UNIVERSIDADE FEDERAL DO RIO GRANDE DO SUL
INSTITUTO DE MATEMÁTICA E ESTATÍSTICA
PROGRAMA DE PÓS-GRADUAÇÃO EM MATEMÁTICA APLICADA

Reduction Techniques Applied to the Oxidation of Ethanol

por

Felipe Crivellaro Minuzzi

Tese submetida como requisito parcial
para a obtenção do grau de

Doutor em Matemática Aplicada

Prof. Dr. Álvaro Luiz De Bortoli
Orientador

Porto Alegre, Junho de 2018.

CIP - CATALOGAÇÃO NA PUBLICAÇÃO

Minuzzi, Felipe Crivellaro

Reduction Techniques Applied to the Oxidation of Ethanol / Felipe Crivellaro Minuzzi.—Porto Alegre: PPGMAp da UFRGS, 2018.

136 p.: il.

Tese (Doutorado) —Universidade Federal do Rio Grande do Sul, Programa de Pós-Graduação em Matemática Aplicada, Porto Alegre, 2018.
Orientador: De Bortoli, Álvaro Luiz

Tese: Matemática Aplicada
Dinâmica dos Fluidos, Combustão, Modelagem Química, REDIM, Mecanismos Esqueleto

Reduction Techniques Applied to the Oxidation of Ethanol

por

Felipe Crivellaro Minuzzi

Tese submetida ao Programa de Pós-Graduação em Matemática Aplicada do Instituto de Matemática da Universidade Federal do Rio Grande do Sul, como requisito parcial para a obtenção do grau de

Doutor em Matemática Aplicada

Linha de Pesquisa: Dinâmica dos Fluidos

Orientador: Prof. Dr. Álvaro Luiz De Bortoli

Banca examinadora:

Prof. Dr. Igor Mozolevski
PPGMTM - UFSC

Prof. Dr. Nilson Romeu Marcilio
PPGEQ - UFRGS

Prof. Dr. Paulo Ricardo de Ávila Zingano
PPGMAp - UFRGS

Tese apresentada e aprovada em
Junho de 2018.

Prof. Dr. Carlos Hoppen
Coordenador

SUMÁRIO

LISTA DE TABELAS

LISTA DE FIGURAS

LISTA DE SIGLAS

ANN	Artificial Neural Network
CSP	Computational Singular Perturbation
CFD	Computational Fluid Dynamics
DNS	Direct Numerical Simulation
DRG	Directed Relation Graph
DRGASA	Directed Relation Graph aided Sensitivity Analysis
DRGEP	Directed Relation Graph with Error Propagation
DRGEPASA	Directed Relation Graph with Error Propagation aided Sensitivity Analysis
DRGX	Directed Relation Graph with Expert Knowledge
FGM	Flamelet Generated Manifolds
FPI	Flamelet Prologation ILDM
ILDM	Intrinsic Low-Dimensional Manifolds
LES	Large Eddy Simulation
LOI	Level of Importance Index
Mtoe	Million tonnes oil equivalent
ODE	Ordinary differential equation
PCA	Principal Component Analysis
PDF	Probability Density Function
PEA	Partial Equilibrium Approximation
PROALCOOL	National Alcohol Program
QSSA	Quasi-Steady-State Assumption
RANS	Reynolds Averaged Navier-Stokes
REDIM	Reaction Diffusion Manifolds
WSR	Well Stirred Reactor

LISTA DE SÍMBOLOS

A	Pre-exponential factor
b	Temperature coefficient
c_p	Constant-pressure specific heat
c_v	Constant-volume specific heat
Da	Damköhler number
E_a	Activation energy
f^o	Constant mass flux
j_i	Mass diffusion of species i
ΔG^o_T	Gibb's function change
$h(T)$	Enthalpy
$h^o_{f,i}$	Enthalpy of formation of species i
$h_i(T)$	Absolute enthalpy of species i
$\Delta h_{s,i}$	Sensible enthalpy change i
K_c	Equilibrium constant
k_b	Backward reaction rate coefficient
k_f	Forward reaction rate coefficient
ℓ^o_R	Reaction zone
ℓ^o_D	Preheat zone
m_i	Mass of species i
m	Total mass of mixture
$\mathcal{M}_i$	Symbol of species i
$\dot{m}$	Flow rate
n_i	Mole number of species i
n	Total number of moles
n_{sp}	Number of species
n_r	Number of reactions
p	Total pressure

Q	Heat of combustion
R	Universal gas constant
s_L^o	Laminar flame speed
s_T	Turbulent flame speed
T	Temperature
T_{ref}	Reference temperature
$u(T)$	Internal energy
V	Volume
W	Mean molar mass
W_i	Molar mass of species i
v_u^o	Flow velocity
X_i	Molar fraction of species i
$[X_i]$	Molar concentration of species i
w_i	Mass fraction of species i
$w_{F,1}$	Initial mass fraction of fuel
$w_{O_x,2}$	Initial mass fraction of oxidant
$w_{i,b}$	Burned mass fraction of species i
$w_{i,u}$	Unburned mass fraction of species i
Ze	Zel'dovich number
	Greek symbols
ρ	Density
τ_{ij}	Lifetime of species i
$\dot{\omega}_i$	Total reaction rate
$\dot{\omega}_T$	Heat release rate
ν_i	Net stoichiometric coefficient of species i
ν_i'	Stoichiometric coefficient of species i as a reactant
ν_i''	Stoichiometric coefficient of species i as a product
λ	Thermal conductivity
ϕ	Equivalence ratio

χ	Scalar dissipation rate
σ	Stoichiometric ratio between fuel and oxidant
ξ	Mixture fraction
ξ_{st}	Stoichiometric mixture fraction

ABSTRACT

Numerical simulation of reactive flows, such as combustion, has a highly non-linear character due to the presence of several chemical reactions that occur among the chemical species that describe the process of fuel's oxidation. Besides, such processes occur at a molecular level, making the system of governing equations stiff, which implies in the need of high order numerical schemes as well as fine meshes and small time step, enhancing considerably the computational cost. In this sense, the use of detailed oxidation mechanisms in the numerical simulation is prohibitive, and chemical reduction techniques are needed in order to develop reduced models with less variables and moderate stiffness, while maintaining the accuracy and comprehensiveness of the detailed model. The objective of the present works if to obtain a comparison between two chemical reduction techniques, the Directed Relation Graph - DRG, based on the skeletal mechanisms generation, and the Reaction Diffusion Manifolds - REDIM, based on the separation of time scales. As validation of the proposed models, one-dimensional numerical simulations of premixed and non-premixed flames, as well as homogeneous reactors, are carry out. Besides, a coupled methodology between DRG and REDIM is presented, that will provide a useful tool for simulation of fuels with very large detailed kinetic mechanisms.

Keywords: Fluid Dynamics, Combustion, Chemical Modelling, REDIM, Skeletal Mechanisms.

RESUMO

A simulação numérica de escoamentos reativos, como a combustão, tem um caráter altamente não-linear devido a presença de diversas reações químicas que acontecem entre as espécies que descrevem o processo de oxidação do combustível. Além disso, tais processos ocorrem a nível molecular, tornando o sistema de equações governantes rígido, o que implica na necessidade de esquemas numéricos de alta ordem bem como malhas finas e passo de tempo pequeno, aumentando consideravelmente o custo computacional. Neste sentido, o uso de mecanismos de oxidação detalhados na simulação numérica é proibitivo, e técnicas de redução química são necessárias de modo a desenvolver modelos reduzidos com menos variáveis e rigidez moderado, mantendo a precisão e abrangência do modelo detalhado. O objetivo do presente trabalho é obter uma comparação dos resultados obtidos para duas técnicas de redução química diferentes, *Directed Relation Graph* - DRG, baseada no desenvolvimento de mecanismos esqueletos, e a *Reaction Diffusion Manifolds* - REDIM, baseada na separação das escalas de tempo. Como validação dos modelos propostos, simulações numéricas 1D de chamas pré-misturadas e não pré-misturadas, bem como de reatores homogêneos, são desenvolvidas. Além disso, uma estratégia que une as duas técnicas de redução é apresentada, com o objetivo de ser aplicada em mecanismos cinéticos grandes.

Palavras-chaves: Dinâmica dos Fluidos, Combustão, Modelagem Química, REDIM, Mecanismos Esqueleto.

RESUMO EXPANDIDO

Título: Técnicas de Redução Aplicadas à Oxidação do Etanol

A busca por eficiência e a preocupação com a emissão de poluentes causando desiquilíbrio ambiental são os principais objetivos da pesquisa em combustão atualmente. O dióxido de carbono, produzido na queima de combustíveis fósseis, é uma dos principais causas do aquecimento global e das mudanças climáticas ocorridas no último século. Nesse contexto, uma alternativa que vem sendo usada mundialmente é o uso de biocombustíveis, tais como o etanol e o biodiesel, como matéria prima para processos de combustão.

Dentre os biocombustíveis, o uso do etanol (C_2H_5OH) como fonte de energia que pode ser produzida através de recursos renováveis se destaca. A maioria deste combustível é derivada da fermentação da cana de açúcar, embora estudos mostram que também pode ser derivado de outros tipos de biomassa, tais como a matéria prima da celulose, milho, arroz, beterraba, polpa de madeira e resíduos sólidos municipais.

A simulação numérica de escoamentos reativos, como a combustão, tem um caráter altamente não-linear devido a presença de diversas reações químicas que acontecem entre as espécies que descrevem o processo de oxidação do combustível. Além disso, tais processos ocorrem a nível molecular, tornando o sistema de equações governantes rígido, o que implica na necessidade de esquemas numéricos de alta ordem bem como malhas finas e passo de tempo pequeno, aumentando consideravelmente o custo computacional. Neste sentido, o uso de mecanismos de oxidação detalhados na simulação numérica é proibitivo, e técnicas de redução química são necessárias de modo a desenvolver modelos reduzidos com menos variáveis e rigidez moderado, mantendo a precisão e abrangência do modelo detalhado.

O objetivo das técnicas de redução química é limitar o número de espécies intermediárias e assim reduzir o número de equações a serem resolvidas de modo a representar com acurácia o comportamento das espécies importantes [108]. As técnicas de redução química podem ser classificadas em termos de redução global do número de reações e refinamento do mecanismo [21]. Nesse contexto, duas categorias principais de redução podem ser identificadas: a análise das escalas de tempo e a geração de mecanismos esqueletos.

Dentre as técnicas de redução esqueleto, o *directed relation graph* - DRG [56] é um método cujo objetivo é resolver de maneira eficiente o complexo acoplamento entre as espécies químicas, de modo que aquelas que têm pequena ou nenhuma influência nas espécies importantes possam ser removidas. Sendo assim, a contribuição da espécie B na produção/consumo da espécie A pode ser quantificada através do índice r_{AB}, dado por

$$r_{AB} = \frac{\sum_{i=1}^{n_r} |\nu_{A,i}\dot{\omega}_i\delta_{B,i}|}{\sum_{i=1}^{n_r} |\nu_{A,i}\dot{\omega}_i|}, \quad (1)$$

onde $\nu_{A,i}$ é o coeficiente estequiométrico de A na reação i, $\dot{\omega}_i$ é a taxa de reação e $\delta_{B,i}$ é

$$\delta_{B,i} = \begin{cases} 1, & \text{se a } i\text{-ésima reação elementar envolve a espécie } B; \\ 0, & \text{caso contrátio.} \end{cases} \quad (2)$$

Os termos no denominador da Eq. (3.21) é a contribuição das reações no consumo/produçao da espécie A, e os termos no numerador são aqueles do denomidador que envolvem a espécie B [57].

Definindo um valor limite ϵ $(0 < \epsilon < 1)$, e se o índice r_{AB} é maior se comparado com ϵ, então a remoção da espécie B pode induzir erro na produção da espécie A, de modo que a espécie B deve ser mantida no mecanismos esqueleto. Geralmente, a espécie A é escolhida entre aquelas que possuem atributos químicos desejáveis que o modelo reduzido deve reproduzir [76]. Diversas mecanismos

esqueletos já foram obtidos usando o DRG para diferentes tipos de combustíveis [3, 53, 56, 60, 61, 68, 69, 93, 119] .

Nas técnicas de análise da escala de tempo, a abordagem através de variedades lentas produzem resultados satisfatórios. Neste contexto, o método *Reaction Diffusion Manifolds* - REDIM possui a vantagem de levar em consideração processos químicos e de transporte. O REDIM afirma que um número definido de parâmetros podem ser usados para descrever a dinâmica do sistema completo. Para obter isso, a hipótese de variedades invariantes é utilizada.

O estado termocinético em um sistema reactivo com n_{sp} espécies pode ser descrito pelo vetor $n = n_{sp} + 2$-dimensional $\mathbf{\Psi} = \left(h, p, \phi_1, \ldots, \phi_{n_{sp}}\right)^T$, onde h é a entalpia específica, p a pressão e ϕ_i é a fração molar específica da espécie i. O estado termocinético varia devido aos processos químicos e de transporte de acordo com a EDP [9]

$$\frac{\partial \mathbf{\Psi}}{\partial t} = \mathbf{F}(\mathbf{\Psi}) - \mathbf{u} \cdot \mathrm{grad}(\mathbf{\Psi}) - \frac{1}{\rho} \left(\mathbf{D} \cdot \mathrm{grad}(\mathbf{\Psi})\right)_\theta \mathrm{grad}(\theta) = \mathbf{\Phi}(\mathbf{\Psi}). \tag{3}$$

Aqui, $\mathbf{u}$ é a velocidade, $\mathbf{D}$ é a $n \times n-$matriz de difusão, $\mathbf{F}$ é termo fonte n-dimensional e ρ a massa específica. $\mathrm{grad}(\theta)$ é uma estimativa do gradiente.

Após as escalas de tempo rápidas relaxarem, a dinâmica do sistema é governada pelos m_s modos lentos ($m_s \ll n$), i.e., a solução do sistema pertence a uma variedade de dimensão m_s no espaço dos estados. Esta variedade $\mathcal{M}$ é definida por

$$\mathcal{M} = \left\{\mathbf{\Psi} : \mathbf{\Psi} = \mathbf{\Psi}(\theta), \mathbf{\Psi} : R^{m_s} \to R^n\right\}, \tag{4}$$

onde θ é o vetor m_s-dimensional que parametriza a variedade. A condição de invariância para a variedade lenta $\mathcal{M}$ implica que

$$\left(I - \mathbf{\Psi}_\theta(\theta) \cdot \mathbf{\Psi}_\theta^+(\theta)\right) \cdot \mathbf{\Phi}\left(\mathbf{\Psi}(\theta)\right) = 0, \tag{5}$$

na qual $\mathbf{\Psi}_\theta^+$ é a pseudo-inversa de Moore-Penrose de $\mathbf{\Psi}_\theta$.

Para encontrar a solução da Eq. (4.40), a seguinte equação de evolução foi proposta para ser resolvida [9]

$$\frac{\partial \mathbf{\Psi}(\theta)}{\partial t} = \left(I - \mathbf{\Psi}_\theta(\theta) \cdot \mathbf{\Psi}_\theta^+(\theta)\right) \cdot \mathbf{\Phi}(\mathbf{\Psi}(\theta)). \tag{6}$$

A solução estacionária $\mathbf{\Psi}(\theta, \infty)$ dada pela Eq. (4.59) fornece a variedade reduzida desejada. As variáveis que parametrizam a variedade são usadas para descrever todas os outros parâmetros da simulação. Para integrar a equação REDIM até a convergência, é necessário definir uma estimativa inicial $\mathbf{\Psi}^0 = \mathbf{\Psi}^{init}(\theta)$ para a variedade.

É importante salientar que, embora o objetivo final das estratégias de redução sejam as mesmas, a formulação é diferente. A redução esqueleto utiliza as informações cinéticas para reduzir o número de espécies, resultando em um novo mecanismo para a oxidação do combustível. No REDIM, não há a intenção de explicitamente desenvolver um novo mecanismo mas, baseado na formulação detalhada do sistema, descrever as variáveis termodinâmicas como função das outras que parametrizam o sistema.

Embora diversos trabalhos usando REDIM são encontrados na literatura, não existe um que lide com etanol e sua validação. Além disso, um estudo compreensivo que compare quais tipos de técnicas de redução, esqueleto ou escalas de tempo, produz um resultado mais aceitável com menor custo computacional. Sendo assim, este trabalho possui os seguintes objetivos:

1. Desenvolver um mecanismo esqueleto usando DRG e construir a REDIM para o etanol e validar os resultados;

2. Comparar os resultados obtidos pelas duas estratégias;

3. Desenvolver uma abordagem unindo DRG e REDIM de modo a obter uma ferramenta para a simulação de mecanismos detalhados grandes.

A técnica DRG foi implementada na linguagem Python, usando o software de código aberto Cantera, o qual consiste em um software orientado a objetos que permite incorporar parâmetros termodinâmicos de de cinética química nas simulações. Já a abordagem REDIM foi aplicada usando os software INSFLA e HOMREA, os quais já possuem as rotinas para obtenção da variedade implementadas.

A validação dos resultados obtidos com as duas técnicas são feitas para três tipos de processos de combustão: tempo de atraso de ignição, velocidade de chama e chamas difusivas contra-corrente. O tempo de atraso de ignição mostra que o mecanismo esqueleto obtido pode ser usado em sistemas de baixa temperatura, e com possível reprodução de fenômenos como ignição e re-ignição, sob diferentes pressões e razões de equivalência. Estes resultados podem ser vistos nas Figs. 5.1 e 5.2.

Uma chama plana de livre propagação é usada para o cálculo da velocidade de chama. As simulações consideram pressão atmosférica e temperatura inicial de $T = 298K$, e a razão de equivalência (que influencia a composição da mistura) varia entre 0.5 e 2.0. Os resultados podem ser vistos nas Figs. 5.3, 5.4 e 5.5.

A terceira aplicação utilizada para validação foi de uma chama difusiva contra-corrente. Esta chama é muito usada para validação de modelos, pois possui um efeito de transporte difusivo evidente. Os resultados da simulação numérica, tanto com o REDIM como com o mecanismo esqueleto, são comparados com dados experimentais disponíveis na literatura. Estes podem ser encontrados nas Figs. 5.6 e 5.7.

Conclui-se, portanto, que a vantagem de usar o REDIM é, com uma escolha correta de parametrização e condição inicial, este vai reproduzir o modelo detalhado com quase nenhuma diferença. De fato, o REDIM independe do mecanismo detalhado utilizado. Isto não é visto na redução via DRG, já que, mesmo com uma precisão aceitável, alguns parâmetros apresentam variações. As diferenças po-

dem ser extendidas para as técnicas que envolvem o desenvolvimento de mecanismos esqueletos e redução de modelo, já que esta irá sempre usar informações termodinâmicas do próprio sistema para obter o resultado, enquanto a primeira necessita de conhecimento *a priori* sobre a cinética do modelo. Todavia, o REDIM não é universal, e diferentes REDIMs devem ser produzidas para cada tipo de processo de combustão. O caráter mais universal do DRG é uma vantagem, já que mesmo se uma aplicação não é usada na sua implementação, o mecanismo esqueleto resultante pode gerar resultados satisfatórios para essa simulação.

Além disso, uma estratégia híbrida entre as duas abordagens, DRG e REDIM, é proposta de modo a ser utilizada na combustão de hidrocarbonetos de cadeia longa ou alcoóis com moléculas grandes, como o biodiesel. O DRG é aplicado em um primeiro estágio, para diminuir o custo computacional da obtenção da condição inicial do REDIM. Se o mecanismo esqueleto obtido reproduzir com precisão o completo, a REDIM construída para este seguirá o mesmo padrão.

Assim, as contribuições deste trabalho podem ser resumidas em:

1. um novo mecanismo esqueleto para o etanol, com 37 espécies e 184 reações, que reproduz o mecanismo detalhado com precisão e possui tamanho comparável com outros disponíveis na literatura.

2. a REDIM para o etanol que pode ser utilizada em simulações de dinâmica dos fluidos computacional.

3. uma nova metodologia que consiste em acoplar as estratégias DRG e REDIM, a qual produz resultados satisfatórios e é destinada à aplicação em mecanismos cinéticos grandes.

ACKNOWLEDGEMENTS

This work is the result of a cooperation between my home institution, UFRGS, and KIT - Karlsruhe Institute of Technology, where I spent a period of my Doctorate. I would like to thank both institutions, for giving me the opportunity to achieve this goal. I thank Prof. De Bortoli, which accepted to be my advisor, and Prof. Maas, that kindly received me in his Institute and gave all the opportunities to finish this work. Furthermore, I would like to acknowledge CAPES and CNPq for their financial support.

I would like to thank my family: my father Valdir, mother Diva, brother Rafael, aunts, uncles and cousins, for their support and for always looking after me. To Adilção, Angela and Mariane, for kindly receiving me as a member of their family and for always encouraging me.

I know I only come this far because I had friends. For those that are always with me, thank you for your friendship (you know who you are!). I must cite some of the colleagues/friends I achieve in this period: from PPGMAp, Bruna, César, Fábio, Francisco, Lucélia, Marcelo, Vinicius, Rhuany and all of those who made my days lighter. A special thank to Jean, who has supported and helped me a lot to finish this work. To all kind friends I made in Germany, from ITT, Jörg, Robert, Slava, Sylvia, Marcus, Andrey, Christina, Simon and Martin. A special thanks to Philipp and Chunkan. Also, I thank Naiá, Felix and Liége for their friendship and company.

And last, but definitely not the least, I would like to thank the woman of my life, Bruna. Thank you, specially, for your patience and understanding in all the time absent, and the time I invest in this goal. For the supportive and the encouraging words. For always sticking with me. I know I would not had finished this Thesis without you. Thank you, and I love you!

1 INTRODUCTION

Energy conversion is a fundamental resource of today's society well-being. In 2016, world consumption of energy was approximately 13276.3 Mtoe (million tonnes oil equivalent), of which 32% was derived from oil, 23% from natural gas, 28% from coal and, in this scenario, only 2% is related with renewable energy sources [16]. Most of the consumed energy worldwide is due to fossil fuels, a process that generates several gaseous and particulate emissions, such as the carbon dioxide (CO_2), carbon monoxide (CO), nitrous oxides (NO_x) and soot, which are harmful to human health and motive environmental imbalance.

Combustion can be defined as the conversion of the energy contained in the chemical reactions into heat, and its application ranges from different fields of engineering, such as industrial processes, piston engines, gas turbines, heating, electrical systems, among others. Despite the growth in using renewable energy, combustion will remain being the major source of conversion for several years [83]. Nonetheless, the fuel to be burned will be different, and considerable studies are being focused in the use of biofuels, such as ethanol and biodiesel.

Two main products of the combustion of hydrocarbons or alcohols cannot be avoided, even when using biofuels: the carbon dioxide (CO_2) and water vapour (H_2O). The latter is not a problem, but the first is, being the leading cause of the global warming and climate changes of the last century. Svante Arrhenius (1859 - 1927) was the pioneer to relate carbon dioxide's emission with the growth of Earth's temperature. His calculations revealed that "the Arctic temperature could ascend between eight and nine degrees Celsius, if CO_2 emission increases among 2.5 and 3 times its actual value." The central challenge of combustion research nowadays is to maximize the efficiency in order to produce energy with the least amount of fuel possible. The less fuel is burned, the lower emission of carbon dioxide. In

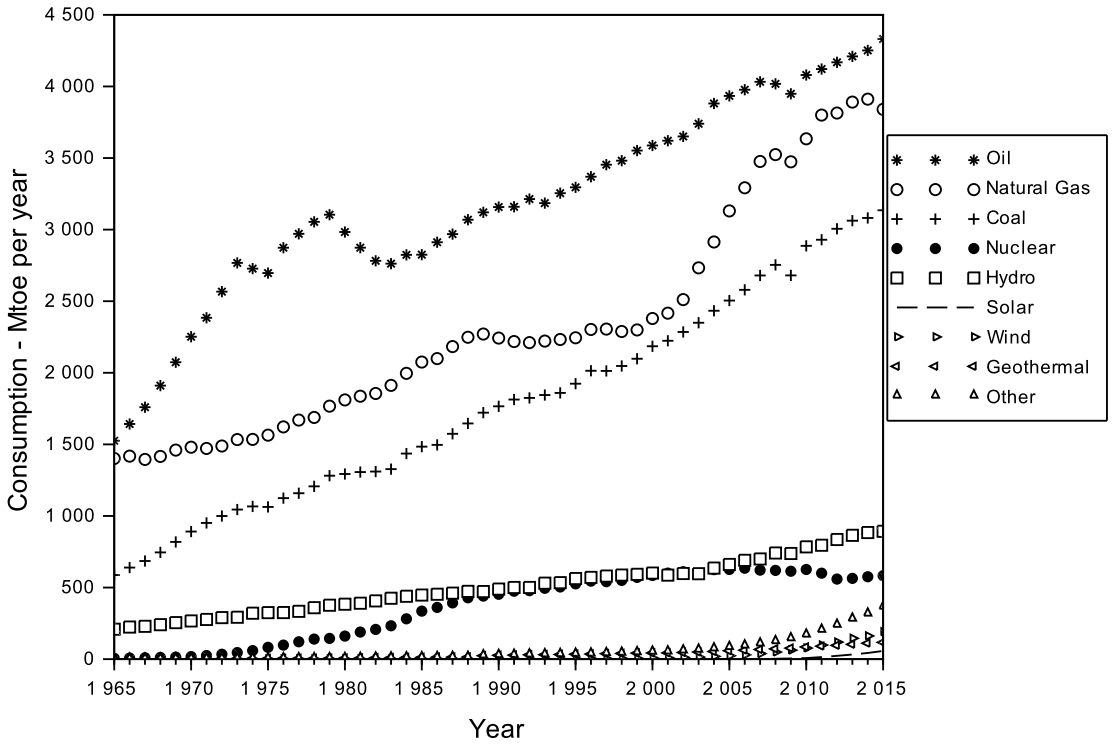

Figure 1.1: Worldwide consumption of energy, in million tonnes oil equivalent (Mtoe), by fuel. One Mtoe produces approximately 4.4 terawatts/hour of electricity in a modern factory.

this context, biofuels carry an important role, as the CO_2 produced from this fuels rebounds to the nature, so it's cycle is complete.

Among biofuels, the use of ethanol (C_2H_5OH) as an energy source that can be produced through renewable resources stands out. Most of this fuel is derived from the fermentation of sugar cane, although studies show that it can also be derived from other types of biomass, such as raw material of cellulose, corn stalk, rice straw, beet, wood pulp and municipal solid waste.

In Brazil, the use of ethanol as a source of renewable energy was achieved since the beginning of the 1970s, with the implementation of the National Alcohol Program (PROÁLCOOL), created to reduce dependence on gasoline and

reduce oil imports [13]. Nowadays, ethanol replaces around 50% of gasoline consumption and its production has increased from 0.6 billion of liters in 1975/1976 to around 24 billions in 2012/2013. In 2015/2016, Brazilian production reached 30 billion liters [84]. The United States and Brazil are the two countries that have efficiently implemented ethanol as an alternative energy source, and have shown that ethanol is a competitive fuel with gasoline and suitable for use in other countries.

Therefore, it is natural that studies regarding the oxidation of ethanol emerges. Saxena and Williams [90] proposed a detailed kinetic mechanism for ethanol oxidation and developed numerical and experimental studies to validate it. The concentration of pollutants were also investigated. Marinov [64] proposed a detailed kinetic mechanism for ethanol oxidation in high temperatures. The validation was performed with simulations of constant volume bomb and counterflow flames for laminar flame speed, shock wave to catch ignition delay time and ethanol oxidation product profiles from jet-stirred and turbulent flow reactor. Ignition of ethanol in a shock tube reactor was studied both numerically and experimentally by Curran *et al.* [20]. Egolfopoulos *et al.* [24] did an experimental and numerical study on ethanol oxidation kinetics, using counterflow premixed flame to determine laminar flame speed, flow and shock tube reactors. Several researches concerning numerical and experimental oxidation of ethanol in reactors or one-dimensional flames can also be found [22, 23, 48, 49]. Turbulent non-premixed spray flames of ethanol has also been interest of study. Masri and Gounder [65] performed an experimental study for a pilot-stabilized jet flame of ethanol to measure mean temperature, axial velocity and droplets velocity. This study was used as reference for numerical simulations using RANS [89] and also using LES [14, 34, 86].

The simulation of reactive flows involves a complex modeling and knowledge in thermodynamics, chemical kinetics, molecular transport and fluid dynamics. Combustion is a process that releases heat and generates instabilities in the flow due to fluctuations and gas expansion, which propitiate the transition to tur-

bulence. In most cases, in practical devices, combustion occurs in turbulent flows [42], and the understanding of these topics is crucial for the physical description of the phenomenon. Turbulence models are based on the Navier-Stokes equations and in closures hypothesis, which depend on dimensional arguments and empirical data. According to Peters [79], this semi-empirical nature of turbulence models places them in the category of an art rather than science.

This multidisciplinary character of combustion requires an extremely complex numerical simulation with a high computational cost. For instance, one can consider the oxidation of a laminar flame of hydrogen (H_2), a robust and simple fuel, which is described by 21 elementary reversible chemical reactions and 9 chemical species [71]. This reactive flow is modelled by a rigid (or stiff) system of partial differential equations, where five equations carry out the conservation of mass, momentum and energy. Besides, nine equations for the conservation of mass for each species are added, which describe the mass diffusion and the effects of chemical reactions in the production/consumption of each species. The source terms of these equations have a high non-linear character and sensitive to any change of parameters, enhancing numerical instability.

Even though hydrogen is a simple fuel, its oxidation shows how complex can be the modelling of combustion. To deal with more complicated fuels, such as hydrocarbons and alcohols, one can expect thousand of elementary reactions and hundreds of chemical species and, also, turbulence can enhance the complexity and dimension of the system. Therefore, using detailed kinetic mechanisms in the simulation is computationally prohibitive, so that techniques for chemical reduction are mandatory in order to develop reduced models with less variables and moderate stiffness, while maintaining the accuracy and comprehensiveness of the detailed model.

The purpose of techniques for chemical reduction is to limit the number of intermediary species and reduce the number of equations to be solved in order to

represent with accuracy the behaviour of the main species [108]. The techniques for chemical reduction can be classified in terms of global reduction in the number of reactions and refinement of the mechanism [21]. A complete review of the chemical reduction techniques can be found in the works of Goussis and Maas [32], Griffiths [33], Løvås [54] and Tomlin *et al* [101].

There are two main categories of reduction techniques for kinetic mechanisms: time scale analysis and the generation of skeletal mechanisms [58]. The latter consists in identifying the important and necessary species and to generating the mechanism only with those. Some examples are the directed relation graph (DRG) [56] and directed relation graph with error propagation (DRGEP) [76], sensitivity analysis based on Jacobian analysis [108] and even artificial neural networks (ANN). Time scale analysis is used primarily to identify a gap in species trajectory on the composition state space, so that the system dynamics can be described using only the slow time scales. Examples are the Quasi-Steady-State Assumption (QSSA) [7] and Partial Equilibrium (PE), Intrinsic Low-Dimensional Manifolds (ILDM) [63], Flame Prologation of ILDM (FPI) [27] Reaction Diffusion Manifolds (REDIM) [9], Computational Singular Perturbation (CSP) [43, 44], Flamelet approach [124] and its developments, as Flamelet with Progress Variable [81] and Flamelet Generated Manifolds (FGM) [72].

Among the skeletal reduction techniques, the directed relation graph - DRG [56] consists in evaluate the error produced when one species is withdraw of the full mechanism. It has a simple theory an it is easy to implement, generating good results. Lu and Law [57] developed a skeletal mechanism for n-heptane with 842 reactions and 290 species, and for the iso-octane, with 233 and 959 reations. Also, Lu and Law [56] applied the DRG technique for ethylene, obtaining 33 species and 205 reactions. The final reduced mechanism, after applying the QSSA and CSP strategies, consists in 16 reactions. Using DRGEP, Niemeyer *et al.* [69] developed a mechanism with 868 reactions and 173 species for n-heptane and, using the DRG,

1044 reactions and 211 species were obtained. For the iso-octane, the DRGEP produced a mechanism of 1140 reactions and 232 species, while the DRG produced 722 reactions and 275 species. Now, for the n-decane, the DRGEP generated an initial skeletal mechanism of 1865 reactions and 381 species.

The DRG technique can also be used for very large reaction mechanisms, such as those of biodiesel. Wang *et al.* [119] developed a skeletal mechanism using DRG for methyl decanoate with 410 species and 1321 reactions. Lu *et al* [61] utilized a surrogate of the tri-component biodiesel formed by methyl decanoate, n-heptane and methyl 9-decenoate and, with DRG and directed relation graph with sensitivity analysis - DRGASA, a skeletal mechanism of 115 species and 460 reactions were developed. This mechanism was also reduced by An *et al.* [3] with directed relation graph with error propagation and sensitivity analysis - DRGEPSA, among others, resulting in a 112 species and 498 reactions. Ng *et al.* [68] reduced the methyl butanoate mechanism and methyl crotonate to 33 species among 101 reactions and 47 species among 210 reactions, respectively.

Seshadri *et al* [93] used DRG to develop a reduced mechanism for methyl decanoate, obtaining a skeletal mechanism with 125 species among 713 reactions. In the same way, Luo *et al* [60] obtained a skeletal mechanism with 118 species and 837 reactions for the same fuel. Liu *et al* [53] developed two detailed mechanisms for methyl butanoate, one with 301 species among 1516 reactions and another with 275 species among 1549 reactions. Using DRG and other methods, a reduced mechanism with 68 and 60 species was developed. Besides those, other strategies are being employed for the reduction of methyl butanoate, as can be found in the works of Akih-Kumgeh *et al* [2], Brakora *et al* [8] and Lin *et al* [51].

It is important to emphasize that, even though the final goals of the reduction strategies are the same, the formulation differs. Skeletal mechanism reduction uses kinetic information to make the number of species, and consequently the number of reactions, smaller, resulting in a new kinetic mechanism. The tech-

niques based on time scales analysis are quite different in this aspect. They do not intend to explicitly develop a new mechanism but, based on the detailed formulation of the system, to use assumptions such that the reduced model has less equations to be solved. Generally, this idea consists in describing the thermodynamic variables as functions of other parameters in the system.

Among the time scales analysis strategies, the so called slow manifold approach produces very reliable results. In this context, the REDIM has an advantage of taking into account both reaction and transport processes. The REDIM has the property that a defined number of parameters are enough to describe the dynamics of the full system. To achieve that, the assumption of invariant manifolds is used.

REDIM has been used in numerical calculations of a methane/air laminar non-premixed flame, where the flow was simulated using the finite element method [39]. Recently, an algorithm for model reduction for near-wall reactive flows based on the REDIM technique was developed [98]. This study is important because it is necessary to account for the flame-wall interactions that perturbs the system states by heat loss and catalytic reactions. The validation of the methodology was with a methane/air combustion system in a simple geometry and a cold inert wall.

Multi-directional molecular diffusion was also studied in terms of the REDIM [91]. Gradients from direct numerical simulations (DNS) of a turbulent flame was incorporated into the REDIM, and it was found that the inclusion of multi-directional gradient from the considered DNS data was only of minor influence for the REDIMs. This means that, while the detailed dynamics of a system with multi-directional diffusion might differ from that a system with uni-directional diffusion, the same REDIM can be used to describe both systems.

A coupled strategy between REDIM and Progress Variable Method was developed by Benzinger *et al.* [5], based on a new variable: the normalized strength

of molecular transport. The model was validated with calculations of a homogeneous engine cycle, a non-premixed counterflow flame, premixed free flat flame and premixed hot-spot. In [12], the instationary behaviour of counterflow non-premixed flames with REDIM is studied and the ability of REDIM to describe transient processes of extinction and re-ignition. An eigenvalue analysis of the Jacobian matrix shows that the REDIM can handle the unstable regions of the domain where there is no stationary flamelets solutions. Thus, REDIM not only represents a slow attractive manifold, but is also capable of predicting transient behaviour within the slow manifold. This conclusion is very useful since improved the choice of initial gradients to solve the REDIM equation.

Turbulent simulations are also well described using REDIM. For instance, PDF simulations of the ignition of hot transient jets for different fuels [25] was developed. A comparison between joint velocity-scalar PDF and joint scalar PDF is investigated [66] for bluff-body stabilized jet-type turbulent non-premixed flames. Large eddy simulation is also applied with REDIM and the presumed filtered density function [114, 115, 116], as well as RANS [52, 127].

The global search for new sources of energy, the concern with pollutants emission causing environmental imbalance and the needed for numerical simulations with lower computational cost to describe the combustion phenomena sustain the importance of this work.

1.1 Objectives

Although several works with different fuels are found in the literature using REDIM, there is none that deals with ethanol and its validation. Besides, a comprehensive study that compares which type, skeletal or model reduction, of strategy produces a more reliable result with less computational effort has not been found. The present work aims to answer these questions.

Considering the methods studied and the literature review, this thesis has the following objectives:

1. Develop a methodology to implement a computational code for DRG and use it to generate a skeletal mechanism for ethanol. The result will be validated against premixed and non-premixed 1D flames as well as well-stirred reactor.

2. Built the REDIM for ethanol and validate the result with a counterflow non-premixed flame.

3. Compare the results obtained for the two strategies (REDIM and DRG), analysing difficulties, accuracy and computational cost.

4. Develop a coupled methodology between DRG and REDIM that will provide a useful tool for simulation of fuels with very large detailed kinetic mechanisms.

This thesis is organized as follows: the first chapter is the introduction. The second will present the basic concepts of combustion kinetics, necessary to understand the methods to be studied, exploiting also the difference between combustion regimes. The third chapter is dedicated to the skeletal mechanism generation techniques, with focus to the DRG, aim of this work. The fourth chapter consists in the model reduction techniques, exploiting the time scales separation and how this lead to slow invariant manifolds. Finally, the fifth chapter presents the validation with different combustion situations of the models developed in the two prior chapters, and the sixth presents the conclusions and suggestions for future works.

2 KINETICS OF COMBUSTION

In this chapter, the necessary concepts about thermodynamics and kinetics of the elementary reactions will be introduced. The concepts that will be defined here are required for the precise description of the processes that control reactive flows, besides forming the theoretical foundation for the understanding the mechanism reduction techniques.

2.1 Mass fraction, moles and thermodynamic parameters

In combustion, the energy contained in the chemical reactions is transformed in thermal energy. In this course, chemical species reacts among each other to form new species, which react again, in a dynamical process, until the final products of combustion are formed. The chemical elements are conserved during the reactions, as, for instance, the carbon atom C, being present in the hydrocarbon molecule C_nH_m, will remain present in the molecule of carbon dioxide CO_2, when the combustion is complete. To describe the transformations that occur among the chemical species, it is indispensable to introduce definitions for species concentration, which can have different descriptions in the literature.

We consider a multi-component system, with n_{sp} different chemical species, which contains a huge number of molecules. One mole of compound correspond to 6.023×10^{23} particles (molecules, atoms, etc.), the Avogrado's constant, and the molar fraction X_i of the species i is defined as the ratio between the mole number of species i, n_i, and the total number moles of the system, n,

$$X_i = \frac{n_i}{n}, \tag{2.1}$$

where the total number of moles is obtained from the summation among all species, i.e., $n = \sum_{i=1}^{n_{sp}} n_i$.

The mass m_i of all molecules of species i is related to the number of moles by

$$m_i = W_i n_i, \tag{2.2}$$

where W_i is the molar mass of species i, representing the mass of one mol of this species. The total mass of the mixture is given by $m = \sum_{i=1}^{n_{sp}} m_i$ and the mass fraction of species i is defined as the ratio between the mass of species i and the total mass, i.e.,

$$w_i = \frac{m_i}{m}. \tag{2.3}$$

The mean molar mass W is defined by $m = Wn$ (units usually g/mol) and the relation between molar fraction and mass fraction is given by

$$w_i = \frac{W_i}{W} X_i. \tag{2.4}$$

Another variable defining the concentration, that is frequently used in combustion, is the number of moles per unity of the system volume V, or molar density (units mol/m^3):

$$[X_i] \;=\; \frac{n_i}{V},$$

and is related with the mass fraction through the mass density ($\rho = m/V$, units kg/m^3) by $[X_i] = \rho w_i / W_i$. From the previous definitions, it follows that the summation of all molar or mass fractions of all species in the system must be equal to unity:

$$\sum_{i=1}^{n_{sp}} X_i = 1 \quad \text{e} \quad \sum_{i=1}^{n_{sp}} w_i = 1. \tag{2.5}$$

One can easily verify the expression for the mean molar mass by

$$\frac{\rho}{[X]} \;=\; \frac{m}{n} \;=\; W. \tag{2.6}$$

For gases and gaseous mixtures in combustion processes, an equation of state relates temperature (T), pressure (p) and density of the gas. A satisfactory

relation is given by the ideal gas equation of state [120], given by

$$pV = nRT, \tag{2.7}$$

where R is the universal gas constant, $R = 8314\ J.mol^{-1}.K^{-1}$, p the pressure (in Pa), V the volume (in m^3), T the absolute temperature (in K). From Eq. (2.7), it follows that

$$[X] = \frac{p}{RT} \quad \text{and} \quad \rho = \frac{pW}{RT} = \frac{p}{RT\sum_i \frac{w_i}{W_i}} \tag{2.8}$$

Nevertheless, the ideal gas equation of state is not a good approximation for temperatures close the the critic, or low pressures, situations where the system is better estimated as a real gas. An example of equation of state for a real gas is the equation of van der Waals

$$\left[p + a\left(\frac{n}{V}\right)^2\right](V - nb) = nRT, \tag{2.9}$$

where a and b are the van der Waals's constants, adjustable for each particular gas.

Equations of state can be used to calculate enthalpy h and the internal energy u (unit $J = kg.m^2.s^{-2}$). The calorific equations of state are given by [109]

$$h(T) - h_{\text{ref}} = \int_{T_{\text{ref}}}^{T} c_v\ dT, \tag{2.10}$$

$$u(T) - u_{\text{ref}} = \int_{T_{\text{ref}}}^{T} c_p\ dT, \tag{2.11}$$

where c_v is the constant-volume specific heat and c_p the constant-pressure specific heat. For ideal or real gases, these quantities are generally dependent of the temperature. To any chemical species, the absolute (or standardized) enthalpy h_i is defined as the sum of the enthalpy of formation $h^o_{f,i}$, responsible for the energy associated with chemical bonds, and the sensible enthalpy change, $\Delta h_{s,i}$, associated only with the temperature

$$h_i(T) = h^o_{f,i}(T_{\text{ref}}) + \Delta h_{s,i}(T_{\text{ref}}), \tag{2.12}$$

where the standard reference temperature is normally defined as $T_{\text{ref}} = 298.15K$. Absolute enthalpy can be used to define the heat of combustion Q,

$$Q \;=\; -\Delta h \;=\; -(h_{\text{products}} - h_{\text{reactants}}), \tag{2.13}$$

and indicates the variation of energy released as heat in the system.

Combustion is a multidisciplinary subject and, for its complete understanding, it is necessary knowledge in thermochemistry, chemical kinetics, transport phenomena and fluid dynamics [83]. For the physical description of reactive flows, the concepts introduced above are important, but others should be determined. These concepts can be found in books for the classical theory of the combustion's kinetics [41, 108, 109, 120].

2.2 Kinetics of chemical reactions

Chemical reactions occur when molecules of one species collide with those of other species (reactants) and then new molecules are created (products). The atoms of the reactants are rearranged in the new molecules, and this process arises when the reactant molecules hold enough energy so that the chemical bonds can be broken during the collision, and another bonds are formed.

The oxidation of methane, for instance, can be described by the global chemical reaction:

$$CH_4 + 2O_2 \;\rightarrow\; CO_2 + 2H_2O. \tag{2.14}$$

This reaction indicates that one mole of methane reacting with two moles of oxygen produces one mole of carbon dioxide and two moles of water vapour. The number of atoms of carbon, oxygen and hydrogen are the same in both sides of the equation. This defines a stoichiometric reaction, and occur when the combustion of a determined fuel is complete, that is, the quantity of oxygen is enough to transform all carbon into CO_2 and all hydrogen in H_2O.

However, stoichiometric reactions rarely occur in real combustion systems. In most of the cases, the number of reacting molecules colliding to produce the product's number of molecules are not the same as indicated in the reaction (2.14). Many bonds should be broken and others formed so that the oxidation process becomes complete. In this way, intermediaries species are produced, which react among themselves and with the reactants, and the final products will only be formed after several steps of coupled reactions [109]. Each one of these individual steps is denominated elementary reaction and the set of several elementary reactions that are necessary for the oxidation of the fuel is entitled detailed kinetic mechanism.

Since the rection (2.14) does not occur, the three following elementary reactions appear in a molecular level

$$CH_4 + O \rightarrow CH_3 + OH \tag{2.15}$$

$$CH_4 + H \rightarrow CH_3 + H_2 \tag{2.16}$$

$$CH_4 + OH \rightarrow CH_3 + H_2O \tag{2.17}$$

i.e., several steps are needed to break methane's molecule and form the radicals which will lead to the main products of combustion. These radicals (or free radicals) are intermediary reactive species that have unpaired electrons. The oxidation of methane is the most studied and understood due its unique chatacteristics, such as high ignition temperature and low flame speed, and it is composed by hundreds (or even thousands) of elementary reactions and chemical species. One example of complete mechanism for the combustion of methane is GRI-mech 3.0 [95], which has 325 elementary reactions and 53 chemical species.

2.2.1 Consumption and production of chemical species

A chemical reaction can be formally described by the equation [78]

$$\sum_{i=1}^{n_{sp}} \nu_i' \mathcal{M}_i \underset{k_b}{\overset{k_f}{\rightleftharpoons}} \sum_{i=1}^{n_{sp}} \nu_i'' \mathcal{M}_i \tag{2.18}$$

where $\mathcal{M}_i$ represents the symbol of species i, ν_i' and ν_i'' their stoichiometric coefficients. The symbol $\rightleftharpoons$ express a forward and backward reaction. The net stoichiometric coefficient $\nu_i = \nu_i'' - \nu_i'$ is positive when $\nu_i'' > \nu_i'$, indicating that ν_i moles of specie i is produced. If $\nu_i'' < \nu_i'$, then ν_i moles of specie i are consumed.

All chemical reactions occur at a defined finite rate that depends on the conditions of the system, such as the reactants concentration, temperature and the presence of a catalyst or inhibitor. For a given reaction, the reaction rate is the quantitative measure of its evolution, i.e., the number of moles produced by unit of time and volume [38].

For the chemical reaction (2.18), the molar rate of consumption/production of each species i over time is given by

$$\frac{d\left[X_i\right]}{dt} = \nu_i \dot{\omega} \tag{2.19}$$

where the total reaction rate $\dot{\omega}$ is given by

$$\dot{\omega} = k_f \prod_{i=1}^{n_{sp}} \left[X_i\right]^{\nu_i'} - k_b \prod_{i=1}^{n_{sp}} \left[X_i\right]^{\nu_i''} \tag{2.20}$$

where k_f is the forward reaction rate coefficient and k_b the backwards reaction rate coefficient. Usually, k_b is calculated through the equilibrium constant K_c since, when $\dot{\omega} = 0$, it holds that

$$\frac{k_f}{k_b} = \frac{\prod_{i=1}^{n_{sp}} \left[X_i\right]^{\nu_i''}}{\prod_{i=1}^{n_{sp}} \left[X_i\right]^{\nu_i'}} = K_c. \tag{2.21}$$

The chemical equilibrium can be determined by species concentrations or using the variation of the Gibb's function ΔG_T^o

$$K_c = \exp\left(-\frac{\Delta G_T^o}{RT}\right) \tag{2.22}$$

When the intention is to analyse the consumption/production of a chemical species in a kinetic mechanism of n_r elementary reactions, it is necessary to incorporate the molar rate to the contribution of each one of those. Thus,

the relation (2.20) turns to

$$\dot{\omega}_i = W_i \sum_{j=1}^{n_r} \nu_{kj} \left[k_{fj} \prod_{i=1}^{n_{sp}} [X_i]^{\nu'_{ij}} - k_{bj} \prod_{i=1}^{n_{sp}} [X_i]^{\nu''_{ij}} \right], \tag{2.23}$$

where the net stoichiometric coefficient $\nu_{kj} = \nu''_{kj} - \nu'_{kj}$ is calculated in each reaction j.

The molar rate of each species possess the contribution of several reactions that happens extremely fast, leading to highly non-linear and stiff system of equations [79]. The integration of this system in the context of combustion modelling is in many conditions considered prohibitive. Therefore, there is the requirement to simplify the detailed kinetic mechanism without losing the chemical knowledge of important species. The most used reduction techniques are displayed in the Chapters 3 and 4.

2.2.2 Coefficients of reaction rates

The coefficients of reaction rate, or specific velocity of reaction, introduced in Eq. (2.20), strongly depends on the temperature. This dependence is described by the empirical Arrhenius's law, given by

$$k_{f,b} = A' \exp\left(-\frac{E_a}{RT}\right), \tag{2.24}$$

where A' is the pre-exponetial factor (or frequency factor), E_a the activation energy, T the temperature and R the universal gas constant. More precise measurements indicate that the pre-exponential factor A' also depends on temperature [120], and so the reaction rate can be described by the modified Arrhenius law

$$k_{f,b} = AT^b \exp\left(-\frac{E_a}{RT}\right), \tag{2.25}$$

where b is the temperature coefficient. The activation energy behave as an energy limit in which the reactants should overcome so that the chemical reactions can be broken and the products formed. The activation energies of the forward and

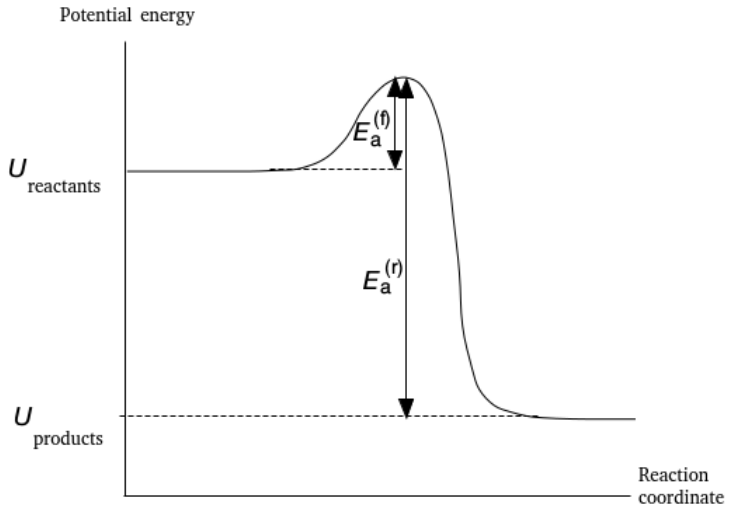

Figure 2.1: Energy diagram for a chemical reaction. The relation $U_{products} - U_{reactants}$ is a result of the chemical equilibrium K_c. Adapted from [120].

backwards reactions are not equal, leading to different reaction rates. Figure 2.1 exhibits the potential energy contained in the species over the reaction coordinate[1] during the reaction. The activation energy can be calculated by the Schröndiger equation of quantumm mechanics, which governs the molecules collision processes [38]. Nonetheless, calculating this equation is very complex, so that semi-empirical procedures are employed to obtain reaction rates coefficients.

Additionally to the temperature, other factors affect the specific velocities. Pressure, mainly in unimolecular reactions of dissociation or termolecular reactions of recombination, also portray an important role and can be described by the Lindemann mechanism. The use of catalysts, which speed up the reaction and are not consumed, allow that the reaction occurs at a lower activation energy. The higher the reactants concentration, as well as the contact surface, the larger will be the reaction velocity.

[1]The reaction coordinate is the path of minimum potential energy from reactants to products with respect to the changing interatomic distance

The heat release rate, $\dot{\omega}_T$, to be used in the governing equation's system of the reactive flow, can be described as the summation over all reactions in the mechanism [79]

$$\dot{\omega}_T = \frac{1}{c_p} \sum_{j=1}^{n_r} Q_j \dot{\omega}_j, \tag{2.26}$$

where Q_j is the heat of combustion of reaction j.

2.2.3 Important reactions in a mechanism

Kinetic mechanism generation starts by the definition of the most important species, which usually comprise reactants and products, beyond required intermediate species [108]. The reaction types that can occur between the group of species should also be identified together with appropriate thermodynamic data.

Reactions that can occur in the oxidation process are defined as [120]: chain initiation steps, chain propagation steps, chain branching steps and chain termination steps.

Initiation reactions are responsible by the chain ignition. They are reactions where the radicals are formed through reacting stable species. The branching reactions are those where the stable molecules are broken by free radicals, increasing the number of the latter. These reactions are generally the most important source of radicals, which participate of the most important reactions of the system.

The propagation reactions are also responsible for breaking molecules via radicals, but not increasing its number. As result, other stable species or chemically excited species are formed. Considering the ratio between the number of radicals in the product by the number of radicals in the reactants, the propagating chain reactions have this ratio equal to one, as the branching reactions have it higher than one. Lastly, the oxidation process finishes with the chain termination reactions, where the radicals react to form the stable products.

The initiation reaction can be illustrated through [41]

$$M + Br_2 \rightarrow 2Br + M \quad \text{and} \quad M + O_2 \rightarrow 2O + M, \tag{2.27}$$

where M is a stable species. Propagation reactions, with the same number of radicals in both sides, can be

$$\begin{aligned} CO + OH &\rightarrow CO_2 + H; \\ \\ Br + H_2 &\rightarrow HBr + H; \\ OH + H_2 &\rightarrow H_2O + H. \end{aligned}$$

Two branching reactions are

$$\begin{aligned} H + O_2 &\rightarrow OH + O; \\ O + H_2 &\rightarrow OH + H, \end{aligned} \tag{2.28}$$

and two termination reactions are

$$\begin{aligned} M + 2O &\rightarrow O_2 + M; \\ M + 2H &\rightarrow H_2 + M. \end{aligned} \tag{2.29}$$

Generally, for hydrocarbons, combustion can be summarized as:

1. initiation: $M \rightarrow R$;
2. branching: $M + R \rightarrow \alpha R + M^*,\ \alpha > 1$;
3. propagation: $M + R \rightarrow M + M^*$;
4. termination: $M + R \rightarrow M$,

where R is a radical and M^* an excited species.

2.3 Types of Flames

Gaseous combustion processes can be divided by which level of mixture is considered: premixed or non-premixed. Premixed flames occur when reactants, fuel and oxidant, are completely mixed prior entering the reaction zone. The non-premixed flames occur when the fuel and oxidant are injected separately in the reaction zone.

The internal combustion engine is an example of premixed mixture [79]. The fuel and the oxidant are mixed through turbulence before an electric spark ignites the mixture. Another example of premixed flame is the gas turbines used for generating energy, where the liquid fuel is vaporized and premixed with air before entering the combustion chamber.

In the gas turbines used in aircraft engines, the fuel is introduced in the combustion chamber where evaporates and burns in a non-premixed flame. Diesel engines also uses the non-premixed configuration. The atmospheric air enters the combustion chamber and is compressed, increasing pressure and temperature. Liquid fuel is injected as a spray, and the droplets absorb the heat from air particles, evaporating, leading to ignition. The explosion pushes the piston down and the resultant gases of combustion exits through the exhausts.

In furnaces, a condition called partially premixed is held. Liquid, gas or solid fuels enter the combustion chamber separately from air and, once the mixture is ignited, the flame propagates towards the nozzle until it stabilizes at a distance, called the lift-off height. In the region between the nozzle and the lift-off height, combustion takes place as a premixed flame, which determine stabilization of the flame. After this point, combustion turns to occur under non-premixed conditions.

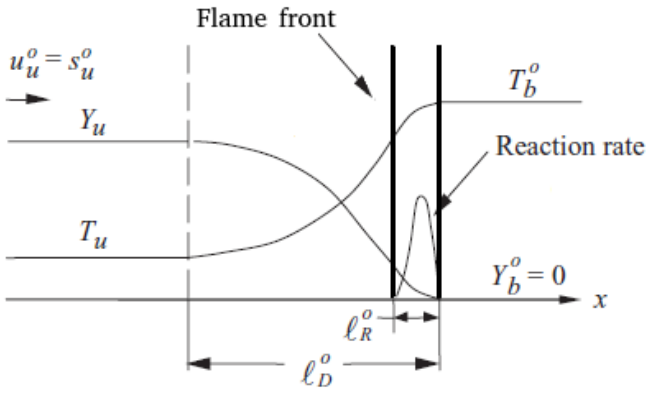

Figure 2.2: Structure of premixed flame, adapted from [46].

2.3.1 Premixed flames

Numerical solution of premixed flames are of interest because this is one of the few configurations where comparisons between experiment, theory and calculation can be performed, besides being useful to validate chemical models [83].

In a standard premixed flame structure (Fig. 2.2-(a)), the unburned gases (Y_u - fuel and oxidant, also called fresh gases) and the burned gases (Y_b^o - products) are separated by an extremely thin reaction zone (ℓ_R^o - typical values between $0.1 - 1$mm, for atmospheric pressure). In this region, the combustion products are formed and the energy is released. One can observe high temperature gradients (order of 5 or 6 times) [113], inducing high heat transfer and density variations.

Prior to this region, a preheat zone (ℓ_D^o) which is always greater then the reaction zone: $\ell_R^o/\ell_D^o \approx Ze^{-1}$, where Ze is the Zel'dovich number[2], is observed, where the mixture approaches the flame and its gradually heated by the heat conducted forward from the chemical heat release region, resulting in an increase of temperature until the burned temperature (T_b^o) is reached [46]. This continuous heating of the mixture leads to the ignition and subsequent reaction. The high

[2]The Zel'dovich number measures the combined effects of the temperature sensitivity of the reaction.

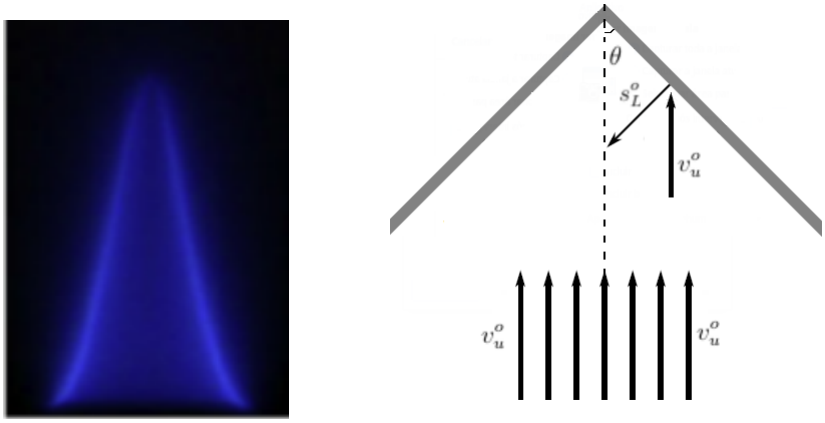

(a) (b)

Figure 2.3: A hydrogen/biogas premixed laminar Bunsen burner flame snapshot (a), obtained from the work of Wei *et al.* [121], and (b) a theoretical flame from a Bunsen burner configuration.

temperature gradients of the reaction zone are responsible for the heat and radicals diffusion towards the preheat zone, allowing the flame to self propagate [17].

One of the main characteristics of premixed flames is its ability to propagate towards the fresh gases. In this sense, a special parameter is defined: the flame speed (or laminar burning velocity) s_L^o. This is defined as the velocity, related with the flame front, in which the reactants move, in the direction perpendicular to the flame [17]. For instance, if we consider the well known Bunsen burner (see Fig. 2.3), the laminar flame speed is given by

$$s_L^o = v_u^o \sin\theta \tag{2.30}$$

in which v_u^o is the flow velocity and θ is the angle between the stream line and the flame front. Furthermore, there are a lot of existing theories for calculating the flame speed, and can be classified in [17, 28]: thermal theory, which assumes the thermal diffusion as the main phenomena; the diffusion theory, which assumes the mass diffusion as the most important phenomena; and the global theory, which assumes both phenomena as equally important. However, these theories are based mostly in a single-step global reaction.

For a multi-step chemical kinetics (i.e., using a detailed mechanism), to obtain the flame speed, the freely propagating, one dimensional, adiabatic laminar premixed flame can be calculated numerically by solving the following system of governing equations for the continuity, mass fractions and temperature [78]:

$$\frac{d\rho u}{dx} = 0, \tag{2.31}$$

$$\rho u \frac{dw_i}{dx} = \frac{dj_i}{dx} + \dot{\omega}_i, \tag{2.32}$$

$$\rho u c_p \frac{dT}{dx} = \frac{d}{dx}\left(\lambda \frac{dT}{dx}\right) - \sum_{i=1}^{n_s} h_i \dot{\omega}_i - \sum_{i=1}^{n_s} c_p j_i \frac{dT}{dx} + \frac{dp}{dt}, \tag{2.33}$$

where j_i is the mass diffusion of species i, h_i the enthalpy of species i, c_p is the heat capacity, λ the thermal conductivity and $\dot{\omega}_i$ is given by (2.23). The continuity equation (2.31) yields

$$f^o = \rho_u s_L^o, \tag{2.34}$$

in which the subscript u denotes the condition at the unburned mixture. f^o is the constant mass flux, also defined as the laminar burning flux, and this is the fundamental parameter characterizing the rate of flame propagation [46]. The flame speed in (2.34) is an eigenvalue of the problem, and must be determined as part of the solution [28, 78], since the unburned mixture density ρ_u is known.

The freely propagating premixed flat flame is a common configuration for analysing premixed flames, whose structure is displayed in Fig. 2.4. Considering v_u the velocity that the unburnt gases enter the burner, if the laminar flame speed s_L is less than v_u, the flame blows-off [120]. Thus, the relation $s_L^o > v_u^o$ has to be fulfilled for flat flames.

Now, the turbulent flame speed propagation s_T is bigger than the corresponding laminar s_L^o, as well as the reaction zones. The analysis developed by Zel'dovich indicates that the flame propagation is the reason for the diffusive process and the expression s_L^o, for a global reaction, is given by [120]

$$s_L^o \approx p^{\frac{n}{2}-1} \exp\left(-\frac{E_a}{2RT_b}\right), \tag{2.35}$$

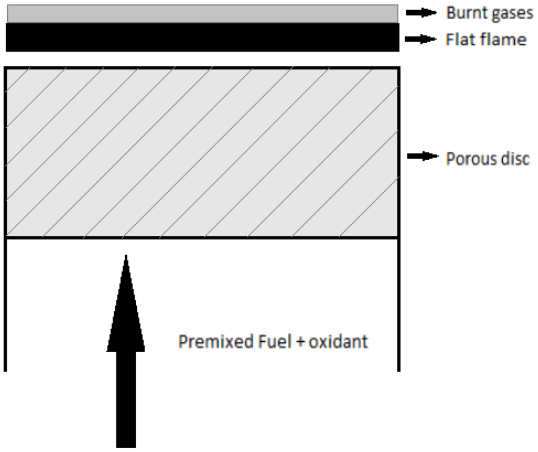

Figure 2.4: Structure of a premixed flat flame

where n is the reaction order, p the pressure and T_b the burned gases temperature.

The turbulent propagation flame speed depends on the laminar, and can be calculated using the following empirical expression

$$\frac{s_T}{s_L^o} = 1 + \alpha \left(\frac{u'}{s_L^o} \right)^k, \tag{2.36}$$

where k and α are constants of order 1 and u' is the rms (root mean square) velocity.

2.3.2 Non-premixed flames

In the non-premixed flames, fuel and oxidant are mixed after entering the combustion chamber, and the mixture occurs mainly by molecular diffusion, which takes reactants to the reaction zone. For this reason, they are also called diffusion flames. The structure of this kind of flame depends on the Damköhler number (ratio between the flow and the chemical characteristic time scales) and consists of three zones, with the reaction zone separating the fuel rich zone of the fuel lean zone [46]. As the fuel and oxidant are transported into each other, they heat up and meet at the reaction zone, where mixture and fast chemical reactions occur.

For many years, the fast chemistry hypothesis were used in non-premixed flames to describe global properties. In this case, the reaction takes place in a very thin zone, practically a reaction sheet. Fuel and oxidant remains confined in their respective regions, and its concentrations decreases as molecular transport lead them into the reaction sheet.

The fast chemistry hypothesis, used in the flame sheet model (also known as Burke-Schumann solution), is justified by the high temperature in the reaction zone. Due to the branching reactions, the fuel molecules bonds generally breaks at between $1300K$ and $1500K$ [79]. Outside this limit, extinction may occur. Thus, industries develop engine far from this extinction limit, where temperature is high enough and therefore reactions occur rapidly. It is also in this limit that products and radicals are formed.

An essential characteristic to calculate a non-premixed flame is the introduction of a conservative variable, called mixture fraction [79]. So, scalars as temperature, concentration as density of species can be described by algebraic relations, which depends only of the mixture fraction.

2.3.2.1 Mixture fraction

Mixture fraction (denoted Z or ξ) is defined as the proportion between fuel and oxidant happening in the mixture. It is a conserved scalar under chemical reactions, so that the terms involving chemical reactions can be dropped from its transport equation [6], and it is a measure of the stoichiometry of the local mixture. The mixture fraction equation depends on diffusion and convection, not on reaction [83].

Generally, non-premixed flames are described as a system with two streams, one for fuel, with mass flux $\dot{m}_1$, and another for the oxidant, with mass flux $\dot{m}_2$. Mixture fraction is defined in any point of the system as the local ratio

between the fuel mass flux and the sum of both mass fluxes, as

$$\xi = \frac{\dot{m}_1}{\dot{m}_1 + \dot{m}_2}. \tag{2.37}$$

The local mass fraction of the fuel, $w_{F,u}$, in the unburned region is related with mixture fraction by

$$w_{F,u} = w_{F,1}\xi, \tag{2.38}$$

where $w_{F,1}$ is the initial mass fraction in the fuel stream. Analogously, the local mass fraction of the oxidant, $w_{O_x,u}$, in the unburned region is

$$w_{O_x,u} = w_{O_x,2}(1-\xi), \tag{2.39}$$

where $w_{O_x,2}$ denotes the initial mass fraction in the oxidant stream. Following from (2.37), (2.38) and (2.39), integrating from the unburned state to the burned state, one can relate the mass fractions of fuel and oxidant with mixture fraction by

$$\xi = \frac{\sigma w_F - w_{O_x} + w_{O_x,2}}{\sigma w_{F,1} + w_{O_x,2}} \tag{2.40}$$

where σ is the stoichiometric ratio between fuel and oxidant, i.e.,

$$\sigma = \frac{\nu'_F W_F}{\nu'_{O_x} W_{O_x}}. \tag{2.41}$$

From Eq. (2.40) one can observe that $\xi = 1$ in the fuel stream, since $w_{O_x} = 0$ and $w_F = w_{F,1}$, and $\xi = 0$ in the oxidant stream, due to $w_F = 0$ and $w_{O_x} = w_{O_x,2}$.

In a stoichiometric mixture, it holds that

$$\frac{w_{O_x}}{w_F} = \sigma \tag{2.42}$$

ans thus, the stoichiometric value for the mixture fraction is given by

$$\xi_{st} = \frac{w_{O_x,2}}{w_{F,1} + w_{O_x,2}} = \left[1 + \frac{\sigma w_{F,1}}{w_{O_x,2}}\right]^{-1}. \tag{2.43}$$

Its worth emphasize that ξ_{st} is generally too small, meaning that a high amount of oxidant is necessary for consuming the fuel.

The equivalence ration ϕ defines the ratio of fuel and air in the unburned mixture normalized by the stoichiometric mixture, and can be related to ξ through the relation

$$\phi = \frac{\sigma w_{F,u}}{w_{O_x,u}} = \frac{\xi}{1-\xi}\frac{(1-\xi_{st})}{\xi_{st}}. \tag{2.44}$$

Assuming that the diffusivity D_i of species i is equal to D_ξ, the mixture fraction satisfies the following transport equation

$$\frac{\partial(\rho\xi)}{\partial t} + \frac{\partial(\rho u_j \xi)}{\partial u_j} = \frac{\partial}{\partial x_j}\left(\rho D_\xi \frac{\partial \xi}{\partial x_j}\right) \tag{2.45}$$

in which the boundary conditions are $\xi = 1$ in the fuel stream and $\xi = 0$ in the oxidant stream. The diffusivity coefficient D_ξ in Eq. (2.45) is arbritary, but as the maximum temperature defines the reaction zone, enthalpy diffusion is the most important transport process in the mixture fraction space. Therefore, thermal diffusion is chosen as the coefficient D_ξ.

The surface defined by $\xi = \xi_{st}$ represents the flame surface. This information permits to establish the relation between species mass fractions and mixture fraction. Next section will present these relations, which were first introduced by Burke and Schumann. Figure 2.5 shows the basic structure of a laminar non-premixed flame.

2.3.2.2 Burke-Schumann solution

Consider the irreversible one-step reaction given by

$$\nu_F F + \nu_{O_x} O_x \rightarrow \nu_{CO_2} CO_2 + \nu_{H_2O} H_2O. \tag{2.46}$$

Assuming the fast chemistry hypothesis, there is a thin reaction zone outside of which the mass fractions of fuel and oxidant are either zero or function of mixture fraction. In the region $\xi < \xi_{st}$, the mixture is considered fuel lean, i.e.,

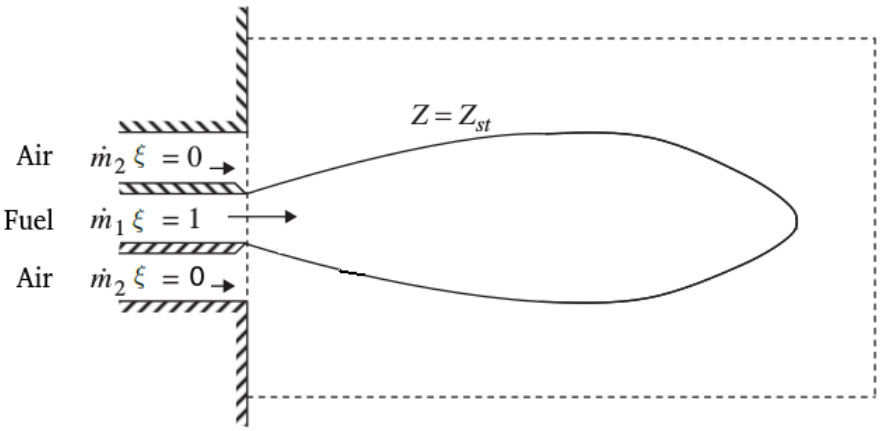

Figure 2.5: Structure of a non-premixed laminar flame with two inlet streams. Note that the stoichiometric value of mixture fraction ξ defines the flame surface.

there is abundant oxidant to completely burn the fuel ($w_{F,b} = 0$). The remaining oxidant is calculated through the mixture fraction by the relation

$$w_{O_x,b} = w_{O_x,2}\left(1 - \frac{\xi}{\xi_{st}}\right), \quad \xi < \xi_{st}. \tag{2.47}$$

Analogously, in the region where $\xi > \xi_{st}$, there is excess of fuel, i.e., the mixture is fuel rich. In this case, the existing amount of oxidant is not enough to burn all the fuel ($w_{O_x,b} = 0$), which can be calculated as

$$w_{F,b} = w_{F,1}\left(\frac{\xi - \xi_{st}}{1 - \xi_{st}}\right), \quad \xi > \xi_{st}. \tag{2.48}$$

Assuming equal and constant heat capacities for the species in the system, besides pressure, and that the Lewis number is equal to unity [79], the temperature can be related to the mixture fraction by

$$T(\xi) = \begin{cases} T_u(\xi) + \dfrac{Qw_{F,1}}{c_p \nu_F W_F}\xi, & \text{if } \xi \leq \xi_{st}, \\ T_u(\xi) + \dfrac{Qw_{O_x,2}}{c_p \nu_{O_x} W_{O_x}}(1-\xi), & \text{if } \xi \geq \xi_{st}. \end{cases} \tag{2.49}$$

Neglecting heat losses (adiabatic flame temperature), the maximumm temperature for a non-premixed flame happens in $\xi = \xi_{st}$ and it is obtained by [83]

$$T_{ad} = \frac{1}{1+\phi}\left(T_1 + T_2\phi + \frac{Qw_{F,u}}{c_p}\right) \tag{2.50}$$

If the fuel considered is a hydrocarbon, C_mH_n, or an alcoohol, $C_mH_nO_p$, the main products of combustion, CO_2 and H_2O can also be related to the mixture fraction through [78]

$$\begin{aligned} w_{CO_2,b} &= w_{F,1} m \frac{W_{CO_2}}{W_F} \xi \\ w_{H_2O,b} &= w_{F,1} \frac{n}{2} \frac{W_{H_2O}}{W_F} \xi \end{aligned} \qquad \text{if } \xi \leq \xi_{St} \tag{2.51}$$

$$\begin{aligned} w_{CO_2,b} &= w_{F,1} \xi_{st} m \frac{W_{CO_2}}{W_F} \left(\frac{1-\xi}{1-\xi_{st}} \right) \\ w_{H_2O,b} &= w_{F,1} \xi_{st} \frac{n}{2} \frac{W_{H_2O}}{W_F} \xi \left(\frac{1-\xi}{1-\xi_{st}} \right) \end{aligned} \qquad \text{if } \xi \geq \xi_{St} \tag{2.52}$$

Figure 2.6 shows the Burke-Schumann solution for mass fractions of fuel, oxidant and species obtained using the above relations, based on the following global reaction of ethanol oxidation

$$C_2H_5OH + 3O_2 \quad \rightarrow \quad 2CO_2 + 3H_2O \tag{2.53}$$

The concept of mixture fraction is defined to systems with two streams, one for the fuel and another for the oxidant. For systems with more than two streams in the combustion zone, several mixture fractions must be defined [42]. In this case, the complexity will turn the mixture fraction approach less interesting for non-premixed flames, and an approach based on mass fractions of the elements can be adopted.

Situations where the Damköhler number is not high enough implicate that the diffusion characteristic time is not very large compared to the chemical characteristic time. Therefore, the fast chemistry hypothesis is not valid and the effects of non-equilibrium should be taken in account. Besides, in real flames, fuel and oxidant don't react in a single global step, and the effects of dissociation should also be considered, as the diffusivity for species and temperature, which are different and lead to discrepant diffusive effects.

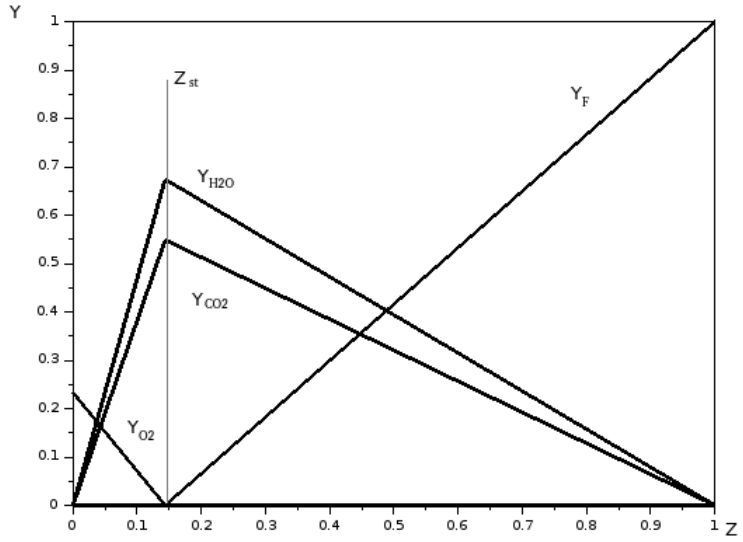

Figure 2.6: Mass fractions of fuel, oxidant and main products of combustion for a non-premixed flame of ethanol (C_2H_5OH), obtained using the Burke-Schumann solution. The initial mass fractions are $w_{F,1} = 1$ and $w_{O_x,2} = 0.233$.

2.4 The counterflow configuration

The counterflow non-premixed flame is the simplest configuration of a steady one-dimensional non-premixed flame, and is often used in experiments and numerical studies [19]. Theoretically, the understanding of a two dimensional non-premixed flame can be done considering that the convection is reduced to one spatial dimension [120]. Figure 2.7 shows the common configuration of a counterflow flame. This type of flame will form the basis for the flamelet concept and is used as initial profile for the REDIM method (discussed in chapter 4).

A laminar flow leaves the fuel duct and stagnates against the flow leaving from the oxidizer duct. The description is, thus, to the flow properties at the stagnation stream line (denoted as a stagnation plane in Fig. 2.7) Using the boundary layer approximation of Prandtl [92], in which the diffusion in the direction or-

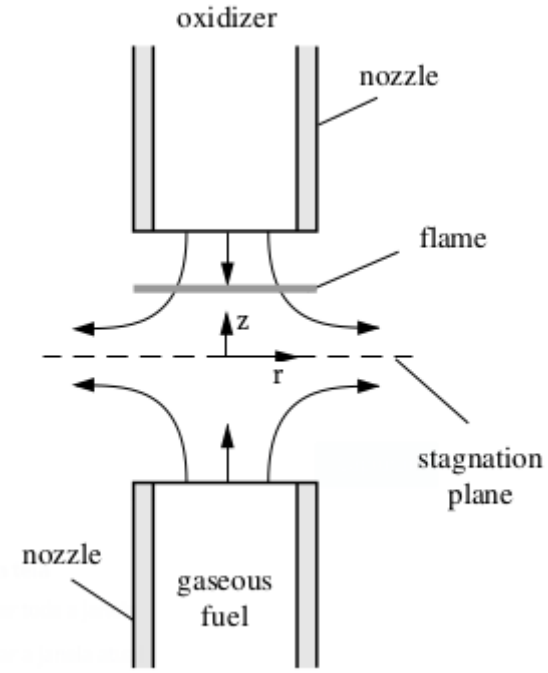

Figure 2.7: Structure of a counterflow flame, adapted from [79].

thogonal to the stream line (i.e., in this case, the r-direction) is neglected. Therefore, the problem reduces to one spatial coordinate, where the gradients in the r-direction of the temperature and mass fractions can be eliminated, so as the velocity in that direction.

One main characteristic of counterflow flames is that the flow velocity along the center line near the stagnation region varies linearly with distance [46]. Thus, the flow can be characterized by a single parameter, namely its velocity gradient a, which constitute the local strain rate. The inverse of the strain rate a represents the characteristic flow time, yielding the Damköhler number, together with the characteristic reaction time.

The strain rate can be used to perturb the counterflow flame. The higher a is chosen, more the flame structure is perturbed by transport processes and its structure changes [25]. An extinguished flame can be obtained by enhancing the

strain rate in one side of the burner so that the reaction zone move towards the wall, losing heat for it and consequently quenching.

The configuration of a counterflow flame yields hypothesis that can be used to simplify the system of equations. These hypothesis are [97, 120]

1. the temperature, the mass fractions of species and the density are all functions of the coordinate z, i.e.,

$$\frac{\partial T}{\partial r} = \frac{\partial w_i}{\partial r} = \frac{\partial \rho}{\partial r} = 0; \tag{2.54}$$

2. the normal component of velocity v_z is a function of z, i.e.,

$$\frac{\partial v_z}{\partial r} = 0; \tag{2.55}$$

3. the tangential velocity component v_r is proportional to the coordinate tangential to the flame r and therefore its gradient is a function only of z, i.e.,

$$\frac{\partial v_r}{\partial r} = \frac{v_r}{r} = G(z,t); \tag{2.56}$$

4. the solutions are considered along the z-axis, that is, for $r = 0$. The first derivative of the density in the r direction vanishes

$$\left.\frac{\partial \rho}{\partial r}\right|_{r=0} = 0. \tag{2.57}$$

The governing system for the counterflow flames comes from the axisymmetric stagnation-flow equations, these derived from the three-dimensional cylindrical Navier-Stokes equations, but considering flow only in the $z - r$ plane. Those

reads [36, 125]

$$\frac{\partial \rho}{\partial t} + \frac{1}{r}\frac{\partial}{\partial r}(\rho r v_r) + \frac{\partial}{\partial z}(\rho v_z) = 0 \tag{2.58}$$

$$\begin{aligned}\rho\frac{\partial v_z}{\partial t} + \rho v_z\frac{\partial v_z}{\partial z} + \rho v_r\frac{\partial v_z}{\partial r} &= -\frac{\partial P}{\partial z} + \frac{\partial}{\partial z}\left[2\mu\frac{\partial v_z}{\partial z} + \kappa\nabla\cdot\mathbf{V}\right] \\ &+ \frac{1}{r}\frac{\partial}{\partial r}\left[\mu r\left(\frac{\partial v_r}{\partial z}\frac{\partial v_z}{\partial r}\right)\right]\end{aligned} \tag{2.59}$$

$$\begin{aligned}\rho\frac{\partial v_r}{\partial t} + \rho v_z\frac{\partial v_r}{\partial z} + \rho v_r\frac{\partial v_r}{\partial r} &= -\frac{\partial P}{\partial r} + \frac{\partial}{\partial z}\left[\mu\left(\frac{\partial v_r}{\partial z} + \frac{\partial v_z}{\partial r}\right)\right] \\ &+ \frac{\partial}{\partial r}\left[2\mu\frac{\partial v_r}{\partial r} + \kappa\nabla\cdot\mathbf{V}\right],\end{aligned} \tag{2.60}$$

corresponding to the continuity, the axial and radial momentum equations, respectively. Here, t is time, r the radial component, z the axial component, ρ is the density, v_r and v_z the radial and axial velocities, respectively, with $\mathbf{V}$ the vector of velocity, P the pressure and μ and κ the dynamic and bulk viscosities, respectively, which by the Stokes hypothesis are related by $\kappa = -2\mu/3$.

The velocity field is presumed to be described in terms of a stream function that has the form

$$\Psi(z, r) = r^2\mathbf{F}(z), \tag{2.61}$$

where $\mathbf{F}(z)$ is an undefined function of z. This function is derived as to satisfy the steady-state continuity equation and thus,

$$\frac{\partial \Psi}{\partial r} = -r\rho v_z \quad \text{and} \quad \frac{\partial \Psi}{\partial z} = r\rho v_r. \tag{2.62}$$

Calculating the derivatives, we have [37]

$$\frac{\partial \Psi}{\partial r} = 2r\mathbf{F} + \underbrace{\frac{\partial \mathbf{F}}{\partial r}}_{=0} r^2 = 2r\mathbf{F} \tag{2.63}$$

$$\frac{\partial \Psi}{\partial z} = r^2\frac{\partial \mathbf{F}}{\partial z} + \underbrace{\frac{\partial r^2}{\partial z}}_{=0}\mathbf{F} = r^2\frac{\partial \mathbf{F}}{\partial z}. \tag{2.64}$$

So,

$$2r\mathbf{F} = -r\rho v_z \quad \text{and} \quad r^2\frac{\partial \mathbf{F}}{\partial z} = r\rho v_r \tag{2.65}$$

The stream function has the physical meaning that the fluid flows at stream lines, which are lines of constant stream functions. Thus, by definition, flow cannot cross stream lines, and the mass flow rate between any two stream lines must be constant [36].

From (2.65), the following relations for the derivatives of v_z and v_r are obtained

$$v_z = -\frac{2\mathbf{F}}{\rho} \quad \Rightarrow \quad \begin{cases} \dfrac{\partial v_z}{\partial z} = \dfrac{\partial}{\partial z}\left(-\dfrac{2\mathbf{F}}{\rho}\right) = -2\dfrac{\partial}{\partial z}\left(\dfrac{\mathbf{F}}{\rho}\right) \\ \dfrac{\partial v_z}{\partial r} = \dfrac{\partial}{\partial r}\left(-\dfrac{2\mathbf{F}}{\rho}\right) = 0 \end{cases} \tag{2.66}$$

$$v_r = \frac{r}{\rho}\frac{\partial \mathbf{F}}{\partial z} \quad \Rightarrow \quad \begin{cases} \dfrac{\partial v_r}{\partial z} = \dfrac{\partial}{\partial z}\left(\dfrac{r}{\rho}\dfrac{\partial \mathbf{F}}{\partial z}\right) = r\dfrac{\partial}{\partial z}\left(\dfrac{1}{\rho}\dfrac{\partial \mathbf{F}}{\partial z}\right) \\ \dfrac{\partial v_r}{\partial r} = \dfrac{\partial}{\partial r}\left(\dfrac{r}{\rho}\dfrac{\partial \mathbf{F}}{\partial z}\right) = \left(\dfrac{1}{\rho}\dfrac{\partial \mathbf{F}}{\partial z}\right) \end{cases} \tag{2.67}$$

Remembering that ρ is a function only of z, so it remains in the derivatives of z. The divergence appearing in the axial and radial momentum equations then can be written as

$$\begin{aligned} \nabla \cdot \mathbf{V} &= \frac{\partial v_z}{\partial z} + \frac{\partial v_r}{\partial r} + \frac{v_r}{r} \\ &= -2\frac{\partial}{\partial z}\left(\frac{\mathbf{F}}{\rho}\right) + \left(\frac{1}{\rho}\frac{\partial \mathbf{F}}{\partial z}\right) + \frac{\rho}{\rho}\frac{1}{r}\frac{r}{\rho}\frac{\partial \mathbf{F}}{\partial z} \\ &= 2\left[-\frac{\partial}{\partial z}\left(\frac{\mathbf{F}}{\rho}\right) + \frac{1}{\rho}\frac{\partial \mathbf{F}}{\partial z}\right] \end{aligned} \tag{2.68}$$

With the hypothesis that $\partial v_r/\partial r$ is a function G that depends only of z, one can rearrange the continuity equation (2.58) as

$$\begin{aligned} \frac{\partial \rho}{\partial t} + \frac{1}{r}\frac{\partial}{\partial r}(\rho r v_r) + \frac{\partial}{\partial z}(\rho v_z) &= \frac{\partial \rho}{\partial t} + \frac{\rho}{r}\left(v_r + r\frac{\partial v_r}{\partial r}\right) + \frac{\partial}{\partial z}(\rho v_z) \\ &= \frac{\partial \rho}{\partial t} + \frac{\rho}{r}\left(v_r + rG\right) + \frac{\partial}{\partial z}(\rho v_z) \\ &= \frac{\partial \rho}{\partial t} + \frac{\rho}{r}\frac{r}{\rho}\frac{\partial \mathbf{F}}{\partial z} + \rho G + \frac{\partial}{\partial z}(\rho v_z) \\ &= \frac{\partial \rho}{\partial t} + \rho G + \rho G + \frac{\partial}{\partial z}(\rho v_z), \end{aligned} \tag{2.69}$$

that is,

$$\frac{\partial \rho}{\partial t} + 2\rho G + \frac{\partial}{\partial z}(\rho v_z) = 0 \tag{2.70}$$

Substituting relations (2.67), (2.67) and (2.68) in the axial momentum equation (2.59), one obtains

$$\begin{aligned}\rho\frac{\partial v_z}{\partial t} + 4\mathbf{F}\frac{\partial}{\partial z}\left(\frac{\mathbf{F}}{\rho}\right) + r\frac{\partial \mathbf{F}}{\partial z}\underbrace{\frac{\partial v_z}{\partial r}}_{=0} &= -\frac{\partial P}{\partial z} + \frac{\partial}{\partial z}\left[2\mu\left(-2\frac{\partial}{\partial z}\left(\frac{\mathbf{F}}{\rho}\right)\right) - \right. \\ \left. -\frac{4}{3}\mu\left(-\frac{\partial}{\partial z}\left(\frac{\mathbf{F}}{\rho}\right) + \frac{1}{\rho}\frac{\partial \mathbf{F}}{\partial z}\right)\right] &+ \frac{1}{r}\frac{\partial}{\partial r}\left[\mu r\left(r\frac{\partial}{\partial z}\left(\frac{1}{\rho}\frac{\mathbf{F}}{\partial z}\right)\right)\underbrace{\frac{\partial v_z}{\partial r}}_{=0}\right],\end{aligned} \tag{2.71}$$

which, divided by the density, yields,

$$\frac{\partial v_z}{\partial t} + \frac{4\mathbf{F}}{\rho}\frac{\partial}{\partial z}\left(\frac{\mathbf{F}}{\rho}\right) = -\frac{1}{\rho}\frac{\partial P}{\partial z} - \frac{4}{3\rho}\frac{\partial}{\partial z}\left[2\mu\frac{\partial}{\partial z}\left(\frac{\mathbf{F}}{\rho}\right) + \frac{\mu}{\rho}\frac{\partial \mathbf{F}}{\partial z}\right] + \frac{2\mu}{\rho^2}\frac{\partial \mathbf{F}}{\partial z}. \tag{2.72}$$

For the radial momentum equation (2.60), one have

$$\begin{aligned}\rho\frac{\partial v_r}{\partial t} - 2r\mathbf{F}\frac{\partial}{\partial z}\left(\frac{1}{\rho}\frac{\partial \mathbf{F}}{\partial z}\right) + \frac{r}{\rho}\left(\frac{\partial \mathbf{F}}{\partial z}\right)^2 &= -\frac{\partial P}{\partial r} + \frac{\partial}{\partial z}\left[\mu\left(r\frac{\partial}{\partial z}\left(\frac{1}{\rho}\frac{\partial \mathbf{F}}{\partial z}\right)\right)\right] + \\ &+\frac{\partial}{\partial r}\left[\frac{2\mu}{\rho}\frac{\partial \mathbf{F}}{\partial z} - \frac{2\mu}{3}\left(2\left(-\frac{\partial}{\partial z}\left(\frac{\mathbf{F}}{\rho}\right) + \frac{1}{\rho}\frac{\partial \mathbf{F}}{\partial z}\right)\right)\right]\end{aligned} \tag{2.73}$$

Observe that the terms inside the brackets in the second line of the above equation depends only on z, so its derivative with respect to r vanishes. Furthermore, dividing by ρ and r, the equation yields,

$$\frac{1}{r}\frac{\partial v_r}{\partial t} - \frac{2\mathbf{F}}{\rho}\frac{\partial}{\partial z}\left(\frac{1}{\rho}\frac{\partial \mathbf{F}}{\partial z}\right) + \frac{1}{\rho^2}\left(\frac{\partial \mathbf{F}}{\partial z}\right)^2 = \frac{1}{r\rho}\frac{\partial P}{\partial r} + \frac{1}{\rho}\frac{\partial}{\partial z}\left[\mu\frac{\partial}{\partial z}\left(\frac{1}{\rho}\frac{\partial \mathbf{F}}{\partial z}\right)\right]. \tag{2.74}$$

The goal now is to eliminate the undefined function $\mathbf{F}$. Using the hypothesis that $\partial v_r/\partial r = G(z, r)$ and (2.67), the following relation is valid

$$\rho G = \frac{\partial \mathbf{F}}{\partial z} \tag{2.75}$$

Substituting in Eq. (2.72),

$$\frac{\partial v_z}{\partial t} + \frac{4\mathbf{F}}{\rho}\frac{\partial}{\partial z}\left(\frac{\mathbf{F}}{\rho}\right) = -\frac{1}{\rho}\frac{\partial P}{\partial z} - \frac{4}{3\rho}\frac{\partial}{\partial z}\left[2\mu\frac{\partial}{\partial z}\left(\frac{\mathbf{F}}{\rho}\right) + \frac{\mu}{\rho}\rho G\right] + \frac{2\mu}{\rho^2}\rho G, \tag{2.76}$$

i.e.,

$$\frac{\partial v_z}{\partial t} + \frac{4\mathbf{F}}{\rho}\frac{\partial}{\partial z}\left(\frac{\mathbf{F}}{\rho}\right) = -\frac{1}{\rho}\frac{\partial P}{\partial z} - \frac{4}{3\rho}\frac{\partial}{\partial z}\left[2\mu\frac{\partial}{\partial z}\left(\frac{\mathbf{F}}{\rho}\right) + \mu G\right] + \frac{2\mu}{\rho}G, \quad (2.77)$$

and for Eq. (2.74),

$$\frac{1}{r}\frac{\partial v_r}{\partial t} - \frac{2\mathbf{F}}{\rho}\frac{\partial}{\partial z}G + \frac{1}{\rho^2}(\rho G)^2 = -\frac{1}{r\rho}\frac{\partial P}{\partial r} + \frac{1}{\rho}\frac{\partial}{\partial z}\left[\mu\frac{\partial}{\partial z}G\right]. \quad (2.78)$$

i.e.,

$$\frac{1}{r}\frac{\partial v_r}{\partial t} - \frac{2\mathbf{F}}{\rho}\frac{\partial}{\partial z}G + G^2 = -\frac{1}{r\rho}\frac{\partial P}{\partial r} + \frac{1}{\rho}\frac{\partial}{\partial z}\left[\mu\frac{\partial}{\partial z}G\right]. \quad (2.79)$$

Isolating the pressure term in equations (2.77) and (2.79), it becomes clear that both $\partial P/\partial z$ and $1/r\partial P/\partial r$ are functions of z alone. Thus, calculating the derivative of $1/r\partial P/\partial r$ with respect to z, the result is a function of z only, that is,

$$\frac{\partial}{\partial z}\left(\frac{1}{r}\frac{\partial P}{\partial r}\right) = w(z). \quad (2.80)$$

However, using the Schwarz's Theorem to change the order of differentiation, one obtains that

$$\frac{\partial}{\partial z}\left(\frac{1}{r}\frac{\partial P}{\partial r}\right) = \frac{1}{r}\frac{\partial}{\partial r}\left(\frac{\partial P}{\partial z}\right) = 0, \quad (2.81)$$

since, as stated, $\partial P/\partial z$ is functions of z only. This is possible since, by hypothesis, the pressure has continuous second derivatives, fulfilling the Schwarz's Theorem hypothesis. Therefore, it must be the case that $1/r\partial P/\partial r$ is a constant, defined as J [97],

$$\frac{1}{r}\frac{\partial P}{\partial r} = J \quad (2.82)$$

throughout the flow field that varies with time. So, Eq. (2.79) becomes

$$\frac{1}{r}\frac{\partial v_r}{\partial t} - \frac{2\mathbf{F}}{\rho}\frac{\partial}{\partial z}G + G^2 = -\frac{J}{\rho} + \frac{1}{\rho}\frac{\partial}{\partial z}\left[\mu\frac{\partial}{\partial z}G\right]. \quad (2.83)$$

Using that $v_r/r = G$ and that $-\mathbf{F} = (\rho v_z)/2$ (see (2.67)), the final form of the radial momentum equations is

$$\frac{\partial G}{\partial t} + v_z\frac{\partial G}{\partial z} + G^2 - \frac{J}{\rho} + \frac{1}{\rho}\frac{\partial}{\partial z}\left[\mu\frac{\partial}{\partial z}G\right] = 0, \tag{2.84}$$

and for the axial momentum equation,

$$\frac{\partial v_z}{\partial t} + \frac{1}{\rho}\frac{\partial P}{\partial z} + v_z\frac{\partial v_z}{\partial z} - \frac{4}{3\rho}\frac{\partial}{\partial z}\left[\mu\frac{\partial v_z}{\partial z}\right] + \frac{4}{3\rho}\frac{\partial}{\partial z}(\mu G) - \frac{2\mu}{\rho}\frac{\partial G}{\partial z} = 0. \tag{2.85}$$

The cylindrical energy and species mass fraction equations are given by [36], respectively

$$\begin{aligned}\rho c_p\left(\frac{\partial T}{\partial t} + v_z\frac{\partial T}{\partial z} + v_r\frac{\partial T}{\partial r}\right) &= \left(\frac{\partial P}{\partial t} + v_z\frac{\partial P}{\partial z} + v_r\frac{\partial P}{\partial r}\right) + \frac{\partial}{\partial z}\left(\lambda\frac{\partial T}{\partial z}\right) + \\ &+\frac{1}{r}\frac{\partial}{\partial r}\left(r\lambda\frac{\partial T}{\partial r}\right) - \sum_{i=1}^{n_{sp}} c_{p,i}\left(j_{i,z}\frac{\partial T}{\partial z} + j_{i,r}\frac{\partial T}{\partial r}\right) - \sum_{i=1}^{n_{sp}}\dot{\omega}_i h_i W_i,\end{aligned} \tag{2.86}$$

and

$$\rho\frac{\partial w_i}{\partial t} + \rho v_z\frac{\partial w_i}{\partial z} + \rho v_r\frac{\partial w_i}{\partial r} = -\left(\frac{\partial j_{i,z}}{\partial z} + \frac{\partial j_{i,r}}{\partial r}\right) + \dot{\omega}_i W_i. \tag{2.87}$$

where T is the temperature, w_i the mass fraction of species i, c_p is the specific heat at constant pressure, λ the thermal conductivity, $j_{i,z}$ and $j_{i,r}$ the diffusions fluxes in z and r directions, respectively, of species i, $\dot{\omega}_i$ is the production/consumption source term of species i, h_i the enthalpy of species i and W_i the molar mass of species i.

Using the hypothesis that temperature and mass fractions are functions only of z, so well as the pressure (deduced above), equations (2.86) and (2.87) turns to

$$\rho c_p\left(\frac{\partial T}{\partial t} + v_z\frac{\partial T}{\partial z}\right) = \left(\frac{\partial P}{\partial t}\right) + \frac{\partial}{\partial z}\left(\lambda\frac{\partial T}{\partial z}\right) - \sum_{i=1}^{n_{sp}} c_{p,i}j_{i,z}\frac{\partial T}{\partial z} - \sum_{i=1}^{n_{sp}}\dot{\omega}_i h_i W_i, \tag{2.88}$$

and

$$\rho\frac{\partial w_i}{\partial t} + \rho v_z\frac{\partial w_i}{\partial z} = -\frac{\partial j_{i,z}}{\partial z} + \dot{\omega}_i W_i. \tag{2.89}$$

Therefore, the governing system for a counterflow diffusion flame, composed by the continuity, momentum, temperature and species mass fractions equations, is summarized as

$$\frac{\partial \rho}{\partial t} + 2\rho G + \frac{\partial}{\partial z}(\rho v_z) = 0; \tag{2.90}$$

$$\frac{\partial v_z}{\partial t} + \frac{1}{\rho}\frac{\partial P}{\partial z} + v_z\frac{\partial v_z}{\partial z} - \frac{4}{3\rho}\frac{\partial}{\partial z}\left[\mu\frac{\partial v_z}{\partial z}\right] + \frac{4}{3\rho}\frac{\partial}{\partial z}(\mu G) - \frac{2\mu}{\rho}\frac{\partial G}{\partial z} = 0, \tag{2.91}$$

$$\frac{\partial G}{\partial t} + v_z\frac{\partial G}{\partial z} + G^2 - \frac{J}{\rho} + \frac{1}{\rho}\frac{\partial}{\partial z}\left[\mu\frac{\partial}{\partial z}G\right] = 0; \tag{2.92}$$

$$\frac{\partial T}{\partial t} + v_z\frac{\partial T}{\partial z} - \frac{1}{\rho}\frac{\partial P}{\partial t} - \frac{1}{\rho c_p}\frac{\partial}{\partial z}\left(\lambda\frac{\partial T}{\partial z}\right) + \frac{1}{\rho c_p}\sum_{i=1}^{n_{sp}} c_{p,i}j_{i,z}\frac{\partial T}{\partial z} + \frac{1}{\rho c_p}\sum_{i=1}^{n_{sp}}\dot{\omega}_i h_i W_i = 0; \tag{2.93}$$

$$\frac{\partial w_i}{\partial t} + v_z\frac{\partial w_i}{\partial z} + \frac{1}{\rho}\frac{\partial j_{i,z}}{\partial z} - \frac{1}{\rho}\dot{\omega}_i W_i = 0, \tag{2.94}$$

with the diffusion fluxes given by [97]

$$j_{i,z} = -\left(\rho D_i^F\frac{w_i}{X_i}\frac{\partial X_i}{\partial z} + \frac{D_i^T}{T}\frac{\partial T}{\partial z}\right), \tag{2.95}$$

where D_i^F and D_i^T is the mass and thermal diffusivity. The system is closed with the equation of state

$$\rho - \frac{PW}{RT} = 0 \tag{2.96}$$

The pressure gradient in the radial direction can be related with the strain rate a by [79]

$$J = -\rho a^2. \tag{2.97}$$

The system is completed with initial and boundary conditions for all the dependent variables and, so, J is an eigenvalue of the system, i.e., for such boundary conditions, J has to adapt so the system has solution [120].

Generally, the velocity profile along the axis has the shape presented in Fig. 2.8. In a non-reactive flow, the velocity is characterized by a transition of the

velocities from the boundaries. Nevertheless, with reacting flow, in the combustion zone, the high temperature of the burnt gas leads to high density changes. Thus, as the velocity is defined by the mass flux ($\dot{m} = \rho v$), the monotonic behaviour of the velocity is lost and a deviation is observed.

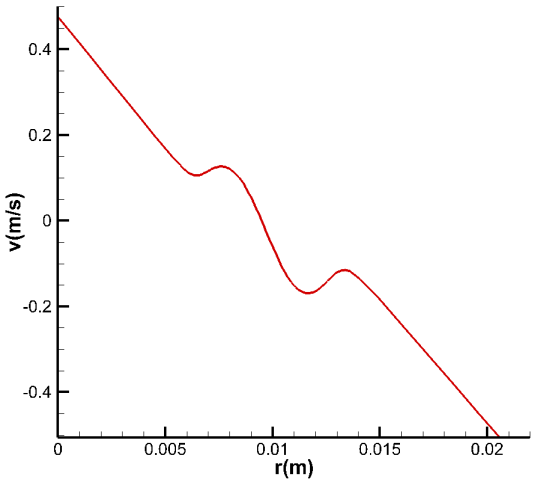

Figure 2.8: Velocity profile of a counterflow non-premixed methane/air flame. The fuel side is fed with 25% CH_4, 75% Air, $T = 294K$, and oxidizer side with 21% O_2, 79% N_2, $T = 291K$.

It is possible to derive analytical solutions for counterflow non-premixed flames, as shown in [46, 79]. The idea, which will provide the basis for the flamelet concept, is to introduce a transformation from the physical space to a mixture fraction space. This transformation reads

$$\frac{\partial}{\partial z} = \frac{\partial \xi}{\partial z}\frac{\partial}{\partial z}. \tag{2.98}$$

Thus, the equations for mass fractions and temperature will be projected in this mixture fraction space. Together with appropriate boundary conditions, one can derive an analytical solution for the mixture fraction by similarity, given by [79]

$$\xi = \frac{1}{2}\mathrm{erfc}\left(\frac{\eta}{\sqrt{2}}\right), \tag{2.99}$$

where η is a non-dimensional coordinate.

2.5 Chemical kinetics reduction

Chemical kinetic modeling became an important tool for interpretation and understanding of the combustion phenomena. The kinetic mechanisms developed for the simulation of flames are focused in a wide range of applications, for low and high temperatures, pressure, initial concentration, among others. To correct describe all these details, thousand of chemical reactions are necessary [74], enhancing considerably the computational cost. Besides, numerical simulations involving detailed kinetic mechanism are complicated due to the existence of highly reactive radicals, which induces significant stiffness to the governing equations due to the huge difference in the time scales of species [57]. Consequently, there exists the need to develop from these detailed mechanisms corresponding reduced mechanism of fewer variables and moderate stiffness, while maintaining the accuracy and comprehensiveness of the detailed mechanism.

In order to simplify the numerical treatment of the chemical kinetics, many methods have been devised, such as the assumption of an infinite reaction rate (mixed is equal to burnt) or one-step chemistry [32]. The first reduced mechanism, for premixed and non-premixed flames of methane, were obtained and published in the mid-1980s and, shortly after, they were used for numerical and asymptotic analysis. Also in this time, several research groups focused their attention in the development of useful techniques for mechanism reduction of short chain fuels [80]. It was verified that kinetic models for hydrocarbons have a hierarchic logic, where the mechanism of the largest chain fuel contains, as a subset, the mechanism for smaller molecules. This comprehension helped to reduce the time and effort required to develop mechanisms for bigger molecules. Figure 2.9 shows this hierarchy for aliphatic hydrocarbons.

In order to reduce a mechanism, the first step is to identify for which application this will be used. For instance, a mechanism developed for analysis

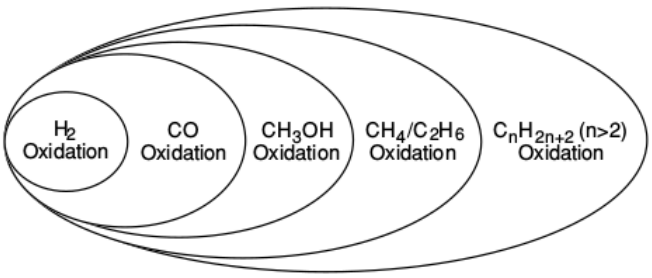

Figure 2.9: Hierarchy of the kinetic mechanisms describing aliphatic hydrocarbons (without aromatic rings).

of equilibrium compositions may not generates satisfactory results if the goal is to investigate pollutant formation, ignition or extinction, adiabatic flame temperature or even flame speed. The second step is to identify species and reactions which are mandatory to describe efficiently the models characteristics [108]. Turányi [102] claims that there are three types of species in a mechanism:

1. Important species (or targets) are those whose precise reproduction of the concentration profiles follows directly from the aim of the investigation. This decision depends on the objective of the modelling.

2. Necessary species (or intermediary) are those for which realistic compositions are necessary to describe accurately the concentrations of the important species.

3. Redundant species are those that can be omitted from the mechanism without significant consequences for the desired calculation.

In this context, there are two main categories of reduction techniques for kinetic mechanisms: time scale analysis and the generation of skeletal mechanisms [58]. The latter consist in identify the important and necessary species and generates the mechanism only with these. Some examples are the directed relation graph (DRG) and directed relation graph with error propagation (DRGEP), sensitivity analysis based on Jacobian analysis and even artificial neural networks (ANN).

Time scale analysis is used primarily to identify a gap in species trajectory on the composition state space, so that the system dynamics can be described using only the slow time scales. Examples are the Quasi-Steady-State Assumption (QSSA), Partial Equilibrium (PE), Intrinsic Low-Dimensional Manifolds (ILDM), Computational Singular Perturbation (CSP), Flamelet approach and Lumping. Next chapters will provide an explanation of some of these techniques.

3 SKELETAL MECHANISM GENERATION

The first strategy for generating reduced mechanism is the identification of species and reactions that are redundant. This step is called skeletal mechanism generation, which can reduced the number of species in the mechanism by $\frac{1}{3}$ or $\frac{2}{3}$.

The modelling of chemical kinetics must consider the accurate description of concentrations profiles of the important species (that can be defined according to the objective of the model) and/or important characteristics (such as, for instance, ignition time and flame speed). For such purpose, necessary species should remain in the model, so that the important characteristics of the important species are well described. All other species can be considered redundant, and thus withdraw of the resulting skeletal mechanism. Subsequently, reactions that contribute little to the remaining species are eliminated.

The methods for skeletal reduction can be applied locally, i.e., for specific pressure, temperature and concentration profiles. In this case, the achievement of a good skeletal scheme for a more complex combustion situation depends on the range of conditions to give the reduced model validity in reproducing certain features.

An important consideration to be made is that since most methods depends on the concentration of the species through an specific application, the process should be repeatedly to different configurations, i.e., several states over the trajectory of a species. The ones that are considered redundant to all relevant simulations and conditions are removed from the mechanism.

3.1 Sensitivity analysis

Mathematical models have been used for investigation of complex chemical systems. The results of these models depend considerably on the appropriate selection of elementary steps, such as the kinetic mechanism and initial data [106]. A rigorously ranking of elementary reactions provides a basis for mechanism reduction, i.e., selecting reactions that are not important in a given condition and that can be eliminated of the scheme without significantly loss of information.

The term sensitivity analysis defines a collection of mathematical methods that can be used to explore the relations between the initial parameters values of a model and its solution [104]. In chemical systems, the sensitivity analysis describes the variation of a species concentration in time t_2 when there is a perturbation in the parameters at time t_1 ($t_1 < t_2$) [105]. Sensitivity analysis is a powerfull tool for mechanism reduction, and has been used to develop mechanisms for several fuels, such as the *n*-heptane and *iso*-octane [69, 94], propane [102], methane [96], ciclohexane [50], gasoline surrogates [70] and kerosene [117], *n*-dodecane [26], *n*-butanol [53, 118] and biodiesel surrogates [3, 87].

The kinetic system of ordinary differential equations defines the relation between the production rate of a species and the reaction rates [108]. For an isothermal, spatially homogeneous dynamical system, the concentration change over time can be obtained solving the following initial value problem [102]:

$$\frac{d\mathbf{c}}{dt} = \mathbf{f}(\mathbf{c}, \mathbf{k}), \quad \text{with} \quad \mathbf{c}(0) = \mathbf{c}_0, \tag{3.1}$$

where $\mathbf{c}(t)$ is the concentration vector, t the time and $\mathbf{k}$ the vector for kinetic parameters, such as Arrhenius coefficient, thermodynamic data, pressure, temperature, etc. The most commom variable used as parameter $\mathbf{k}$ is the reaction velocity coefficient [47, 103, 108]. The right hand side of Eq. (3.1) can be obtained, for each species i,

using

$$f_i(\mathbf{c}, \mathbf{k}) \;=\; \sum_{j=1}^{n_r} \nu_{ij} \dot{\omega}_j, \tag{3.2}$$

where $\dot{\omega}_j$ is given by (2.20) and ν_{ij} is the stoichiometric coefficient of species i in reaction j.

Obtaining the derivative with respect to the parameter k_j in both sides of the kinetic system of ODE's (3.1), and using the chain rule, results the following system of equations:

$$\frac{d}{dt}\frac{\partial \mathbf{c}}{\partial k_j} \;=\; \frac{\partial \mathbf{f}}{\partial \mathbf{c}}\frac{\partial \mathbf{c}}{\partial k_j} + \frac{\partial \mathbf{f}}{\partial k_j}, \qquad j = 1, 2, \ldots, n_r, \tag{3.3}$$

with initial conditions $\dfrac{\partial \mathbf{c}}{\partial k_j}(t_0) = 0$. The matrix form of this system is

$$\frac{d\mathbf{S}}{dt} \;=\; \mathbf{JS} + \mathbf{F}, \tag{3.4}$$

where

$$\mathbf{F} = \frac{\partial \mathbf{f}}{\partial \mathbf{k}} = \begin{bmatrix} \frac{\partial f_1}{\partial k_1} & \cdots & \frac{\partial f_1}{\partial k_n} \\ \vdots & \ddots & \vdots \\ \frac{\partial f_n}{\partial k_1} & \cdots & \frac{\partial f_n}{\partial k_n} \end{bmatrix}, \tag{3.5}$$

is the rate sensitivity matrix,

$$\mathbf{S} = \frac{\partial \mathbf{c}}{\partial \mathbf{k}} = \begin{bmatrix} \frac{\partial c_1}{\partial k_1} & \cdots & \frac{\partial c_1}{\partial k_n} \\ \vdots & \ddots & \vdots \\ \frac{\partial c_n}{\partial k_1} & \cdots & \frac{\partial c_n}{\partial k_n} \end{bmatrix}, \tag{3.6}$$

is the sensitivity matrix of the system, in which each element represents the change of concentration c_i of species i in time t_2, when there is a perturbation in the parameter k_j in time t_1 ($t_2 > t_1$), and

$$\mathbf{J} = \frac{\partial \mathbf{f}}{\partial \mathbf{c}} = \begin{bmatrix} \frac{\partial f_1}{\partial c_1} & \cdots & \frac{\partial f_1}{\partial c_n} \\ \vdots & \ddots & \vdots \\ \frac{\partial f_n}{\partial c_1} & \cdots & \frac{\partial f_n}{\partial c_n} \end{bmatrix} \tag{3.7}$$

is the Jacobian matrix.

The sensitivity coefficients $\partial c_i/\partial k_j$ are of limited applicability in its original form [104]. The parameters and various quantities of a model may have different units and, in this case, the elements of sensitivity matrix are incomparable. To overcome this problem, one introduce the normalized sensitivity coefficients, which form the normalized sensitivity matrix, given by

$$\tilde{\mathbf{S}} \;=\; \left(\frac{k_j}{c_i}\frac{\partial c_i}{\partial k_j}\right) \;=\; \left(\frac{\partial \ln c_i}{\partial \ln k_j}\right). \tag{3.8}$$

The normalized sensitivity matrix exhibits how solutions c_i change as consequence of the change in the values k_j, keeping the other parameters fixed [100]. The normalized form of matrix $\mathbf{F}$ is given by

$$\tilde{\mathbf{F}} \;=\; \frac{k_j}{f_i}\frac{\partial f_i}{\partial k_j}. \tag{3.9}$$

Observe that, for $i = 1$,

$$f_1 \;=\; \sum_{j=1}^{n_r} \nu_{1j}\dot{\omega}_j \;=\; \nu_{11}\dot{\omega}_1 + \nu_{12}\dot{\omega}_2 + \cdots + \nu_{1j}\dot{\omega}_j + \cdots + \nu_{1n_r}\dot{\omega}_{n_r}. \tag{3.10}$$

Calculating the derivative of expression (3.10) with respect to the parameter k_j, only the terms with the j-th reaction rate remains. Thus, for all i, it holds that

$$\frac{\partial f_i}{\partial k_j} \;=\; \nu_{ij}\dot{\omega}_j, \qquad j = 1, \ldots, n_r. \tag{3.11}$$

So, the normalized matrix $\tilde{\mathbf{F}}$ can be calculated as

$$\tilde{\mathbf{F}} \;=\; \frac{\nu_{ij}\dot{\omega}_j}{f_i}, \qquad j = 1, \ldots, n_r. \tag{3.12}$$

Matrix $\tilde{\mathbf{F}}$ represents the connection between the sensitivity analysis of the concentrations and the production rates [103]. One element of $\tilde{\mathbf{F}}$ is the ratio among the molar rate of consumption/production of species i in reaction j and the net change in the concentration of species i.

The investigation and reduction of a complex kinetic mechanism can be performed efficiently via analysis of matrices **F**, **J** and **S**. The methods that calculate these matrices have the characteristic of considering each species equally important and, therefore, redundant species may appear in the reduced mechanism [102]. Thus, the first step in a complete mechanism reduction is to identify the redundant species.

3.1.1 Identification of the redundant species

Elimination of redundant species of a mechanism has two benefits [40]: (i) a smaller mechanism is better interpretable from a chemical point of view, (ii): simulation with reduced mechanisms requires less computational time. Two methods are proposed for identifying redundant species [102]:

1. **Method 1:** Identification of redundant species via reduced models.

   A consequence of the kinetic law of mass action is that, if a species has no consuming reactions, change in its concentration has no influence in the concentration of other species. So, a species is considered redundant if eliminating all its consuming reaction does not cause difference in the model's solution.

   However, a species can be redundant even if eliminating its consuming reaction causes significant changes. This happens when a species is formed by a fast reversible reaction and has a low concentration. If all consuming reactions of this species were dropped out, its concentration will increase significantly, which may cause changes in the concentration of important species. Species presenting this behaviour must be reinvestigated through a simultaneous elimination of its fast consuming and formation reactions.

2. **Method 2:** Identification of redundant species via investigation of the Jacobian.

   Change of the species concentrations changes the reaction rates in which these species are reactant. An element of the normalized Jacobian matrix $\tilde{\mathbf{J}}$ indicate the effect of changing a species concentration in the production rate of another. This effect can be calculated through the sum of squares of normalized Jacobian elements

$$B_i = \sum_{j=1}^{N} \left(\frac{\partial \ln f_j}{\partial \ln c_i} \right)^2 \tag{3.13}$$

   which indicates the influence of the change of the concentration of species i on the rate of production of the species group Ω formed by N species.

   The higher the B_i of a specie i considered non-important, the greater is its direct influence on Ω. Nevertheless, there are necessary species that are coupled with important species through other necessary species. Thus, the group Ω should be identified via a iterative process: species whose B_i are greater than a limit are incorporated to Ω, then the index B_i is recalculated and the process is repeated. The redundant species are those who are not included in Ω as the process finishes.

Results of the first method express directly the consequences in eliminating a specie, while the second is less effective, since some redundant species which are formed in fast reversible reactions cannot be identified if they are not connected by fast reactions to necessary species.

3.1.2 Principal component analysis

Principal component analysis (PCA) is one of the most used method of sensitivity analysis for mechanism reduction. It was introduced by Vajda *et al.*

[110, 111], and consists in an analysis of the eigenvalues and eigenvectors of the sensitivity matrix to extract kinetic informations for several species.

Since the sensitivity matrix is not square, $\tilde{S}$ is transformed in a square symmetrical matrix $\tilde{S}^T\tilde{S}$, whose number of columns and rows are equal to the number of reactions in the mechanism. The eigenvalues of $\tilde{S}^T\tilde{S}$, identify groups of parameters, while the eigenvectors provide information about the efficiency of these groups in the change of concentration of species. A parameter (in this case, an elementary reaction) is considered important if belongs to a significant element of an eigenvector associated to a high eigenvalue

The main goal of PCA is to determine the importance of elementary reactions or certain groups of reactions in the complex mechanism [110]. Let $c_i(t,k)$ be the concentration of specie i in time t under influence of parameters k (temperature, pressure, velocity, etc). The effect of change in the reaction coefficients can be calculated using the funcion defined by [111],

$$Q(k) \;=\; \sum_{j=1}^{q}\sum_{i=1}^{n_{sp}}\left[\frac{c_i(t_j,\alpha)-c_i(t_j,\alpha^0)}{c_i(t_j,\alpha^0)}\right], \tag{3.14}$$

where $\alpha_i = \ln k_i$. This function can be approximated using the sensitivity matrix $\tilde{S}$ through

$$Q(k) \approx Q(\alpha) \;=\; (\Delta\alpha)^T\,\tilde{S}^T\tilde{S}\,(\Delta\alpha)\,. \tag{3.15}$$

Diagonalization of $\tilde{S}^T\tilde{S}$ implies that

$$\tilde{S}^T\tilde{S} \;=\; U\Lambda U^T, \tag{3.16}$$

where U denotes the normalized eigenvectors matrix u_k $(k = 1,\ldots,p)$, i.e., $u_k^T u_k = 1$, and Λ is the diagonal matrix formed by the eigenvalues λ_k. A new set of parameters is defined

$$\Psi \;=\; U^T\alpha, \tag{3.17}$$

called principal components. Then, function Q is defined through the principal components as

$$Q(\Psi) = \sum_{k=1}^{p} \lambda_k \Delta \left(\Psi_k\right)^2, \tag{3.18}$$

where $\Delta\Psi = U^T \Delta\alpha$. Principal components corresponding to the highest eigenvalues are the most relevants for the precise description of important species [47].

Lebedev *et al.* [47] developed an algorithm to explain the PCA application. According to this strategy, each principal component has as many elements as there are reactions in the detailed mechanism, with weights varying from 0 to 1. In order to find the most important reactions in each principal component, the weights are compared with a threshold ϵ_{vec} defined for the eigenvector. The standard threshold of the eigenvector is 0.2. A reaction is excluded from the principal component if its weight is less than ϵ_{vec} or maintained if is higher. Each reaction can be included in different principal components. Finally, the components whose eigenvalues are bigger compared to the threshold ϵ_{val} (standard value 1) are considered important and their reactions are retained in the reduced mechanism.

It is possible to apply PCA to matrix $\tilde{\mathbf{F}}$, expressing $\tilde{\mathbf{F}}^T\tilde{\mathbf{F}}$ as function of it eigenvalue and eigenvectors. The reactions that affect the necessary species the most are identified, as the eigenvectors reveal the coupling between reactions and the eigenvalues the weight of the corresponing eigenvector [35]. So, the ideia is to eliminate the reactions with negligible contribution to the production rate of the necessary species, since the reactions with components from the eigenvectors with high values associated with high eigenvalues are the most important reactions of the mechanism [123].

3.1.3 Quasi-stationary sensitivity analysis

The kinetic information derived by conventional sensitivity analysis belongs to a time interval (t_1, t_2), during which characteristics of important reactions may change. The method of quasi-stationary sensitivity analysis [105] is based in an approximation that replaces the differential equations (3.1) by algebraic equations, and in this way simplifying the analysis.

In stationary systems, the sensitivity coefficients can be considered as dynamic quantities governed by the system (3.1). However, species concentrations, as well as the matrices $\mathbf{J}$ and $\mathbf{F}$, are invariant in time, so the left hand side of Eq. (3.4) vanishes. Thus,

$$0 \;=\; \mathbf{JS} + \mathbf{F}. \tag{3.19}$$

The stationary sensitivity matrix is given by

$$\mathbf{S}^s \;=\; -\mathbf{J}^{-1}\mathbf{F}, \tag{3.20}$$

which represents the change of stationary species concentrations to a differential change in parameters [103]. Matrix $\mathbf{S}^s$ carries information from the kinetic mechanism of the equilibrium chemical process. Using Eq. (3.20) demands that the Jacobian $\mathbf{J}$ is invertible. This can be guaranteed if all species have at least one consuming reaction and if none concentration is zero. If $\mathbf{J}$ is not invertible, a possibility is to use the generalized inverse of $\mathbf{J}$.

The quasi-stationary sensitivity analysis method is an approximation, as the quasi-steady state assumption (see Section 4.1.1). Although this approach does not provides precise values of the sensitivity coefficients, studies indicate that the method can provide useful information for a considerable number of reactions in different conditions.

3.2 Directed relation graph - DRG

The directed relation graph (DRG), developed by Lu and Law in 2005 [56], is a reduction method based on the construction of skeletal mechanisms. The aim of the method is to efficiently solve the species coupling, so that those who has little or none influence on the important species can be removed.

The DRG is applied to identify the unimportant species and, thus, remove of the mechanisms the reactions that are not associated with them, using a numerical criteria. This method has a simple implementation, is capable of generating skeletal mechanisms faster than other available techniques and the results can predict the reaction rates of the remaining species with accuracy [56].

A view in the species coupling complexity can be done using the following example: consider species A, that can be related with species B directly in a fast reaction through intermediary species C, even though they are not in the same reaction. In this case, removing a species from the mechanism can induce removal of a group of species associated to it.

The contribution of species B in the production/consumption rate of species A can be quantified through the normalized index r_{AB}, given by

$$r_{AB} = \frac{\sum_{i=1}^{n_r} |\nu_{A,i}\dot{\omega}_i\delta_{B,i}|}{\sum_{i=1}^{n_r} |\nu_{A,i}\dot{\omega}_i|}, \tag{3.21}$$

where $\nu_{A,i}$ is the stoichiometric coefficient of A in reaction i, $\dot{\omega}_i$ is given by (2.20) and $\delta_{B,i}$ is

$$\delta_{B,i} = \begin{cases} 1, & \text{if the } i\text{th elementary reaction involves species B;} \\ 0, & \text{otherwise.} \end{cases} \tag{3.22}$$

The terms in the denominator of Eq. (3.21) are the contribuition of reactions to the production/consumption of species A, and the terms in the numerator are those from the denominator that involve species B [57].

Defining a threshold limit value ϵ ($0 < \epsilon < 1$), and if index r_{AB} is bigger compared to this threshold ($r_{AB} > \epsilon$), then removing species B can induce error in the production of species A, so that species B must be maintained in the skeletal mechanism. Usually, species A are chosen as those who has some desirable chemical attributes that the reduced mechanism should reproduce [76].

Relations among species using DRG can be illustrated in Fig. 3.1. One can observe that species S_1 depends on S_2 and S_3, but both latter does not depend on species S_1 and, if S_1 is an important species, S_2, S_3 and S_8 must be retained, and S_8 should be retained because of its strong coupling with the necessary species S_2 (indicated by the width of the arrow). Through this scheme, it is possible to identify the dependent set of each species, i.e., the set formed by all species whose index r_{AB} is bigger than the threshold ϵ. The final set of species is formed by uniting all dependent sets of the important species, and only the reactions that involve species in this final set are retained in the mechanism.

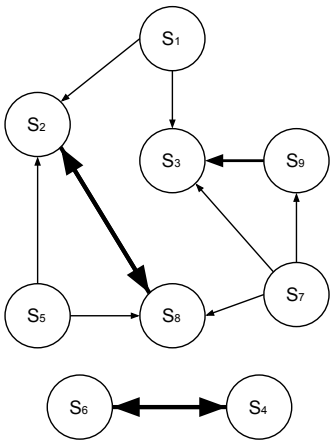

Figure 3.1: DRG method displaying the coupling between species.

A different formulation for the index r_{AB} can be obtained using the maximum over the summation in Eq. (3.21) [54], since that the original formula proved to be unefficient for large number os isomers. According to Lu and Law [58], there is also two alternatives for r_{AB}: the first considering the net rate of production for species A in the denominator of (3.21)

$$r_{AB} = \frac{\sum_{i=1}^{n_r} |\nu_{A,i}\dot{\omega}_i\delta_{B,i}|}{|\dot{\omega}_A|}, \tag{3.23}$$

and the second dealing with the forward and backward coefficients of each reversible reaction as two different reactions, i.e.,

$$r_{AB} = \frac{\sum_{i=1}^{n_r} \left(|\nu_{A,i}\dot{\omega}_{f,i}| + |\nu_{A,i}\dot{\omega}_{b,i}|\right)\delta_{B,i}}{\sum_{i=1}^{n_r} |\nu_{A,i}\dot{\omega}_{f,i}| + \sum_{i=1}^{n_r} |\nu_{A,i}\dot{\omega}_{b,i}|}. \tag{3.24}$$

Xia *et al* [126] considerate $\delta_{B,i}$ equals to 1 only if B is a reactant and in the reaction rate $\dot{\omega}_i$, only forward reactions were accounted.

The resulting skeletal mechanism obtained has errors according to the user-specified threshold ϵ for the conditions under which it is developed [56]. Therefore, mechanisms with different levels of accuracy can be obtained by assigning different values for ϵ. The skeletal mechanism will converge to the detailed as ϵ is approaching zero, and the number of species can vary abruptly as the threshold is varied.

To obtain a mechanism over a sufficiently wide range of parameters, such as pressure, temperature, equivalence ratio and resident time, a group of points in the parametric space are sampled for typical applications, including perfectly stirred reactor and ignition, laminar flame propagation as well as counterflow flames. Consequently, for each application, a skeletal sub-mechanism can be obtained for each point considered, and the union of these consists the application-specific skeletal

mechanism. Finally, the union of those generates an efficient skeletal mechanism that can describe the applications for which was developed over all the parameters.

From a practical point of view, index r_{AB} defines an error estimate in predicting species A if B is neglected. Therefore, consumption and production reactions must be considered equally [76]. However, removing a species that contributes exclusively for the consumption of species A will not have the same effect that removing a species that contributes the same way for the production and consumption of A. In the first case, the error will be bigger than the second, for the error generated by removing the production term is compensated for also removing the associated consumption term.

The biggest advantage in using the DRG is that the reduction is accomplished in a time that is proportional to the number of reactions in the detailed mechanism [57]. In addition, DRG is easy to implement and automate, and has become popular for very huge mechanisms [54].

Among the disadvantages of the method, it is worth pointing out that DRG assumes the same level of importance for all species, without considering kinetic parameters when setting the coupling. For Løvås [54], DRG has some limitations, and so some extensions were developed, as the DRG with error propagation (DRGEP) [76], DRG with expert knowledge (DRGX) [59] and DRG with sensitivity analysis (DRGASA) [128]. In the latter, some characteristics of the original DRG were amended, like analysing the error by important species [67], so that the resulting mechanism is the smallest possible and further elimination of species induce errors above acceptable.

3.3 Methodology for implementing DRG

This section will provide the basic steps that were taken to implement the DRG technique. The computational code was developed in Python, using the open-source software Cantera [30] for the 0D and 1D simulations. Cantera is a suite of object-oriented software tools for problems involving chemical kinetics, thermodynamics, and/or transport processes. It provides types (or classes) of objects representing phases of matter, interfaces between these phases, reaction managers, time-dependent reactor networks, and steady one-dimensional reacting flows. The choice for this software was due to its easy usage and the possibility of using function that facilitate the implementation of DRG.

The DRG algorithm itself is not very complicated. The idea is to calculate index (3.21) to set which species will remain in the skeletal mechanism. Having defined the species, only the reactions happening with those species are retained. Nevertheless, as explained in Section 3.2, it is mandatory to define for which applications and range of parameters the DRG will be used.

The goal of this work is to apply the DRG for ethanol (C_2H_5OH). The detailed mechanism chosen was developed by Marinov, and consists of 57 species among 383 reversible elementary reactions [64]. This mechanism was validated using experimental data from shock tube reactor and flame speed measurements. The applications that will be applied are a batch reactor, with constant volume and internal energy, aiming to catch the ignition time, and a freely propagating premixed flat flame, to catch the flame speed. These situations will be calculated varying initial temperature, pressure and equivalence ratio.

Firstly, the targets species for the DRG was chosen, consisting of the fuel, C_2H_5OH, oxygen, O_2, and the main products of combustion, CO_2 and H_2O. However, it was observed that some species that was important to maintain the path of oxidation from fuel to products was not being retained by DRG, even for small ϵ.

It is the case of C_2H_6 and CH_3CO. Also, C_2H_4, which appears to be produced only in one reaction, so its index will also be very small, was defined as a target species, since its presence is observed to be very important to maintain accuracy. Thus, the final set of target species used for DRG is: C_2H_5OH, O_2, CO_2, H_2O, C_2H_6, CH_3CO and C_2H_4. These species will play the role of A-species in the index (3.21), while the B-species are all species of the detailed mechanism. The threshold value used was $\epsilon = 0.018$. This value was achieved for a simple DRG calculation for stoichiometric mixture in the ideal gas reactor.

The calculation is performed as follows: the detailed mechanism is used to simulate a freely-propagating premixed flat flame in order to find the flame speed. Then, the DRG is applied using the species concentrations and temperature from this flat flame calculations. The species that has its index greater than the threshold is retained in a set, the others are discarded. The next step is to use the detailed mechanism to simulate an ideal gas reactor to catch the ignition time. Again, for each time step, the DRG is applied using concentrations and temperature from the reactor calculations, and the species with the index greater than the threshold are retained. Finally, the final set of species is found by the union of each application species set. The reactions containing only those species then are selected to be in the skeletal mechanism. It is important to emphasize that the flat flame simulation is performed varying equivalence ratio from 0.5 to 2.0, while the pressure and temperature is varied from 1atm to 100atm and 500K to 2000K, respectively, in the reactor. For each of these parameters and time-step, the DRG is applied. Figure 3.2 presents a flow chart of the proposed methodology.

The skeletal mechanism obtained with this strategy consists in 37 species and 184 reactions, which represents a decrease of 35% in the number of species and almost 52% in the number of reactions. This reduction is satisfactory since the remaining variables reproduce the detailed mechanism with accuracy. Error in flame speed and ignition time are less than 9% for all range of parameters.

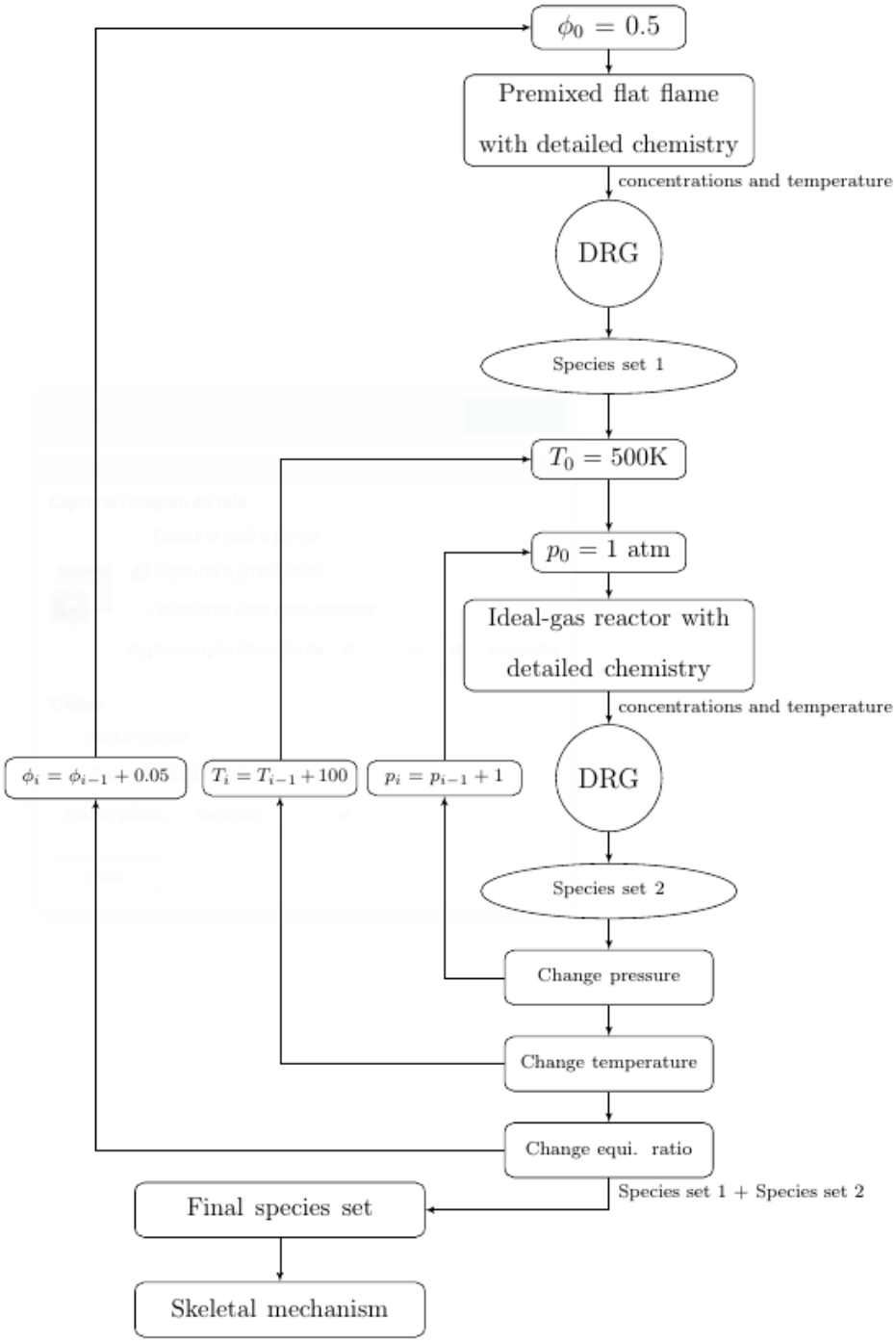

Figure 3.2: Flow chart to obtain the skeletal mechanism.

The skeletal mechanism is shown in Appendix A and the validation of it will be shown in Chapter 5. Also, the number of species and reactions are smaller

then some of the mechanisms shown in the literature for ethanol oxidation, as can be seen in Table 3.1.

Table 3.1: Number of species and reactions of different kinetic mechanism for the oxidation of ethanol.

Mechanism	Ref.	Number of species	Number of reactions
Marinov	[64]	57	383
Saxena and Williams	[90]	46	235
Röhl & Peters	[88]	38	228
Okuyama *et al.*	[73]	46	215

3.4 Validation of the mechanisms

The validation of a kinetic mechanism is an important step in the development of the reduced mechanism. The degree of reliability and accuracy of the obtained model depends on the reproduction, within an acceptable error, of the main characteristics of the mechanism.

Historically, validation of reduced mechanisms have been performed in simulations of homogeneous systems, such as reactors of rapid compression machines, given that simulations of the flame structure, laminar or turbulent, are not useful for validation [122].

The modeling of a well-stirred reactor (WSR) and auto-ignition allow comparisons between the results of the detailed mechanism and the skeletal. The simulations with WSR provide analysis for several values of temperature and pressure, covering ignition and extinction of the system, while the auto-ignition is relevant for low and mean temperatures [46]. These analysis should be performed for different equivalence ratios, so rich, lean and stoichiometric mixtures can be analyzed.

As WSR and auto-ignition are homogeneous system, it is important to extend the validation to simulations that involve the diffusive transport among the

species that are not included in the reduction step. In this sense, the calculation of flame speed in premixed flames, through the modeling of a free flat flame, and simulation of counterflow diffusion flames must be employed, comparing results of the detailed, reduced mechanisms and experimental data, if available.

4 MODEL REDUCTION

Model reduction methods are a collection of techniques that use thermodynamic information of the problem to produce a less difficult system to be solved. Almost all strategies will reduce the number of species mass fractions equations to be solved, using ideas that allow that some thermo-kinetics properties can be calculated in function of other ones. One such strategy is the slow manifold approach, which uses the separation of time scale to find an attractive manifold in the state space that describes the system's dynamics.

4.1 Time scale analysis

Development of skeletal mechanisms may provide a significant reduction in the number of species that are necessary for modelling combustion but, for incorporation in 2D or 3D CFD codes, the number of variables may still be prohibitive [108]. Complex fuels, such as long chain hydrocarbons or alcohols, can contain a significant quantity of isomers[1], which lead to several intermediary species and reactions. A possible overcome to this issue is the time scale analysis.

Models for chemical kinetics have several different time scales, which are related to the dynamical behaviour of the model, considering perturbation in the system. Depending on the species, consumption rate can change in different orders of magnitude within a mechanism, and one example is the intermediate radicals, which react faster than stable species. This difference enhances the stiffness of the calculations and leads to numerical problems when solving the system of ODE (3.1). The separation of time scales is an interesting approach to overcome this problem, since then fast variables can be determined by the slow variables values.

[1]Species that have the same molecular form, but differs in the structure.

For a general kinetic mechanism, the lifetime τ of a species i is given by

$$\tau_i = -\frac{1}{J_{ii}}, \tag{4.1}$$

where J_{ii} is the i-th element of the Jacobian matrix (3.7). Note that if species i has consuming reactions, the term J_{ii} is usually negative, since the derivative of the right-hand side of (3.1) with respect to the species itself has only negative terms. If i does not have any consuming reaction, then $J_{ii} = 0$. A slow variable can be defined as that who has a slow reactivity, i.e., a long lifetime and, analogously, a fast variable is the one that reacts really fast, and therefore has a short lifetime [108].

Figure 4.1 shows the trajectory of species concentration over time for a fast (A) and slow (B) variable. When a slow variable undergo a perturbation, the distance between the perturbed and the original trajectories remains almost constant in time, whilst for the fast variable, the perturbed variable quickly approaches the original trajectory.

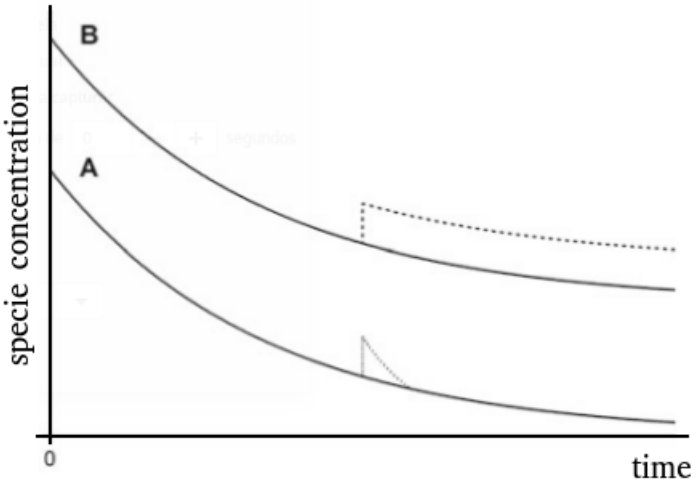

Figure 4.1: Perturbed (dashed) and original trajectories for a fast (A) and slow (B) variable. Adapted from [108]

One important consideration is that the definition of slow or fast variable doesn't have relation with the magnitude of the production rate of the species. The separation in fast/slow variables depends on the system's response when there

is a perturbation in the species concentration trajectory. The implication of this separation is that after the perturbation, fast variables can be determined by the slow variables values.

Changing the concentration of a species $\mathbf{c}$ during the path of oxidation in an arbitrary time $t_0 = 0$ according to the vector $\Delta\mathbf{c}^0$, one has the perturbed vector $\tilde{\mathbf{c}}$ given by

$$\tilde{\mathbf{c}}(0) = \mathbf{c}(0) + \Delta\mathbf{c}^0. \tag{4.2}$$

For a later time t, the perturbed vector is

$$\tilde{\mathbf{c}}(t) = \mathbf{c}(t) + \Delta\mathbf{c}. \tag{4.3}$$

Calculating the time derivative of the above expression, using linearisation and neglecting the high order terms of the Taylor expansion, one obtains

$$\begin{aligned} \frac{d}{dt}\tilde{\mathbf{c}}(t) &= \frac{d}{dt}\left(\mathbf{c}(t) + \Delta\mathbf{c}\right) \\ &\approx \mathbf{f}(\mathbf{c}, \mathbf{k}) + \frac{\partial \mathbf{f}}{\partial \mathbf{c}}\Delta\mathbf{c} \\ &= \mathbf{f}(\mathbf{c}, \mathbf{k}) + \mathbf{J}\Delta\mathbf{c}. \end{aligned} \tag{4.4}$$

Note that one can also express the derivative of (4.3) as a simple sum of the derivative, as

$$\frac{d}{dt}\tilde{\mathbf{c}}(t) = \frac{d}{dt}\left(\mathbf{c}(t) + \Delta\mathbf{c}\right) = \frac{d\mathbf{c}}{dt} + \frac{d\Delta\mathbf{c}}{dt}. \tag{4.5}$$

Comparing (4.4) and (4.5), the derivative of the perturbed concentration is equal to the product of the Jacobian and the perturbation itself, that is,

$$\frac{d\Delta\mathbf{c}(t)}{dt} = \mathbf{J}\Delta\mathbf{c}. \tag{4.6}$$

Although the Jacobian is time dependent, in a short time interval, it doesn't change significantly, so it can be considered constant. Therefore, Eq. (4.6) can be solved analytically:

$$\Delta\mathbf{c}(t) = \Delta\mathbf{c}^0 \exp\left(\mathbf{J}t\right), \tag{4.7}$$

which represents the concentration change in the time t when there is a perturbation in time t_0. Supposing that $\mathbf{J}$ can be diagonalized, then

$$\mathbf{J} = \mathbf{W}^{-1}\Lambda\mathbf{W}, \tag{4.8}$$

where $\Lambda = \mathrm{diag}(\lambda_1, \ldots, \lambda_n)$, with λ_l the eigenvalues of $\mathbf{J}$. Substituting in Eq. (4.7),

$$\begin{aligned} \Delta\mathbf{c}(t) &= \Delta\mathbf{c}^0 \exp\left(\mathbf{W}^{-1}\Lambda\mathbf{W}\right) \\ &= \Delta\mathbf{c}^0\mathbf{W}^{-1}\mathrm{diag}\left(e^{t\lambda_1}, \ldots, e^{t\lambda_n}\right)\mathbf{W} \\ &= \Delta\mathbf{c}^0\sum_{l=1}^{n} e^{t\lambda_l}(v_l \cdot w_l^t), \end{aligned} \tag{4.9}$$

where v_l are the column-vectors of $\mathbf{W}^{-1}$ and w_l are the column-vectors of $\mathbf{W}$.

The analytical solution of (4.7) is a summation of exponential. Supposing that the eigenvalues have zero imaginary part, and since $\mathbf{J}$ is diagonalizable, the number of eigenvalues is equal to the number of variables of the system, and each eigenvalue is associated to a different time scale of the local linear solution of the system. This analysis is local due to setting the Jacobian constant.

The eigenvalue with the largest negative real part (i.e., more negative) correspond to a perturbation which decays very quickly, that is, represents the fastest time scale. However, it is not possible to make an one-to-one association of the eigenvalues with the variables (species concentrations), since for a system with several species coupling, different time scales can contribute to the consumption/production of each perturbed species trajectory.

According to these small perturbations of concentrations, lifetimes can be related to chemical kinetic systems. The lifetimes do not belong to a species, but to combinations of species concentrations defined by the left eigenvectors of the Jacobian [108]: the matrix $\mathbf{W}$. These left eigenvectors are called modes, and the vector $\mathbf{z}$ of modes can be calculated as

$$\mathbf{z} = \mathbf{W}\mathbf{c}, \tag{4.10}$$

with the i-th mode coordinate given by

$$z_i \;=\; w_i \cdot \mathbf{c} \tag{4.11}$$

Therefore, concentrations can be calculated by

$$\mathbf{c} \;=\; \mathbf{W}^{-1}\mathbf{z} \;=\; \mathbf{V}\mathbf{z}, \tag{4.12}$$

or

$$c_i \;=\; v_i \cdot \mathbf{z}. \tag{4.13}$$

The change in time of the modes is given by the initial value problem, deduced from (3.1),

$$\begin{aligned} \frac{d\mathbf{c}}{dt} = \mathbf{f}(\mathbf{c},\mathbf{k}) \;\Longrightarrow\; & \frac{d\mathbf{V}\mathbf{z}}{dt} = \mathbf{f}(\mathbf{V}\mathbf{z},\mathbf{k}) \\ & \mathbf{V}\frac{d\mathbf{z}}{dt} = \mathbf{f}(\mathbf{V}\mathbf{z},\mathbf{k}) \\ & \frac{d\mathbf{z}}{dt} = \mathbf{V}^{-1}\cdot\mathbf{f}(\mathbf{V}\mathbf{z},\mathbf{k}) \\ & \frac{d\mathbf{z}}{dt} = \mathbf{W}\cdot\mathbf{f}(\mathbf{V}\mathbf{z},\mathbf{k}), \end{aligned} \tag{4.14}$$

with initial condition $\mathbf{z}_0 = \mathbf{W}\mathbf{c}_0$.

A perturbation in the concentration vector can be transferred to the modes using the relation

$$\Delta\mathbf{z} \;=\; \mathbf{W}\Delta\mathbf{c}. \tag{4.15}$$

With the ODE for the concentrations (4.6), a similar equation for $\mathbf{z}$ can be obtained

$$\begin{aligned} \mathbf{W}\frac{d\Delta\mathbf{c}}{dt} = \mathbf{W}\mathbf{J}\mathbf{V}\mathbf{W}\Delta\mathbf{c} \;\Longrightarrow\; & \mathbf{W}\frac{d\Delta\mathbf{c}}{dt} = \Lambda\mathbf{W}\Delta\mathbf{c} \\ & \frac{d}{dt}\left(\mathbf{W}\Delta\mathbf{c}\right) = \Lambda\Delta\mathbf{c} \\ & \frac{d\Delta\mathbf{c}}{dt} = \Lambda\Delta\mathbf{z}, \end{aligned} \tag{4.16}$$

whose analytical solution is

$$\Delta \mathbf{z} \;=\; \Delta \mathbf{c}_0 \exp\left(\Lambda t\right). \tag{4.17}$$

Since Λ is a diagonal matrix, the solution for each coordinate i of the modes is

$$\Delta z_i \;=\; \Delta z_i^0 e^{\lambda_i t}, \tag{4.18}$$

i.e., the perturbations in each of the modes are independent of each other.

The number of modes of the system is equal to the number of variables. Physically, the transformation matrix $\mathbf{W}$ shows how each species contributes to the modes associated with each eigenvalue. Ordering the eigenvalues, one can see which species are associated with the slow or fast modes of the system and therefore to identify those contributing with the fast modes (fast decay) and those contributing to the slower modes which may dominate the longer-term dynamics of the model.

The wide range of time scales in combustion is one of the reasons why chemical systems are computationally expensive to solve and stiff. Since very fast time scales are usually associated with local equilibrium processes, it is natural to base a method of mechanism reduction in some kind of time scale analysis [101]. It is often possible to separate and decouple these processes, and assume a local equilibrium with respect to the fastest time scales leading to a reduced set of equations. The next sections will describe the most common techniques of mechanism reduction based on time scale analysis.

4.1.1 Partial equilibrium hypothesis and quasi-steady-state assumption

The more straightforward and simple strategy in mechanism reduction is to identify and remove species and reactions that have negligible contributions to the phenomena of interest [75]. The traditional methodology for simplifying kinetics mechanism involve the use of the Quasi-Steady-State Assumption (QSSA) and/or the Partial Equilibrium approximation (PEA) [32]. This technique started

to be used in the 1980s and continues to be employed as final step in mechanism reduction.

The QSSA is justified when the rates of production and destruction, in both forward and reverse reactions, of a number of species are much larger than the their net rate of formation. When applied to a species i, using Eq. (2.23), one sets $\dot{\omega}_i \approx 0$, and the following relation is obtained

$$0 \approx W_i \sum_{j=1}^{n_r} \nu_{kj} \left[k_{fj} \prod_{i=1}^{n_{sp}} [X_i]^{\nu'_{ij}} - k_{bj} \prod_{i=1}^{n_{sp}} [X_i]^{\nu''_{ij}} \right], \tag{4.19}$$

which can be used to estimate the concentration of a species as a function of the other species in the mechanism. This equality yields a system of algebraic relations among the elementary rates.

The PEA assumes that the forward and/or backward rates of some reactions are so large that they form a number of equilibria, expressed by an equal number of algebraic relations among the elementary reaction rates. Therefore, the forward and backward rates of certain reversible reactions are almost equal, such as the net rate is approximately zero, that is,

$$k_f \prod_{i=1}^{n_{sp}} [X_i]^{\nu'_i} - k_b \prod_{i=1}^{n_{sp}} [X_i]^{\nu''_i} = \dot{\omega} \approx 0 \tag{4.20}$$

$$k_f \prod_{i=1}^{n_{sp}} [X_i]^{\nu'_i} \approx k_b \prod_{i=1}^{n_{sp}} [X_i]^{\nu''_i} . \tag{4.21}$$

The algebraic relations obtained from QSSA and PEA is used to compute the concentration of species and to simplify the differential equations of the remaining species in the mechanism [32].

An important feature in QSSA is to choose which species are in steady-state. The following algorithm was proposed by Turányi *et al* [107]:

1. Firstly, the local error, associated with each species, of QSSA is calculated over the whole domain of the application;

2. A group of species to be in steady-state is selected following a user defined tolerence;

3. Local error is calculated for the group of species from step 2;

4. If the error remains low, the assumption is applied to the group of species from step 2. Otherwise, the tolerance is decreased.

Others techniques also can be used to find the species that are in QSSA, such as the level of importance index (LOI) [55] or the computational singular perturbation (see Section 4.1.2).

The use of QSSA and PEA methodologies is associated with the existence of dissipative times scales which are faster than the ones that characterize the long-term evolution of the system. Thus, separation of time scales are definitive to help chose the QSSA species or PEA reactions, since those are associated with the fast processes (equilibrium state).

4.1.2 Computational singular perturbation - CSP

The computational singular perturbation theory is a family of methods that uses variables transformation so that the time scales in complex chemistry systems can be separated. Lam e Goussis [43, 44, 45] developed a detailed theory based on the application of perturbation in species concentrations to find informations about the presence of QSSA species and PEA reactions inside a detailed mechanism, without any chemistry knownledge [101]. In other words, CSP helps to chose which species are in QSS and reactions in PE.

Consider a system with n variables. The eigenvalue analysis of the Jacobian provides n_f fast time scales, that is, eigenvalues with the largest negative real part. Then, the solution is quickly attracted to a surface Ω with dimension $(n-n_f)$, hereafter denominated slow manifold. Let $S_{\mathbf{c}}\Omega$ and $S_{\mathbf{c}}F$ be two subspaces of

Ω, where the first is the space of trajectories in Ω and the latter the space containing the directions of fast approaches to the manifold. These subspaces are spanned by

$$S_{\mathbf{c}}\Omega = \text{span}\left(\mathbf{a}_i\right), i = n_f + 1, \ldots, n; \tag{4.22}$$

$$S_{\mathbf{c}}F = \text{span}\left(\mathbf{a}_i\right), i = 1, \ldots, n_f. \tag{4.23}$$

The vectors $\mathbf{a}_i$ are the eigenvectors of the Jacobian and form the columns of the matrices

$$\mathbf{A}_R = \begin{bmatrix} | & & | \\ \mathbf{a}_{n_f+1} & \ldots & \mathbf{a}_n \\ | & & | \end{bmatrix} \quad \text{and} \quad \mathbf{A}_S = \begin{bmatrix} | & & | \\ \mathbf{a}_1 & \ldots & \mathbf{a}_{n_f} \\ | & & | \end{bmatrix}. \tag{4.24}$$

In these basis, the right-hand side of Eq. (3.1) can be decomposed in

$$\mathbf{f}(\mathbf{c}, \mathbf{k}) = \mathbf{f}_{\text{fast}}(\mathbf{c}, \mathbf{k}) + \mathbf{f}_{\text{slow}}(\mathbf{c}, \mathbf{k}), \tag{4.25}$$

where

$$\mathbf{f}_{\text{fast}} = \mathbf{A}_R \cdot \mathbf{z}^R \quad \text{and} \quad \mathbf{f}_{\text{slow}} = \mathbf{A}_S \cdot \mathbf{z}^S, \tag{4.26}$$

and $\mathbf{z}$ are the amplitudes defined by

$$\mathbf{z}^R = \mathbf{B}^R\mathbf{f} \quad \text{and} \quad \mathbf{z}^S = \mathbf{B}^S\mathbf{f}. \tag{4.27}$$

Vectors $\mathbf{b}^i$ are defined by $\mathbf{b}^i\mathbf{a}_j = \delta^j_i$.

When the trajectories reach the slow manifold, the fast time scales become exhausted and $\mathbf{f}$ has no components in the fast subspace $S_{\mathbf{c}}F$, and it is entirely in $S_{\mathbf{c}}\Omega$. Thus, the solution evolves inside Ω according to the slow time scales and the kinetics is governed by the equation

$$\frac{d\mathbf{c}}{dt} \approx \mathbf{f}_{\text{slow}}(\mathbf{c}, \mathbf{k}). \tag{4.28}$$

The equation $\mathbf{z}^R \approx 0$ can be interpreted as a generalization of QSSA and PEA.

The advantage in using CSP is that a simple analysis of eigenvalues and eigenvectors of the system provides information about which species or reactions are associated with the fastest modes, although the computational cost of evaluating the Jacobian could be elevated.

4.1.3 Intrinsic Low Dimensional Manifolds

The concept of slow manifold introduced in the last section will provide a base for the theory of the intrinsic low dimensional manifolds (ILDM). The ILDM extracts the essential information of the full system to describe the most interesting and essential details of the system's chemical kinetics. It was developed by Maas and Pope [63] and allows to decouple the fast time-scales and globally reduce the dimension of the model. The main idea is to find a manifold of low dimension inside the vector space of thermochemical states (state space) that attracts the reactive processes.

As already explained, there is a difference in the time scales within a chemical system, which can be obtained via inspection of the eigenvalues of the Jacobian. Consider the local solution given by Eq. (4.9), describing the evolution of a perturbed chemical species. For each species, there is a summation of exponential, and each of these is associated with one time scale. Therefore, in general, all time scales affects the dynamics of each species, although the amount of how much each term affects a given species concentration is not the same for each species. Some species will evolve more quickly than the others for a initial period of time, i.e., governed by the fast time scales in this initial period. When enough time has passed, the slower time scales terms of the solutions begin to dominate the system and thus the evolution of each species concentration. This analysis yields the conclusion that the system behaviour is often contained in the terms correlated to the slower time scales.

The summary is that as the trajectories of the concentrations evolve in the state space, the fast time scales will become exhausted. If a system has n_s slow time scales, the trajectories will approach a n_s-dimensional surface inside the state space, denominated low-dimensional manifold. If all time scales in the system become exhausted, an equilibrium chemical model arises, which represents a

zero-dimensional manifold. This manifold is not characterized by any species concentrations, but by temperature and, in non-premixed flames, the mixture fraction, and the most usual example of this is the Burke-Schumann solution (mass fractions depending on mixture fraction). The low-dimensional manifold has the property to attract reaction trajectories, and the reaction path inside the detailed mechanism will approach the manifold rapidly, where the subsequently movement in the manifold will be slow. This slow movements in the manifolds are parametrized by the variables that it defines.

The question addressed in the precursor work of Maas and Pope was that [63]: If there is a low-dimensional attracting manifold in the state space with the property that if a trajectory is near the manifold, it will remain close to it for all times? And if so, can it be used to provide a simplified model of chemical kinetics? The answer for this question is affirmative, and the theory is the ILDM, presented below.

Consider a homogeneous, isobaric and adiabatic chemical reaction system with n_{sp} species given by

$$\frac{\partial h}{\partial t} = 0 \tag{4.29}$$

$$\frac{\partial p}{\partial t} = 0 \tag{4.30}$$

$$\frac{\partial \phi_i}{\partial t} = \dot{\omega}_i, \qquad i = 1, \ldots n_{sp}, \tag{4.31}$$

where h is the enthalpy, p the pressure and ϕ_i the specific mole fraction ($\phi = Y_i/W_i$) of species i. This system is often written in terms of vectors, i.e.,

$$\frac{\partial \mathbf{\Psi}}{\partial t} = \mathbf{F}(\mathbf{\Psi}), \tag{4.32}$$

where $\mathbf{\Psi} = \left(h, p, \phi_i, \ldots, \phi_{n_{sp}}\right)^T$ and $\mathbf{F} = \left(0, 0, f_1, \ldots, f_{n_{sp}}\right)^T$ are n-dimensional vectors ($n = n_{sp} + 2$).

For each point in the state space, the eigenvalues of the Jacobian matrix ($\mathbf{F}_{\mathbf{\Psi}}$) are calculated to identify the n time scales of the system. The corresponding

eigenvectors describe the characteristic directions associated with those time scales. The general idea is to look for points in the state space for which components in the direction of certain eigenvectors, those associated with fast time scales, vanishes.

Generally, the eigenvectors provided by diagonalization are not orthogonal, and the elimination of characteristic directions associated with fast time scales are more easily carried out when the directions associated with each time scale are orthogonal [85]. Therefore, one way to accomplish that is using the Schur decomposition of the Jacobian at each point of the state space, that is,

$$\mathbf{Q}^T \mathbf{F}_{\mathbf{\Psi}} \mathbf{Q} \;=\; N, \tag{4.33}$$

where the eigenvalues λ_i of the Jacobian appear in the diagonal of the upper triangular matrix N in the order of descending real parts [63]. For chemical systems, the Jacobian contain real numbers and it has been proved that the Schur decomposition always exists for a matrix whose elements are real [29]. Matrix $\mathbf{Q}$ is orthonormal, and its vector columns provides the desired orthogonal set of directions in the state space associated with fast time scales.

Thus, supposing that the Schur decomposition exists for every point in the solution space, a n_l-dimensional manifold ($n_l < n$) is obtained, whose points are calculated by

$$\mathbf{Q}_L^T(\mathbf{\Psi}) \cdot \mathbf{F}(\mathbf{\Psi}) \;=\; 0 \tag{4.34}$$

where $\mathbf{Q}_L^T(\mathbf{\Psi})$ is a $n_f \times n$ matrix ($n_f = n - n_l$). Equation (4.34) is called ILDM equation, and the matrix $\mathbf{Q}_L^T$ is obtained by eliminating the n_l first rows of $\mathbf{Q}^T$, namely, the rows that correspond to the conserved and slowly changing variables.

One problem arising from Eq. (4.34) is that the system is not closed. There are other n_l additional parameters equations necessary to complete the equation system. These new equations will affect the uniqueness and existence of the manifold, but not the construction of the manifold itself [63]. Thus, to identify the

low-dimensional manifold, the following system has to be solved

$$\begin{bmatrix} \mathbf{Q}_L^T(\mathbf{\Psi}) \cdot \mathbf{F}(\mathbf{\Psi}) \\ \mathbf{P}(\mathbf{\Psi}, \tau) \end{bmatrix} = 0, \tag{4.35}$$

with $\mathbf{P}(\mathbf{\Psi}, \tau)$ being the n_l additional parameters equations.

A proper numerical scheme should be used to solve Eq. (4.35), such as the Newton's method. The ILDM gives an accurate description if the application is not required at extremely small times. Thus, in regions of low temperatures, the ILDM is not well predicted. For instance, ignition delay times calculation, since for this processes, the phenomena occurs very quickly within a low temperature region. Another drawback is that ILDM does not consider the transport processes. One alternative for this is the Reaction Diffusion Manifold technique, exploited in Section 4.3.

4.2 Flamelet concept

The flamelet concept is briefly discussed here since consist in a very good approximation for the REDIM, and is tightly close to the counterflow configuration. It was first introduced by Peters [77] for non-premixed turbulent combustion, and consists in a variety of physical models in which the turbulent flame is viewed as a collection of laminar flame elements embedded in a turbulent flow and interacting with it. The main advantage of the flamelet concept is that decouples the complex chemical structure of the flame from the fluid dynamics, which can be modeled independently [19].

For a non-premixed flame, the local structure of the flame in each point of the flame front (i.e., the surface where $\xi(t, \mathbf{x}) = \xi_{st}$), is defined by a laminar flamelet. Using the transformation $(t, \mathbf{x}) \rightarrow (t, \xi)$, the coordinate system becomes the flame front and the physical space is transformed to a mixture fraction space where the only independent variable is ξ [15]. The unsteady equations for temper-

ature and mass fractions, respectively, are therefore given by

$$\rho\frac{\partial w_i}{\partial t} = \frac{\rho\chi}{2Le_i}\frac{\partial^2 w_i}{\partial \xi^2} + \dot{\omega}_i \tag{4.36}$$

$$\rho\frac{\partial T}{\partial t} = \frac{\rho\chi}{2}\frac{\partial^2 T}{\partial \xi^2} - \frac{1}{c_p}\left(\sum_{i=1}^{n_{sp}} h_i\dot{\omega}_i - Q_R\right). \tag{4.37}$$

The scalar dissipation rate χ is given by

$$\chi = 2D_\xi\left(\nabla\xi\cdot\nabla\xi\right). \tag{4.38}$$

The instantaneous scalar dissipation rate consists a very important characteristic in non-premixed combustion, specially χ in stoichiometric conditions, χ_{st}, which denotes how far the flame is from the equilibrium point [15]. Since diffusion fluxes arising from spatial gradients are described as function of the mixture fraction gradients [82], the influence of the flow field on the flamelet structure is completely described by χ. Also, χ can be interpreted as the inverse of the characteristic diffusion time [79]. Thus, the higher is χ, the lower is the characteristic diffusion time scale, and consequently the lower is the Damköhler number. It is straightforward then that if $\chi = 0$, the flamelet concept becomes the Burke-Schumann solution.

The solution for a non-premixed flame is therefore calculated solving the fluid dynamic equations and the mixture fraction Eq. (2.45). Nevertheless, a key difficult in integrating Eqs. (4.36) and (4.37) is to know a priori informations of the scalar dissipation rate dependence of the mixture fraction. Thus, flamelet libraries are usually computed in advance in a pre-processing step, totally independent of the flow. Generally, those libraries are built using counterflow non-premixed flames solutions with detailed chemistry.

If chemistry is considered infinitely fast, the time derivative in the flamelet equations (4.36) and (4.37) vanishes. An important condition for the flamelet approach is that the flame thickness is sufficiently small compared to the length scales [19]. The great advantage of the flamelet compared to the flame sheet

model is that it doesn't need to imply hypothesis to the reaction rates and so complete detailed mechanisms can be used.

For a given steady solution, the flamelet equations define an one dimensional manifold in the state space, parametrized by the mixture fraction, that is, all the thermodynamic properties are functions only of the mixture fractions ξ [38]. That is the great disadvantage of this method, since the reactive scalars are constant throughout the iso-surfaces of the mixture fraction. Nevertheless, several methods for chemistry modeling were developed using the flamelet approach, the best know being the flamelet generated manifold (FGM) [112] which combines the idea of flamelet and slow manifolds, and is used in the commercial CFD code FLUENT.

4.3 Reaction diffusion manifolds - REDIM

The ideas exploited for building the ILDM in Section 4.1.3 regarding the separation of time scales will be used to develop the theory of Reaction Diffusion Manifolds - REDIM. This technique is an improvement of the ILDM, since takes into account the transport processes, and not only reaction. It will be shown that the thermodynamic states of the system evolves towards a low dimensional manifold, that can be calculated using the diffusion and reaction terms of the equation of the variables, such as convection is not necessary.

The time scales separation which leads to the idea that the system dynamics approach a slow manifold in the space states so that all thermodynamic variables can be predicted as a function of the ones that parametrizes the manifold is extended for diffusion and convection systems. Evolution in time of the thermodynamics properties consists of a reaction, a convection and a diffusion term. The major drawback of the ILDM technique is that, since the diffusive/convective terms

of the equations are dominant in the pre-heat zones, that is, the zone before ignition, using only the reaction term, this area of the state space is not covered.

The first attempt of overcoming this problem was developed by Bykov and Maas [10], which suggested a procedure to use ILDM in the whole domain of the state space. They subdivided the domain of interest in three different sub-domains: in the first one, only the chemical kinetic governs the system dynamics; in the second, chemical and convection/diffusion processes are strongly coupled and the third one, where an infinitly slow chemstry assumption is used so that the reaction term is neglected and the system dynamics is governed only by convection/diffusion. The domais were treated separately and three different slow manifolds were obtained. Nevertheless, this approach also had some problems, due to the assumption that the second domain asymptotically shrinks into the boundary between the first and third domain.

The REDIM technique was later introduced also by Bykov and Maas in 2007 [9], whose used the invariant condition to obtain the slow manifold in the state space. This hypothesis were very useful since provided the basic assumption for developing the REDIM equation. The dimension of the REDIM can be choose depending on the complexity of the combustion process to be modeled, and it has been proved that the 1D-REDIM is equivalent to the flamelet concept [9, 39], while 2D and 3D-REDIM are sufficient to calculate complex chemistry calculations, such as turbulent three dimensional flames.

From a numerical point of view, the advantage of using a method where the system is governed only by the slow time scales is in the fact that one can use higher time steps in the numerical schemes, decreasing the stiffness of the system. The next section will introduce the concept of invariant manifolds so that later the REDIM equation can be developed.

4.3.1 The invariance condition

The thermochemical state in a reactive system with n_{sp} species can be described by the $n = n_{sp} + 2$ dimension vector

$$\boldsymbol{\Psi} \;=\; \left(h, p, \phi_1, \ldots, \phi_{n_{sp}}\right), \tag{4.39}$$

where h is the specific enthalpy, p the pressure and ϕ_i is the specific mole fraction of species i, defined as $\phi_i = w_i/W_i$. The thermochemical state changes over chemical and transport processes due the PDE, in vector notation, [9]

$$\frac{\partial \boldsymbol{\Psi}}{\partial t} \;=\; \mathbf{F}(\boldsymbol{\Psi}) - \mathbf{u}\cdot\mathbf{grad}(\boldsymbol{\Psi}) - \frac{1}{\rho}\mathbf{div}\left(\mathbf{D}\cdot\mathbf{grad}(\boldsymbol{\Psi})\right) = \boldsymbol{\Phi}(\boldsymbol{\Psi}) \tag{4.40}$$

Here, $\mathbf{u}$ is the velocity, $\mathbf{D}$ is the $n \times n$ diffusion matrix, $\mathbf{F}$ is the n-dimensional source term that accounts for the chemical reactions and ρ the density. The second term of the right-hand side in Eq. (4.40) represents convection and the third term diffusion.

After the fast time scales are exhausted, the system dynamics is governed by the m_s slowest modes ($m_s < n$), i.e., the system solution is within a m_s-dimensional manifold in the state space. This manifold $\mathcal{M}$ is defined as

$$\mathcal{M} \;=\; \left\{\boldsymbol{\Psi} : \boldsymbol{\Psi} = \boldsymbol{\Psi}(\boldsymbol{\theta}), \boldsymbol{\Psi} : \mathbb{R}^{m_s} \to \mathbb{R}^n\right\}, \tag{4.41}$$

where $\boldsymbol{\theta}$ is the m_s-dimensional vector that parametrizes the manifold. The explicit function $\boldsymbol{\Psi}(\boldsymbol{\theta})$ defines a surface in $\mathbb{R}^n$ with dimension m_s.

The manifold $\mathcal{M}$ is said invariant if, and only if, for some θ_*, such that $\boldsymbol{\Psi}(\theta_*) \in \mathcal{M}$, then for all $\theta > \theta_*$, $\boldsymbol{\Psi}(\theta) \in \mathcal{M}$ (this definition can be found in Gorban and Karlin [31]). The consequence of this definition is that for every $\boldsymbol{\Psi} \in \mathcal{M}$, it holds that $\boldsymbol{\Phi}(\boldsymbol{\Psi}) \in T_\Psi \mathcal{M}$, that is, the field $\boldsymbol{\Phi}$ (defined by the right-hand side of Eq. (4.40)) applied to the vectors of the manifold belong to the tangent space of $\mathcal{M}$. To exemplify this, lets consider a two dimensional system with only the reaction term, that is,

$$\frac{\partial \boldsymbol{\Psi}}{\partial t} \;=\; \mathbf{F}(\boldsymbol{\Psi}). \tag{4.42}$$

In this case, the invariant manifold $\mathcal{M}$ will have dimension equal to one. In the point $\theta_* \in \mathcal{M}$, the derivative of $\mathbf{\Psi}$ in this point is equal to

$$\left.\frac{\partial \Psi}{\partial t}\right|_{\theta=\theta_*} = \mathbf{F}(\mathbf{\Psi}(\theta_*)) \tag{4.43}$$

Considering that for every point θ in the manifold, $\mathbf{F}(\mathbf{\Psi}(\theta)) \in \mathcal{M}$, the derivative of $\mathbf{\Psi}$ in the point θ_* will belong to the manifold, and, since this derivative is equal to the field $\mathbf{F}$ applied in the vector, and also since this will hold for every $\theta > \theta_*$, it can be concluded that, for the points within the manifold, $\mathbf{F}(\mathbf{\Psi}(\theta)) \in T_\Psi \mathcal{M}$. The generalization of this for the filed $\mathbf{\Phi}$ follows analogously.

Therefore, as $\mathbf{\Phi}(\mathbf{\Psi})$ belongs to the tangent space of the manifold, it follows that it is orthogonal to the normal space of $\mathcal{M}$. This implies that

$$(\mathbf{\Psi}_{\boldsymbol{\theta}}^{\perp}(\boldsymbol{\theta}))^T \cdot \mathbf{\Phi}(\mathbf{\Psi}) = 0, \tag{4.44}$$

for all $\boldsymbol{\theta}$. Here, $\mathbf{\Psi}_{\boldsymbol{\theta}}^{\perp}$ represents the normal space of $\mathcal{M}$, i.e.,

$$(\mathbf{\Psi}_{\boldsymbol{\theta}}^{\perp})^T \cdot \mathbf{\Psi}_{\boldsymbol{\theta}} = 0. \tag{4.45}$$

The condition (4.44) implies that the projection of the field $\mathbf{\Phi}$ in the normal space of $\mathcal{M}$ is also orthogonal to the field, that is,

$$P_{(T\mathcal{M})^\perp}[\mathbf{\Phi}(\mathbf{\Psi})] \cdot \mathbf{\Phi}(\mathbf{\Psi}) = 0 \tag{4.46}$$

But,

$$P_{(T\mathcal{M})^\perp}[\mathbf{\Phi}(\mathbf{\Psi})] = \left(\mathbf{\Psi}_{\boldsymbol{\theta}}^{\perp}(\boldsymbol{\theta}) \cdot \mathbf{\Psi}_{\boldsymbol{\theta}}^{+}(\boldsymbol{\theta})\right) \cdot \mathbf{\Phi}(\mathbf{\Psi}) \tag{4.47}$$

where $\mathbf{\Psi}_{\boldsymbol{\theta}}^{+}$ is the Moore-Penrose pseudo-inverse, defined by

$$\mathbf{\Psi}_{\boldsymbol{\theta}}^{+} = \left(\mathbf{\Psi}_{\boldsymbol{\theta}}^T \cdot \mathbf{\Psi}_{\boldsymbol{\theta}}\right)^{-1} \cdot \mathbf{\Psi}_{\boldsymbol{\theta}}^T. \tag{4.48}$$

This pseudo-inverse always exists when the columns of $\mathbf{\Psi}_{\boldsymbol{\theta}}$ are linearly independent (i.e., the matrix $\mathbf{\Psi}_{\boldsymbol{\theta}}^T \cdot \mathbf{\Psi}_{\boldsymbol{\theta}}$ is non-singular). This can always be achieved by a suitable

choice of the local coordinates $\boldsymbol{\theta}$. Then, using (4.47) in (4.46), one obtains

$$\begin{aligned} P_{(T\mathcal{M})^\perp}\left[\boldsymbol{\Phi}(\boldsymbol{\Psi})\right]\cdot\boldsymbol{\Phi}(\boldsymbol{\Psi}) &= \left[\left(\boldsymbol{\Psi}^{\perp}_{\boldsymbol{\theta}}(\boldsymbol{\theta})\cdot\boldsymbol{\Psi}^{+}_{\boldsymbol{\theta}}(\boldsymbol{\theta})\right)\cdot\boldsymbol{\Phi}\left(\boldsymbol{\Psi}(\boldsymbol{\theta})\right)\right]\cdot\boldsymbol{\Phi}\left(\boldsymbol{\Psi}(\boldsymbol{\theta})\right) \\ &= \left(I-\boldsymbol{\Psi}_{\boldsymbol{\theta}}(\boldsymbol{\theta})\cdot\boldsymbol{\Psi}^{+}_{\boldsymbol{\theta}}(\boldsymbol{\theta})\right)\cdot\boldsymbol{\Phi}\left(\boldsymbol{\Psi}(\boldsymbol{\theta})\right). \end{aligned} \tag{4.49}$$

Hence,

$$\left(I-\boldsymbol{\Psi}_{\boldsymbol{\theta}}(\boldsymbol{\theta})\cdot\boldsymbol{\Psi}^{+}_{\boldsymbol{\theta}}(\boldsymbol{\theta})\right)\cdot\boldsymbol{\Phi}\left(\boldsymbol{\Psi}(\boldsymbol{\theta})\right) = 0. \tag{4.50}$$

The relation (4.50) is very important in the REDIM formulation since allows to simplify Eq. (4.40) and to find an approximation for the low-dimensional manifold [9]. Nevertheless, to solve (4.50), two difficulties arise [39]: first, the dependence of $\boldsymbol{\Psi}\in\mathcal{M}$ as a function of the local coordinates $\boldsymbol{\theta}$ should be explicitly determined and second, $\boldsymbol{\Phi}(\boldsymbol{\Psi}(\boldsymbol{\theta}))$ depends on the spatial gradients of $\boldsymbol{\theta}$, i.e., the transport processes, that cannot be known *a priori*. In the next section, these difficulties will be discussed.

4.3.2 REDIM equation

To solve the difficulties highlighted in last section, the right-hand side of Eq. (4.40) has to be analysed. First, observe that

$$\mathbf{grad}(\boldsymbol{\Psi}(\boldsymbol{\theta})) = \begin{pmatrix} \sum_{k=1}^{m_s}\dfrac{\partial\Psi_1}{\partial\theta_k}\dfrac{\partial\theta_k}{\partial x_k} \\ \vdots \\ \sum_{k=1}^{m_s}\dfrac{\partial\Psi_n}{\partial\theta_k}\dfrac{\partial\theta_k}{\partial x_k} \end{pmatrix} \tag{4.51}$$

$$= \begin{pmatrix} \dfrac{\partial\Psi_1}{\partial\theta_1} & \cdots & \dfrac{\partial\Psi_1}{\partial\theta_{m_s}} \\ \vdots & \ddots & \vdots \\ \dfrac{\partial\Psi_n}{\partial\theta_1} & \cdots & \dfrac{\partial\Psi_n}{\partial\theta_{m_s}} \end{pmatrix} \begin{pmatrix} \dfrac{\partial\theta_1}{\partial x_1} \\ \vdots \\ \dfrac{\partial\theta_{m_s}}{\partial x_j} \end{pmatrix} \tag{4.52}$$

$$= \boldsymbol{\Psi}_{\boldsymbol{\theta}}\mathbf{grad}(\theta) \tag{4.53}$$

Thus, the convective term of Eq. (4.40) reads

$$\mathbf{u}\cdot\mathbf{grad}(\boldsymbol{\Psi}) \;=\; \mathbf{u}\cdot(\boldsymbol{\Psi_\theta}\mathbf{grad}(\theta))\,. \tag{4.54}$$

The diffusive term in Eq. (4.40) is rearranged as [38]:

$$\begin{aligned}
\frac{1}{\rho}\mathbf{div}\left(\mathbf{D}\cdot\mathbf{grad}(\boldsymbol{\Psi})\right) &= \frac{1}{\rho}\mathbf{div}\left[\mathbf{D}\cdot(\boldsymbol{\Psi_\theta}\mathbf{grad}(\theta))\right]\\
&= \frac{1}{\rho}\sum_{i=1}^{3}\frac{\partial}{\partial x_i}\left(\sum_{j=1}^{n}\sum_{k=1}^{m_s}D_j\frac{\partial\Psi_j}{\partial\theta_k}\frac{\partial\theta_k}{\partial x_i}\right)\\
&= \frac{1}{\rho}\sum_{i=1}^{3}\sum_{j=1}^{n}\sum_{k=1}^{m_s}\left[\frac{\partial}{\partial x_i}\left(D_j\frac{\partial\Psi_j}{\partial\theta_k}\right)\frac{\partial\theta_k}{\partial x_i}+D_j\frac{\partial\Psi_j}{\partial\theta_k}\frac{\partial}{\partial x_i}\frac{\partial\theta_k}{\partial x_i}\right]\\
&= \frac{1}{\rho}\sum_{i=1}^{3}\sum_{j=1}^{n}\sum_{k=1}^{m_s}\left[\sum_{h=1}^{m_s}\frac{\partial}{\partial\theta_h}\left(D_j\frac{\partial\Psi_j}{\partial\theta_k}\right)\frac{\partial\theta_h}{\partial x_i}\frac{\partial\theta_k}{\partial x_i}+D_j\frac{\partial\Psi_j}{\partial\theta_k}\frac{\partial}{\partial x_i}\frac{\partial\theta_k}{\partial x_i}\right]\\
&= \frac{1}{\rho}\left[(\mathbf{D}\cdot\boldsymbol{\Psi}_\theta)_\theta\circ\mathbf{grad}(\theta)\circ\mathbf{grad}(\theta)+(\mathbf{D}\cdot\boldsymbol{\Psi}_\theta)\cdot\mathbf{div}(\mathbf{grad}(\theta))\right].
\end{aligned}$$

Equation (4.40) becomes

$$\begin{aligned}
\frac{\partial\boldsymbol{\Psi}}{\partial t}=\mathbf{F}(\boldsymbol{\Psi})-\mathbf{u}\cdot(\boldsymbol{\Psi_\theta}\mathbf{grad}(\theta)) \;&-\; \frac{1}{\rho}\left[(\mathbf{D}\cdot\boldsymbol{\Psi}_\theta)_\theta\circ\mathbf{grad}(\theta)\circ\mathbf{grad}(\theta)\right.\\
&+\; \left.(\mathbf{D}\cdot\boldsymbol{\Psi}_\theta)\cdot\mathbf{div}(\mathbf{grad}(\theta))\right].
\end{aligned}\tag{4.55}$$

For simplicity, two hypothesis will be assumed: the Lewis number equal to unity and equal diffusivities for all species, so that the diffusion matrix $\mathbf{D}$ is given by $\mathbf{D} = d\cdot I$. These hypothesis are very common in numerical simulations of combustion processes. Applying the projection operator of Eq. (4.55) to each term of Eq. (4.40), some simplifications can be made. For instance,

$$\begin{aligned}
\left(I-\boldsymbol{\Psi_\theta}(\boldsymbol{\theta})\cdot\boldsymbol{\Psi}^{+}_{\boldsymbol{\theta}}(\boldsymbol{\theta})\right)\cdot(\mathbf{u}\cdot(\boldsymbol{\Psi_\theta}\mathbf{grad}(\theta))) &= \mathbf{u}\cdot(\boldsymbol{\Psi_\theta}\mathbf{grad}(\theta))\\
&- \underbrace{\boldsymbol{\Psi}^{+}_{\boldsymbol{\theta}}(\boldsymbol{\theta})\cdot\boldsymbol{\Psi_\theta}(\boldsymbol{\theta})}_{=\;I}\mathbf{u}\cdot(\boldsymbol{\Psi_\theta}\mathbf{grad}(\theta))\\
&= \mathbf{u}\cdot(\boldsymbol{\Psi_\theta}\mathbf{grad}(\theta))-\mathbf{u}\cdot(\boldsymbol{\Psi_\theta}\mathbf{grad}(\theta))\\
&= 0
\end{aligned}\tag{4.56}$$

This proves that the convection term vanishes in the invariant manifold. Also, it is valid that

$$\begin{aligned}\left(I - \boldsymbol{\Psi}_{\boldsymbol{\theta}}(\boldsymbol{\theta}) \cdot \boldsymbol{\Psi}_{\boldsymbol{\theta}}^{+}(\boldsymbol{\theta})\right) \quad \cdot \quad & [(d \cdot \boldsymbol{\Psi}_{\theta}) \cdot \mathbf{div}(\mathbf{grad}(\theta))] \\ = \quad & d\left[\boldsymbol{\Psi}_{\theta} \cdot \mathbf{div}(\mathbf{grad}(\theta)) - \boldsymbol{\Psi}_{\boldsymbol{\theta}}(\boldsymbol{\theta}) \cdot \underbrace{\boldsymbol{\Psi}_{\boldsymbol{\theta}}^{+}(\boldsymbol{\theta})\boldsymbol{\Psi}_{\theta}}_{=\ I} \cdot \mathbf{div}(\mathbf{grad}(\theta))\right] \\ = \quad & d\left[\boldsymbol{\Psi}_{\theta} \cdot \mathbf{div}(\mathbf{grad}(\theta)) - \boldsymbol{\Psi}_{\theta} \cdot \mathbf{div}(\mathbf{grad}(\theta))\right] \\ = \quad & 0 \end{aligned} \tag{4.57}$$

Therefore, using the relation given in (4.50), one obtains that

$$\left(I - \boldsymbol{\Psi}_{\boldsymbol{\theta}}(\boldsymbol{\theta}) \cdot \boldsymbol{\Psi}_{\boldsymbol{\theta}}^{+}(\boldsymbol{\theta})\right) \cdot \left[\mathbf{F}(\boldsymbol{\Psi}) - \frac{d}{\rho}\boldsymbol{\Psi}_{\theta\theta} \circ \mathbf{grad}(\theta) \circ \mathbf{grad}(\theta)\right] \quad = \quad 0 \tag{4.58}$$

The relation above implies that if the equality is fulfilled, then the vector $\boldsymbol{\Psi}(\theta)$ is in the reduced manifold within the state space. Besides, it is important that the spatial dependence of the gradient of θ can be eliminated, that is, $\mathbf{grad}(\theta) = f(\theta)$. To obtain a numerical solution of Eq. (4.58), the strategy proposed by Bykov and Maas was to reformulate the equation into a system of parabolic PDEs, with appropriate boundary and initial conditions. Thus, the REDIM equations read [9]

$$\begin{cases} \dfrac{\partial \boldsymbol{\Psi}(\theta)}{\partial t} = \left(I - \boldsymbol{\Psi}_{\boldsymbol{\theta}}(\boldsymbol{\theta}) \cdot \boldsymbol{\Psi}_{\boldsymbol{\theta}}^{+}(\boldsymbol{\theta})\right) \cdot \left[\mathbf{F}(\boldsymbol{\Psi}) - \dfrac{d}{\rho}\boldsymbol{\Psi}_{\theta\theta} \circ \mathbf{grad}(\theta) \circ \mathbf{grad}(\theta)\right]; \\ \boldsymbol{\Psi}^{0} = \boldsymbol{\Psi}^{\text{init}}(\theta), \end{cases} \tag{4.59}$$

where $\boldsymbol{\Psi}^{\text{init}}$ is an initial guess for the reduced manifold. The stationary solution $\boldsymbol{\Psi}(\theta, \infty)$ given by Eq. (4.59) yields the desired reduced manifold. To integrate the REDIM equation until it converges, it is necessary to approximate the gradient of θ and to define a good initial guess for the starting manifold.

In the precursor work of Bykov and Maas [9], the dependence of the local gradients were studied for a two dimensional system, in order that the reduced manifold have one dimension. Four different cases were studied for the gradients:

(i) The exact gradients, obtained from a detailed simulation: $\mathbf{grad}(\theta) = \mathbf{grad}_{\text{exact}}(\theta)$;

(ii) the maximum value of the exact gradients calculated in (i): $\mathbf{grad}(\theta) = \max(\mathbf{grad}_{\text{exact}}(\theta))$;

(iii) one order of magnitude less than (ii): $\mathbf{grad}(\theta) = 0.1\max(\mathbf{grad}_{\text{exact}}(\theta))$;

(iv) one order of magnitude higher than (ii): $\mathbf{grad}(\theta) = 10\max(\mathbf{grad}_{\text{exact}}(\theta))$.

As expected, the best results were for the gradients obtained from a detailed simulation, while the third and fourth cases above produced the worst results. It is worth noting that the one-dimensional REDIM built in this example using exact gradients is equivalent to the flamelet approach. By the observations, it was possible to conclude that the low dimensional manifolds are not very sensitive to the local coordinate gradients. As a comparison with the FGM method, the problem of estimating the gradients in REDIM is comparable with defining the scalar dissipation rate χ.

Another issue that is important when solving the system (4.59) is the choice of parametrization, i.e. defining the parameters for the vector θ. Albeit it does not affects the manifold itself (the manifold is independent of the parametrization), it affects the existence and the uniqueness of the REDIM equation (4.59). There is no physical motivation for the parametrization, which can be done using temperature, enthalpy, specific mole fractions of species or elements, species concentrations or even a combination of these.

It is generally a good strategy to define, for a 2D-REDIM, one variable accounting for mixture progress and another for reaction progress. For instance, the solution of a methane/air flame is provided in Fig. 4.2. It can be observed that $\theta_1 = N_2$ and $\theta_2 = CO_2$ are a good choice for parametrization, since the projection of the solution in this space is well defined. However, if one chooses for the same

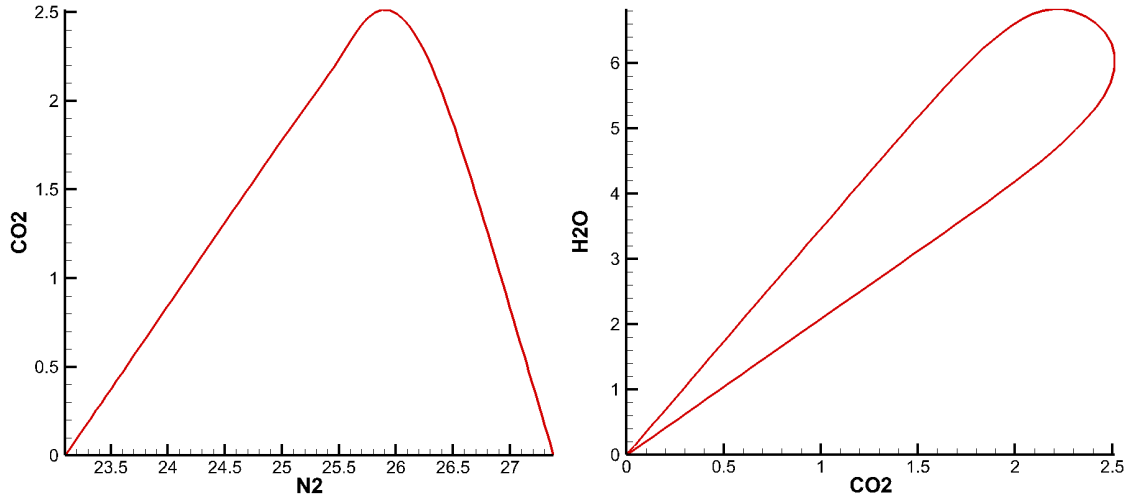

(a) (b)

Figure 4.2: Solution of a counterflow non-premixed flame projected in (a) $\theta_1 = N_2$ and $\theta_2 = CO_2$ plane and (b) $\theta_1 = CO_2$ and $\theta_2 = H_2O$ as parametrization. It is clear that the uniqueness of solution in the second case is lost.

simulation $\theta_1 = CO_2$ and $\theta_2 = H_2O$ as parametrization, the monotonic behaviour of the solution is lost and thus the uniqueness of the solution.

Several types of parametrization and gradients estimatives has been observed in the literature. For instance, in the work of Steinhilber and Maas [99], for a premixed lean methane turbulent flame, the 2D-REDIM was used with $\theta_1 = N_2$ and $\theta_2 = CO_2$ as parametrization. For the gradients, two one-dimensional simulations were performed. For the nitrogen, it was estimated a constant value of $\mathbf{grad}(N_2) = -500\ mol/kg.m$, through solution of a counterflow flame with same boundary and initial conditions that the turbulent flame to be simulated. For the carbon dioxide, the gradients were obtained using a detailed premixed flat flame.

The work of Fischer *et al.* [25], PDF simulations were performed to analyse the ignition of free turbulent jets of propane, ethylene and hydrogen. A 2D-REDIM was built and the parametrization variables were the enthalpy and, for hydrogen, the specific mole fraction of H_2O and for the hydrocarbons, the specific

mole fraction of CO_2. A counterflow scheme with detailed chemistry were used to provide the gradients estimative.

In the works of Wang *et al.* [115, 116], large eddy simulation with filtered density functions were used with REDIM to simulate turbulent flames. In the first work, a 1D-REDIM was used with CO_2 as parametrization, since the simulation considered a fully premixed methane/air flame with constant equivalence ratio and without local extinction phenomena. The second work uses a 2D-REDIM with N_2 and CO_2 as parametrization of the manifold to study the local extinction and re-ignition of two lean premixed piloted natural gas/air flames. Schiessl *et al.* [91] used a direct numerical simulation (DNS) of a non-premixed turbulent planar flame of H_2 and air to obtain the gradients for the REDIM equation to study multi-directional molecular diffusion.

It is concluded by the literature that a good choice for parametrization of a 2D-REDIM is nitrogen and carbon dioxide. The fact that N_2 remains almost unchanged in the evolution of the system makes it a good choice to account for mixture progress, in the role of a conserved scalar. The CO_2 is a good choice for reaction progress since generally its quantity is large compared to all others species. Also, the estimative of the gradients provided by detailed one dimensional simulations is the best choice.

The gradient estimative and the parametrization helps to solve Eq. (4.59). Nevertheless, a suitable choice for the initial guess of the manifold is a crucial point to obtain a good (and fast) converged solution. Next section will treat with initial and boundary conditions for the REDIM equation.

4.3.3 Initial and boundary conditions

The REDIM is independent of initial condition's choice. This is clear since, as mentioned in section 4.1.3, as the fast time scales are dumped, the system

dynamics will always approach the equilibrium point. This means also that for any starting point, the state will achieve the slow manifold. It is understood here that the initial and boundaries conditions will form the initial guess for integration of Eq. (4.59).

Nonetheless, since Eq. (4.59) denotes a stiff system of PDEs, a suitable choice for the initial condition avoid numerical instabilities and speed up the convergence. For instance, the extended ILDM, which represents the limiting case where the reaction term $\mathbf{F}(\mathbf{\Psi})$ is dominant and the transport processes can be neglected, can be used as initial condition. In this matter, the reaction curve can also be used.

Generally, one-dimensional simulations with detailed chemistry can provide a good initial condition for the REDIM equation. As already mentioned, since the 1D-REDIM is equivalent to the flamelet technique, it seems proper to use a flamelet with same boundary conditions (defined by the unburned mixtures) as initial condition for 1D-REDIM.

For a 2D-REDIM, several flamelets with the same conditions for the unburned mixtures can be computed and used to form the initial guess. The only drawback here is to define the boundary of the manifold, since the unburned mixtures do not provide conditions for all the boundary [38].

One strategy would be to take the flamelets with different strain rates, to cover the domain from stable flames until the extinction limit. As explained by Bykov *et al.* [12], the flamelet approach used for the initial guess represents a stationary solution set of detailed systems that are theoretically close to the REDIM for specific estimates of the gradient. To cover the domain where the flamelets do not exist, non-stationary flamelets (extinguishing) flames are chosen. The lower boundary will be a mixture line, i.e., a linear trajectory that connect the unburned mixture in the state space. Figure 4.3 shows the initial guess constructed with this approach for a methane/air flame, using N_2 and CO_2 parametrization.

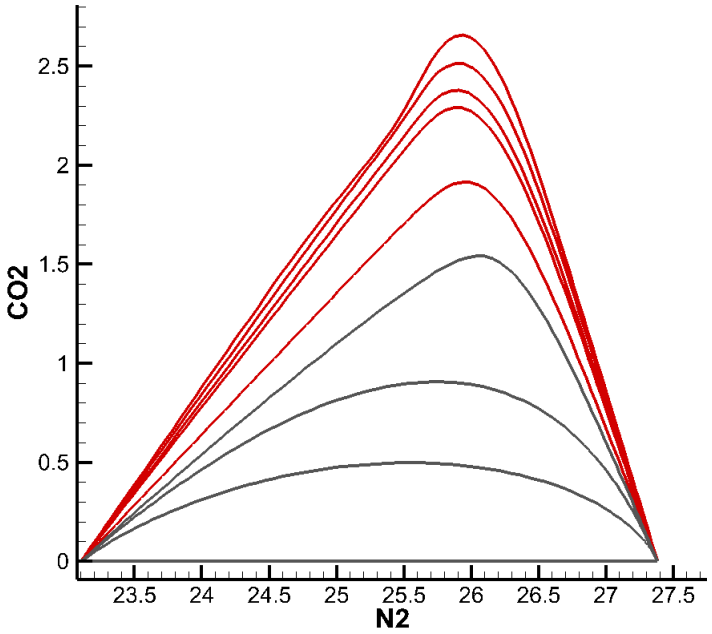

Figure 4.3: Initial guess manifold for the REDIM equation based on stationary and non-stationary flamelets solutions. Red lines show stable stationary flamelets solutions, while the gray lines show extinguishing non-stationary flamelets.

This strategy seems appropriate considering that the flamelet solution already consist in a low dimensional manifold itself. To obtain even better results, suitable boundary conditions should be applied to the flamelets, which ought to be the same as the flame to be simulated. One example could be the initial guess produced for the Sandia Flame D [1, 4], a turbulent piloted methane/air flame, presented in Fig. 4.4. The configuration of this flame consist in the main jet of fuel, a pilot, and a coflow of air. The initial manifold built considering the boundary conditions of the main jet, the pilot and the coflow covers a bigger region in the state space compared to the one build considering only the main jet and the coflow.

Having defined the initial guess, as the parametrization choice and the estimative of the gradients, the REDIM equation (4.59) is ready to be numerically solved. The next section will present an algorithm to solve it.

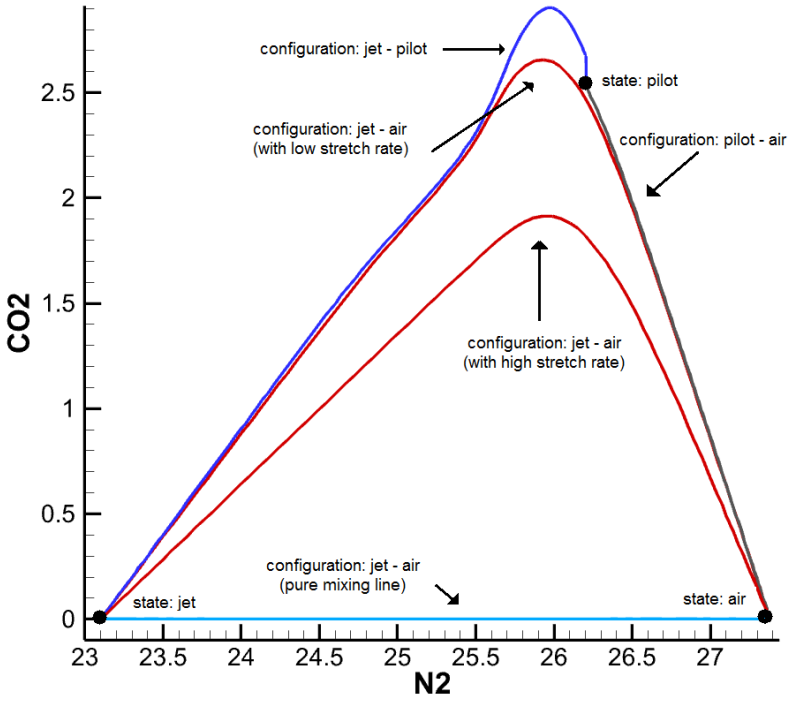

Figure 4.4: Initial guess based on specific mole fractions of N_2 and CO_2 as parametrization of the REDIM. Black dots represent the different states of Sandia Flame, colored lines represent different critical flamelets of laminar counterflow non-premixed flames.

4.3.4 REDIM algorithm

The method for solving Eq. (4.59) proposed by Bykov and Maas [11] are based on the assumption that existence, uniqueness and smoothness of the solution. The idea is to have an algorithm that is independent on the gradient estimates and represents a better way to overcome the dependence on the spatial coordinates.

Thus, an iterative process is suggested by determining automatically the parameter gradient as a function of the parameter itself. First, a constant approximation for the gradient $\mathbf{grad}(\theta) = \mathbf{c}$ is assumed for Eq. (4.59) in order to obtain the first approximation of the slow manifold $\mathbf{\Psi}^1(\theta)$. This constant approximation already provides an appropriate result for the reduced model, if the dimension of the reduced model is reasonably high [9].

The next step is to use the first approximation $\mathbf{\Psi}^1(\theta)$ to solve the following reduced model

$$\frac{\partial \theta}{\partial t} = \mathbf{\Psi}_\theta^{1+}\mathbf{\Phi}(\mathbf{\Psi}^1(\theta)), \tag{4.60}$$

which was derived from Eq. (4.40) using the chain rule and multiplying by $\mathbf{\Psi}_\theta^{1+}$. The solution of Eq. (4.60) provides a stationary solution $\theta^1(x)$ of the reduced model.

Then, θ^1 is used to correct the approximation of the gradient, making $\mathbf{grad}(\theta) = \mathbf{f}_1(\theta)$, where

$$\mathbf{f}_1(\theta) = \left.\frac{\partial \theta^1}{\partial x}\right|_{x=x^*} \tag{4.61}$$

The point $x = x^*$ is determined as follows: within the range of θ, a spatial coordinate x^* is defined which corresponds to some fixed value of the parameter θ^*.

With the improved approximation of the gradient, a new solution of Eq. (4.59) is calculated, $\mathbf{\Psi}^2(\theta)$, using $\mathbf{\Psi}^1(\theta)$ as initial guess. Then, $\mathbf{\Psi}^2(\theta)$ is used in Eq. (4.60) to update the gradient dependence $\mathbf{grad}(\theta) = \mathbf{f}_2(\theta)$. This iterative process is repeated until convergence is achieved.

The main steps to solve the REDIM equation an obtain the reduced slow manifold is summarized as:

1. An initial guess $\mathbf{\Psi}^0(\theta)$ is estimated for the reduced manifold;
2. The local coordinates gradient is estimated by $\mathbf{grad}(\theta) = \mathbf{f}_i(\theta)$, where $\mathbf{f}_0(\theta) = \mathbf{c}$;
3. Equation (4.59) is integrated to obtain a stationary solution $\mathbf{\Psi} = \mathbf{\Psi}^i(\theta)$;
4. Equation (4.60) is integrated to obtain a stationary solution $\theta = \theta^1$ and improve the gradients using Eq. (4.61);
5. Set $i = i + 1$ and return the step 2 until convergence is achieved.$\mathbf{\Psi}^2(\theta)$.

Therefore, as the gradient estimates is updated at each step of the integration, and the first estimate is always constant, the method depends only of the initial guess provided for initialization of the process.

4.4 REDIM calculated for ethanol

In this section, the methodology for generating the 2D-REDIM for ethanol is presented, whose validation will be shown in Chapter 5. The algorithm explained in last section was used. Therefore, it was only needed to find the initial guess for integration of Eq. (4.59). The variables chosen for parametrization are the specific mole fraction of N_2 and CO_2, accounting for the mixture process and the reaction progress, respectively.

The initial manifold is given by detailed simulations of counterflow non-premixed flames, varying the pressure gradient J. A non-stationary flamelet was also simulated to fill out a major part of the state space. The boundary conditions are the same as the experimental conditions used in the work of Saxena and Williams [90]. This is because the data from this work will be used to validate the REDIM. The conditions are shown in table 4.1. The simulations were done with the codes INSFLA and HOMREA, which integrates Eq. (4.59) [62].

The pressure gradient varied from $J = -1.0 \times 10^3$ to $J = -1.0 \times 10^5$, the last stable flame considered. The extinguished flame is simulated with $J = -2.0 \times 10^5$, as well as the non-stationary solutions. This is shown in Fig. 4.5 where the solutions are projected in the $N_2 - CO_2$ plane.

The initial guess is used to start the integration of Eq. (4.59), where the estimation of the gradients follows the algorithm of the last section. After convergence, the REDIM built is presented in Fig. 4.6 in the $N_2 \times CO_2 \times OH$ and $N_2 \times CO_2$ planes. The initial counterflow flames are also displayed to show that

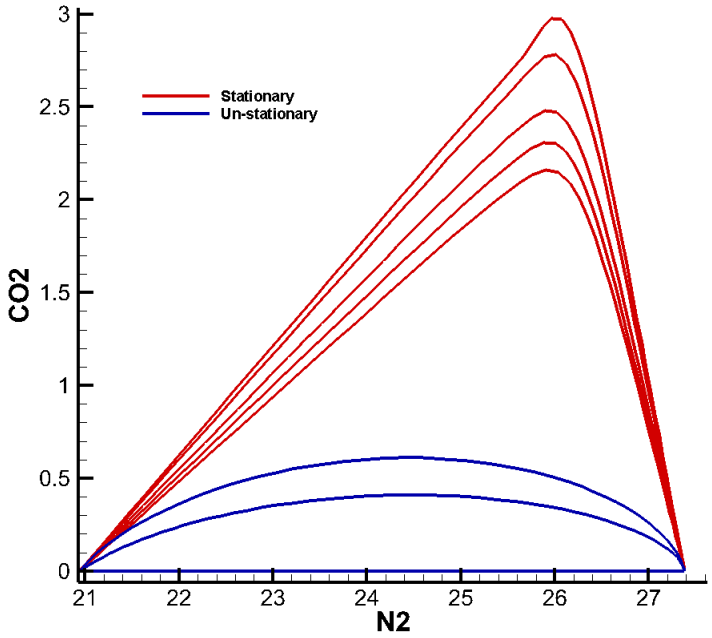

Figure 4.5: Initial guess for the REDIM of ethanol based on counterflow non-premixed flames. The red lines represent the stable flames and the blue the non-stationary and extinguished flames.

the initial guess is already within the manifold, and thus confirming the already mentioned that the flamelet is equivalent to a 1D-REDIM. The projections of temperature, specific mole fractions of H_2O, CO and OH in the 2D-REDIM is shown in Fig. 4.7.

It can be observed that the reaction zone is very well defined in the REDIM in the region of high temperature. It is also in that region that important

Table 4.1: Conditions used in the simulation of counterflow flames to obtain an initial guess for REDIM. The species quantities are given in mole fractions.

	Fuel stream	Oxidizer stream
$X_{C_2H_5OH}$	0.3	0
X_{N_2}	0.7	0.79
X_{O_2}	0	0.21
Velocity (cm/s)	29.8	30
Temperature (Kelvin)	340	298
Pressure (atm)	1	1

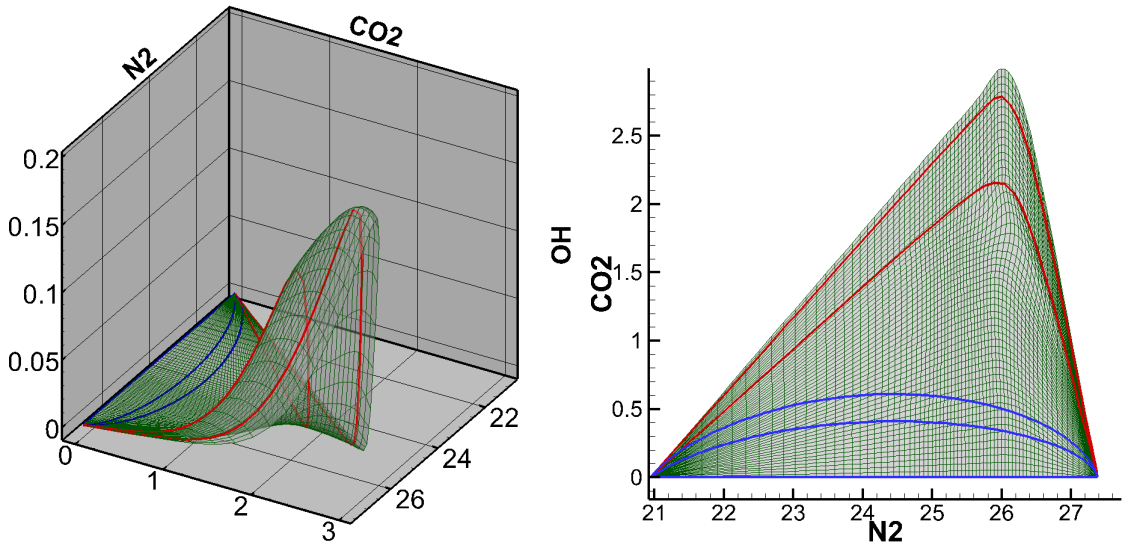

(a) (b)

Figure 4.6: Representation of the REDIM in the (a) $N_2 \times CO_2 \times OH$ and (b) $N_2 \times CO_2$ planes. The initial guess is also displayed to show its validity.

intermediate species are formed, such as CO and OH. Water is formed almost in all the region reached by the REDIM, where the highest amount is formed not in the region of the highest temperature, but slightly prior to that. This results show that the dynamics of the production/consumption of species are greatly described by the chosen parametrization.

The results presented here show that the reduced model will reproduce with accuracy the dynamics of the solution of counterflow non-premixed flame of ethanol. The task now is to validate this result using the REDIM to calculate a flame, that is, describe the thermodynamics parameters as a function of the two chosen parametrization variables N_2 and CO_2. This will be showed in Chapter 5.

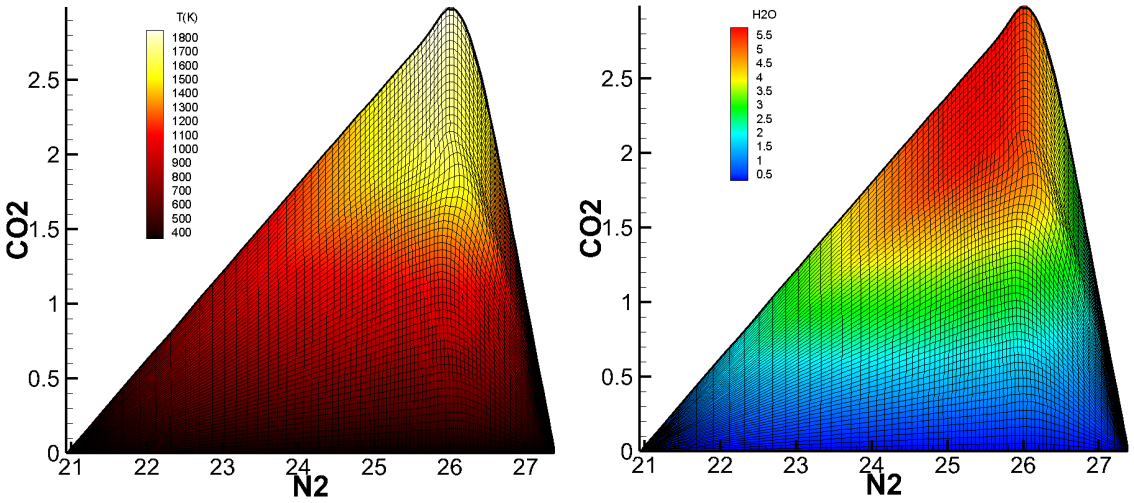

(a)

(b)

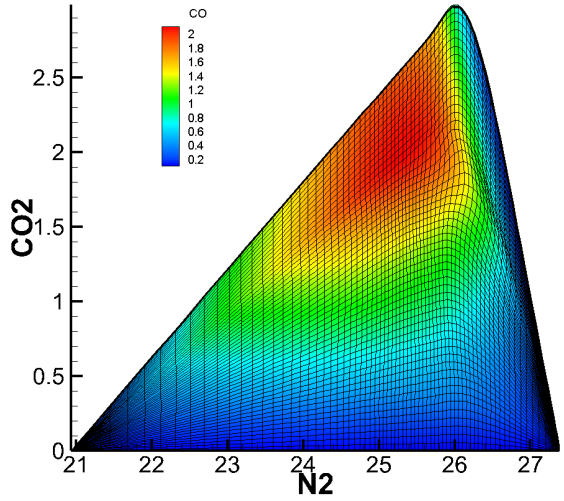

(c)

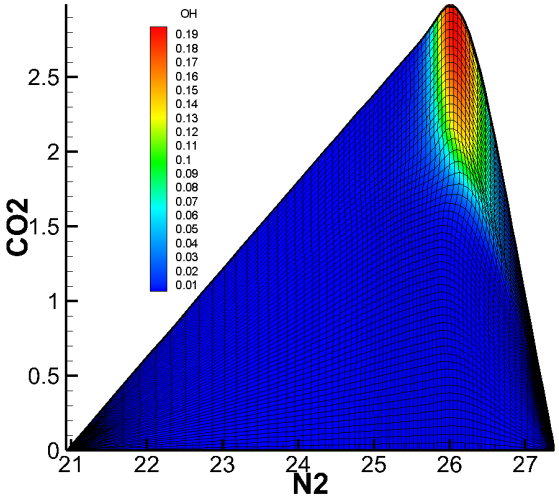

(d)

Figure 4.7: Projections of (a) temperature and specific mole fractions of (b) H_2O, (c) CO and (d) OH in the 2D-REDIM.

5 VALIDATION AND NUMERICAL RESULTS

This chapter has the goal of presenting the validation of the skeletal mechanism presented in Chapter 3 and that of the reduced model based on REDIM developed in Chapter 4. For the DRG, validation is carried out comparing the results of both the detailed and the skeletal mechanisms in a freely propagation premixed flat flame and an ideal gas reactor. Counterflow flames are simulated also for non-premixed and premixed configurations, and these calculations are compared with data available in the literature.

5.1 Skeletal mechanism validation

This section presents the numerical simulations for validating the skeletal mechanism developed with DRG. The simulations of this section were all carried out with Cantera.

5.1.1 Reactor simulations

A chemical reactor is defined as a device developed in order to let reactions occur under controlled conditions. This is a 0D simulation, that is, it varies only time and it has non spatial dependence, and consists in the simplest form of a chemically reaction system. The first simulation performed is a batch reactor, a closed adiabatic thermodynamic system with constant pressure.

The batch reactor is used to catch the autoignition time of the mixture. With Cantera, a reactor can be viewed as a box reduced to a single point, such that there is no spatial evolution but only temporal evolution of the quantities it contains. Thus, the evolution in time is carried out with a network of reactors, i.e., multiple reactors are interconnected, and the mass and heat flow among them are realized.

The total mass of the reactor's contents changes as a result of flow through the reactor's inlet and outlets, and production of homogeneous phase species on the reactor walls [30]

$$\frac{dm}{dt} = \sum_{in} \dot{m}_{in} - \sum_{out} \dot{m}_{out} + \dot{m}_{wall}, \tag{5.1}$$

where m is the mass of the reactor's content (in kg), $\dot{m}_{in}$, $\dot{m}_{out}$ and $\dot{m}_{wall}$ the inlet, outlet and wall mass flow. The species conservation equation is given by

$$m\frac{dw_i}{dt} = \sum_{in} \left[\dot{m}_{in}\left(w_{k,in} - w_k\right)\right] + \dot{m}_{k,gen} - w_k\dot{m}_{wall}, \tag{5.2}$$

where $\dot{m}_{k,gen}$ is the total rate at which species k is generated. The energy equation is given in terms of temperature,

$$\begin{aligned} mc_v\frac{dT}{dt} &= \sum_{in}\left[\dot{m}_{in}\left(h_{in} - \sum_k u_k w_{k,in}\right)\right] \\ &- \frac{pV}{m}\sum_{out}\dot{m}_{out} - \sum_k \dot{m}_{k,gen}u_k - \dot{Q}, \end{aligned} \tag{5.3}$$

in which V is the volume (in m^3), h the enthalpy, p the pressure, u the internal energy and $\dot{Q}$ the heat release.

Cantera uses CVODE from SUNDIALS (a suite of nonlinear and differential/algebraic equations solver) for ODE integration, developed by Lawrence Livermore National Laboratory [18]. CVODE is a package for solving initial value problems both stiff and non-stiff, using variable-coefficient Adams and varying-order backward differentiation formulas (BDF) methods.

The autoignition time is defined as the point where the temperature increases considerably from low to high values, and the simulations are calculated varying the equivalence ratio and pressure. The initial temperature is $T = 800K$, and the time step is set to $\Delta t = 5 \times 10^{-2}$. The same configuration is applied to the detailed and skeletal mechanism. The results are presented in Fig 5.1

Results show that the skeletal mechanism predicts very well the detailed model. This is expected, since the DRG was used using autoignition as an

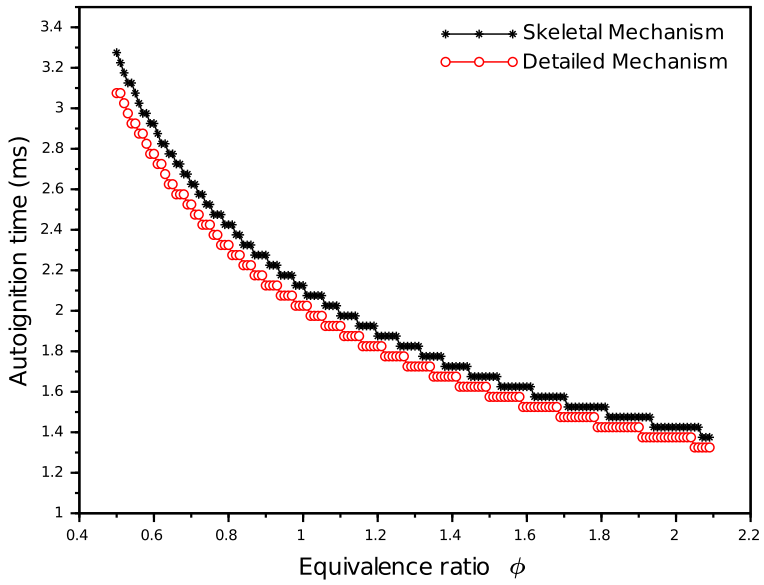

(a)

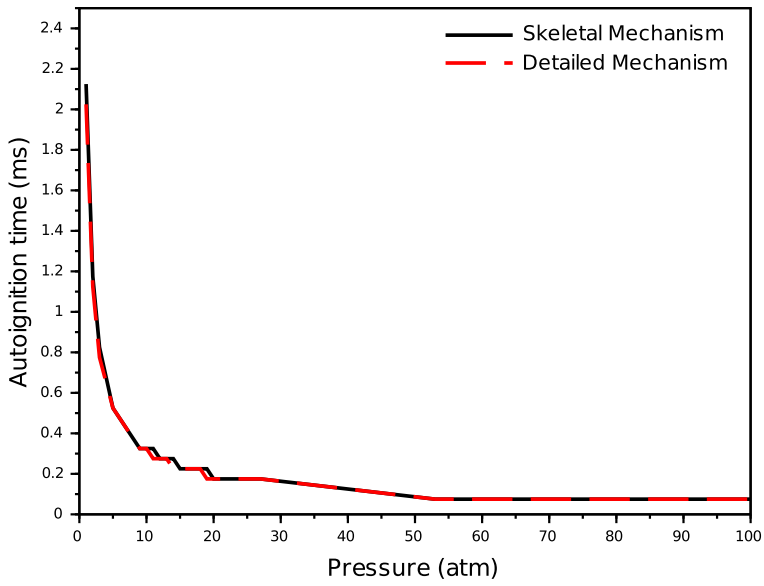

(b)

Figure 5.1: Autoignition time in milliseconds (ms) for both skeletal (black) and detailed (red) mechanisms for different (a) equivalence ratios and (b) pressure.

Table 5.1: Error percentage for selected values of equivalence ratio and pressure for the autoignition calculates in a batch reactor. Pressure is given in atm and autoignition times in milliseconds (ms).

Equivalence ratio				Pressure			
ϕ	Skeletal ignition	Detailed Ignition	Error	Pressure	Skeletal ignition	Detailed Ignition	Error
0.5	3.274	3.074	6%	1	2.125	2.025	4%
0.6	2.874	2.724	5%	2	1.175	1.125	4%
0.7	2.624	2.474	6%	3	0.825	0.775	6%
0.8	2.424	2.324	4%	5	0.524	0.524	0%
0.9	2.274	2.125	7%	6	0.474	0.474	0%
1.0	2.125	2.025	4%	7	0.424	0.424	0%
1.1	1.975	1.925	2%	9	0.324	0.324	0%
1.2	1.875	1.825	2%	10	0.324	0.324	0%
1.3	1.825	1.725	5%	12	0.275	0.275	0%
1.4	1.725	1.675	2%	13	0.275	0.275	0%
1.5	1.675	1.575	6%	15	0.225	0.225	0%
1.6	1.625	1.525	6%	16	0.225	0.225	0%
1.7	1.575	1.475	6%	17	0.225	0.225	0%
1.8	1.525	1.425	7%	18	0.225	0.225	0%
1.9	1.475	1.425	3%	20	0.175	0.175	0%
2.0	1.425	1.375	3%	100	0.075	0.075	0%

application. All errors are below 7%, as can be seen in Tab. 5.1. From pressures above 20 atm, there is no difference in the predictions of the detailed and skeletal mechanisms, and this happens since for higher pressures, the temperature within the reactor is increased. Thus, the initial temperature is enough to set the gas almost close to ignition. This justifies also why for this range ($p > 20$ atm), the autoignition time remains almost constant. Figure 5.1(a) shows that a lean flame has higher autoignition time that a very rich flame ($\phi = 2.0$), that is, the higher the amount of oxidizer, the higher is the time inside the reactor before ignition.

The reactor network was also calculated for a stoichiometric mixture of ethanol and air

$$C_2H_5OH + 3(O_2 + 3.76N_2) \quad \Rightarrow \quad 2CO_2 + 3H_2O + 11.28N_2. \tag{5.4}$$

The initial temperature is also $T = 800K$ and the time step is $\Delta t = 5 \times 10^{-3}$.

Results are displayed in Fig. 5.2. It can be observed that the temperature and the fuel mass fraction is precisely well described by the skeletal mechanism, while the species mass fractions of OH, CO_2, O_2 and CO show very good result, despite a small deviance.

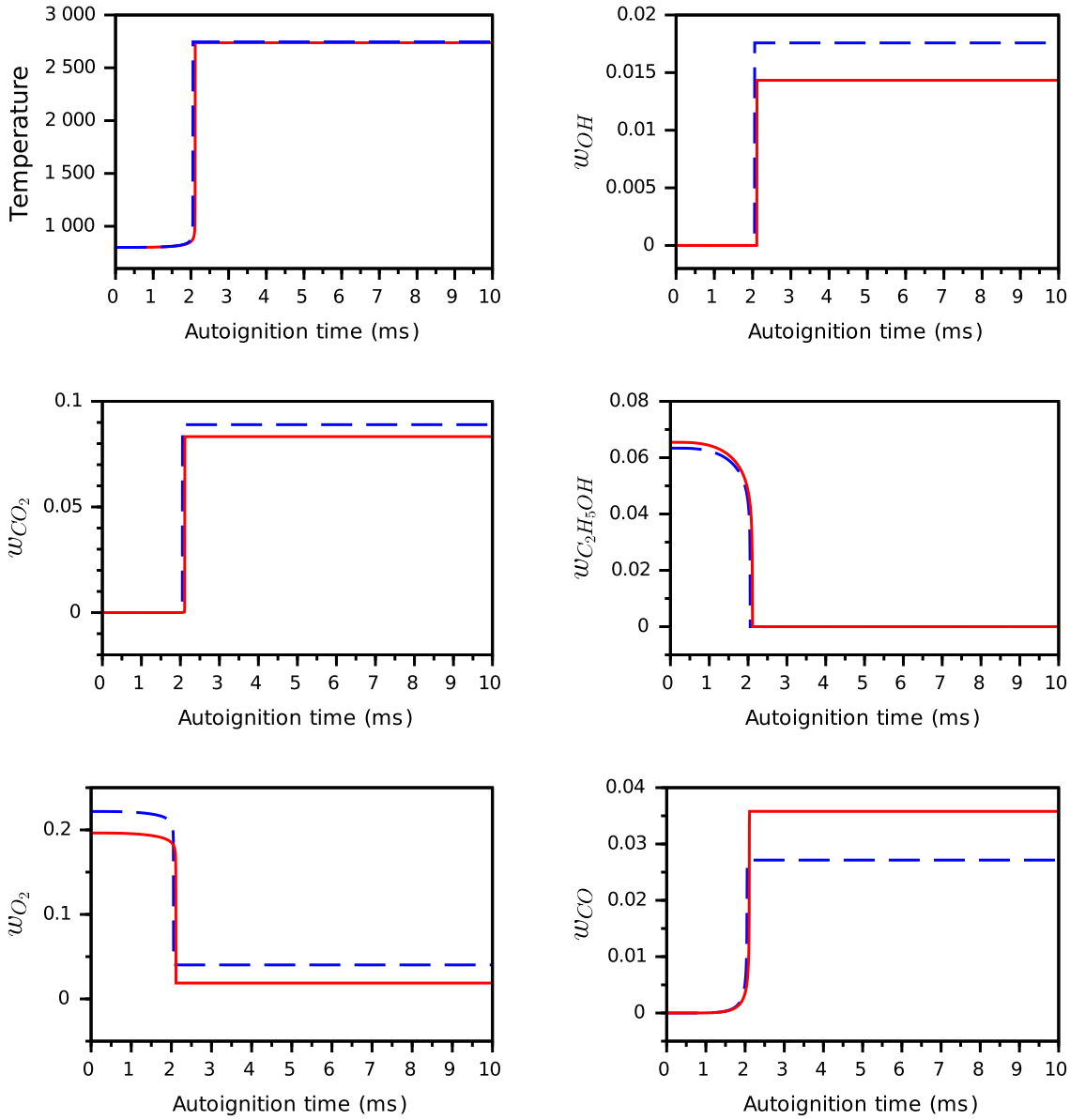

Figure 5.2: Autoignition time in milliseconds (ms) for a stoichiometric mixture of ethanol of selected species. The blue dashed line represent the detailed mechanism while the red line is the skeletal.

5.1.2 Premixed flame

The solution of a freely propagation premixed flat flame with Cantera follows the axisymmetric stagnation-flow equations presented in section 2.3.1. The goal is to calculate the laminar flame speed for different values of equivalence ratio, for both the skeletal and detailed mechanism.

The integration of equations with Cantera uses the following user-specified values:

a) tolerance values for the Newton integration;

b) maximum number of iterations before a Jacobian is re-computed;

c) time stepping values for the Newton time-stepping iterations;

d) grid refinement settings.

The finite-difference method is used to discretize the flow equations and form a system of non-linear algebraic equations. A hybrid using Newton method with time-stepping algorithm is them applied to solve the system. For transient problems, if the Newton iteration fails to find the steady-state solution, a pseudo-transient problem with a larger domain is attempted to be solved. This problem is constructed by adding transient terms in each conservation equation where this is physically reasonable. Thus, the proceeding solution is to take a few time steps and try to solve the steady-state problem. If this is not achieved, more time steps are taken and the calculation is repeated until steady-state Newton succeeds.

Cantera uses an initial coarse grid, with few points, to obtain a converged solution, in which the procedure of solution was explained above. A first flame is calculated and the results are saved and used for a new simulation, refining the grid, specially in the boundary values and reaction zone. This procedure is repeated until a converged solution is obtained in a thin grid.

For the inlet boundary located at a point z_0 where there is an inflow, values are supplied for the temperature, the species mass fractions for fuel and oxidizer. In the outlet boundary, Neumann boundary conditions is applied for those values.

The simulations for this work is as follows: the initial temperature $T = 298K$ and initial pressure $p = 1$atm is defined, as well as the initial compositions of the mixture, which depends on the equivalence ratio ϕ considered. The initial ϕ is set to $\phi = 0.5$ and ranges until $\phi = 2.0$, covering very lean and rich flames. An initial grid is also defined in the z-direction for a domain with 0.02cm. The relative and absolute error tolerances for the Newton integration and the time-stepping is defined as 1×10^{-5} and 1×10^{-9}. The maximum number of iterations that the Jacobian will be used before it must be re-evaluated is 50. The time step is set to $\Delta t = 1 \times 10^{-5}$.

The first flame calculated is without the energy equation, to obtain a first converged solution. With this result stored, another flame is calculated, now with the energy equation. A total of eight flames is used to obtain the steady-state converged solution for the problem of this work.

Figure 5.3 shows the comparison of the results between skeletal and detailed mechanism for the laminar flame speed calculated with the flat flame. It can be seen that the lean zone of the flame shows practically the same results, and for $\phi > 0.8$, results show a small deviance. This is normal since several intermediate reactions were withdraw of the mechanism, which influences in the calculated laminar flame speed s_L, which depends of the activation energy. For $1.4 \leq \phi \leq 1.8$, the deviations between the models are bigger, which does not influence the validity of the model, since in most practice applications, combustion processes occur in lean-stoichiometric configurations.

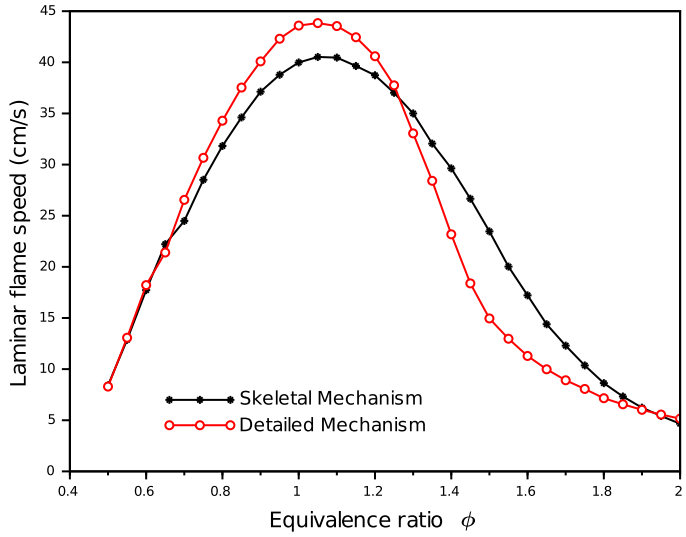

Figure 5.3: Laminar flame speed calculated in a freely propagating flat flame for ethanol. Black lines describe the skeletal and red lines the detailed mechanism.

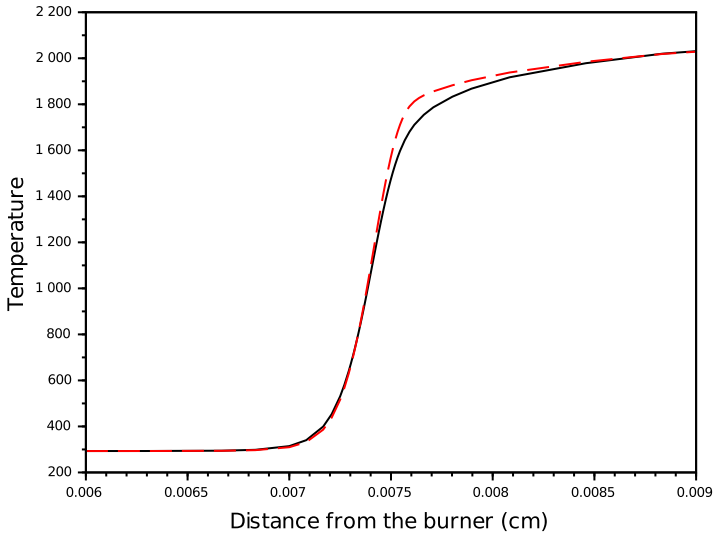

Figure 5.4: Premixed flat flame results profiles of temperature for both the skeletal (black) and detailed (red) mechanisms.

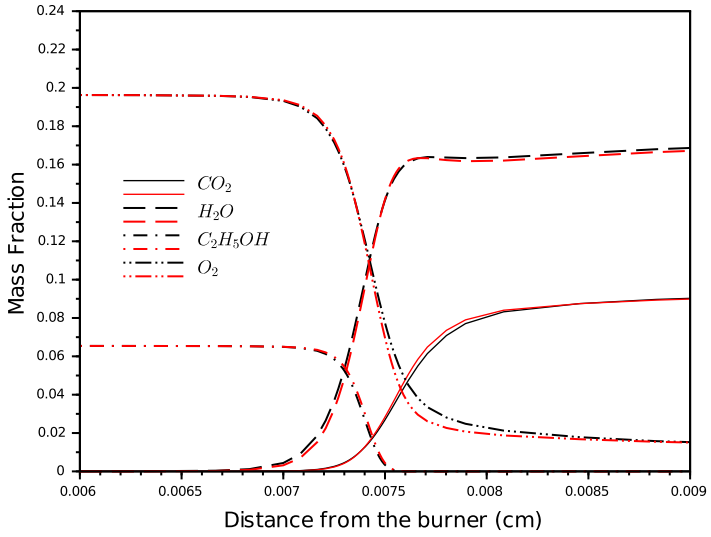

(a)

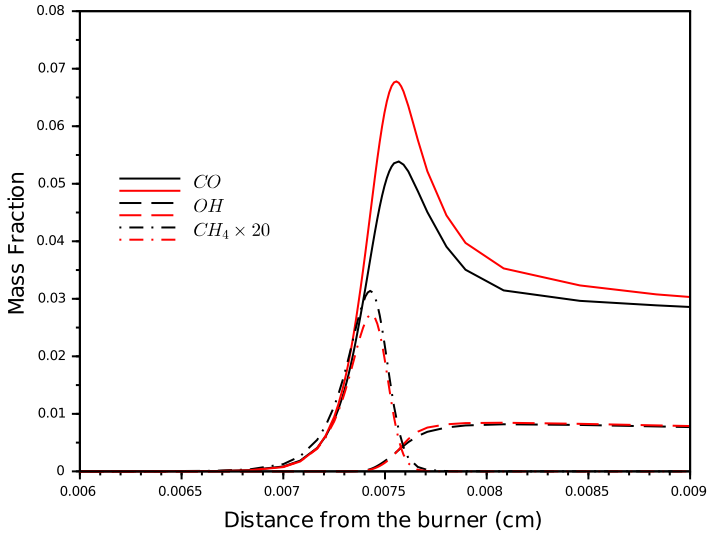

(b)

Figure 5.5: Premixed flat flame results profiles for mass fractions of (a) C_2H_5OH, O_2, CO_2, H_2O and (b) CO, OH, CH_4 for both the skeletal (black) and detailed (red) mechanisms.

Results for temperature and mass fractions of C_2H_5OH, O_2, CO_2, H_2O, CO, OH and CH_4 for a stoichiometric freely ($\phi = 1$) propagating premixed flat flame, with initial temperature $T = 298K$, are shown in Figs. 5.4 - 5.5. The skeletal mechanism reproduces very well all quantities displayed, consisting in the main products of combustion and some important species and radicals. The domain in calculations were also set to 0.02cm, but the figures display the region from 0.006cm to 0.009cm, where the preheat and the reaction zones are more visible.

5.1.3 Counterflow flames

Albeit counterflow flames is not used in DRG as an application, it consists in one of the best simulations to validate a reduced model, since this type of flame takes into account diffusion processes. Besides that, a good result from counterflow simulations can indicate that the skeletal mechanism will provide a good and reliable result for 2D or 3D CFD simulations, specially turbulent flows modeled using the flamelet concept.

The numerical procedure to calculate a counterflow flame with Cantera follows the same procedure explained in the last section, although Eqs. (2.90) - (2.94) are used for integration. Other difference from the calculations of the flat flame is that both boundary conditions are prescribed, and for this work, the values used for temperature, initial mole fractions and velocity is displayed in Table 4.1 for both streams. Those values are for a non-premixed flame and are used since consists in the same values of the experiment carried out by Saxena and Williams [90].

The experimental counterflow burner consists of two opposing ducts of 23.1mm inner diameter with shielding of annular nitrogen curtains separated by 12mm. Air flows from the top duct and fuel through the bottom duct at flow rates adjusted according to a momentum balance to maintain the stagnation plane halfway between the duct exits. An insulated vaporizer, temperature-controlled to provide

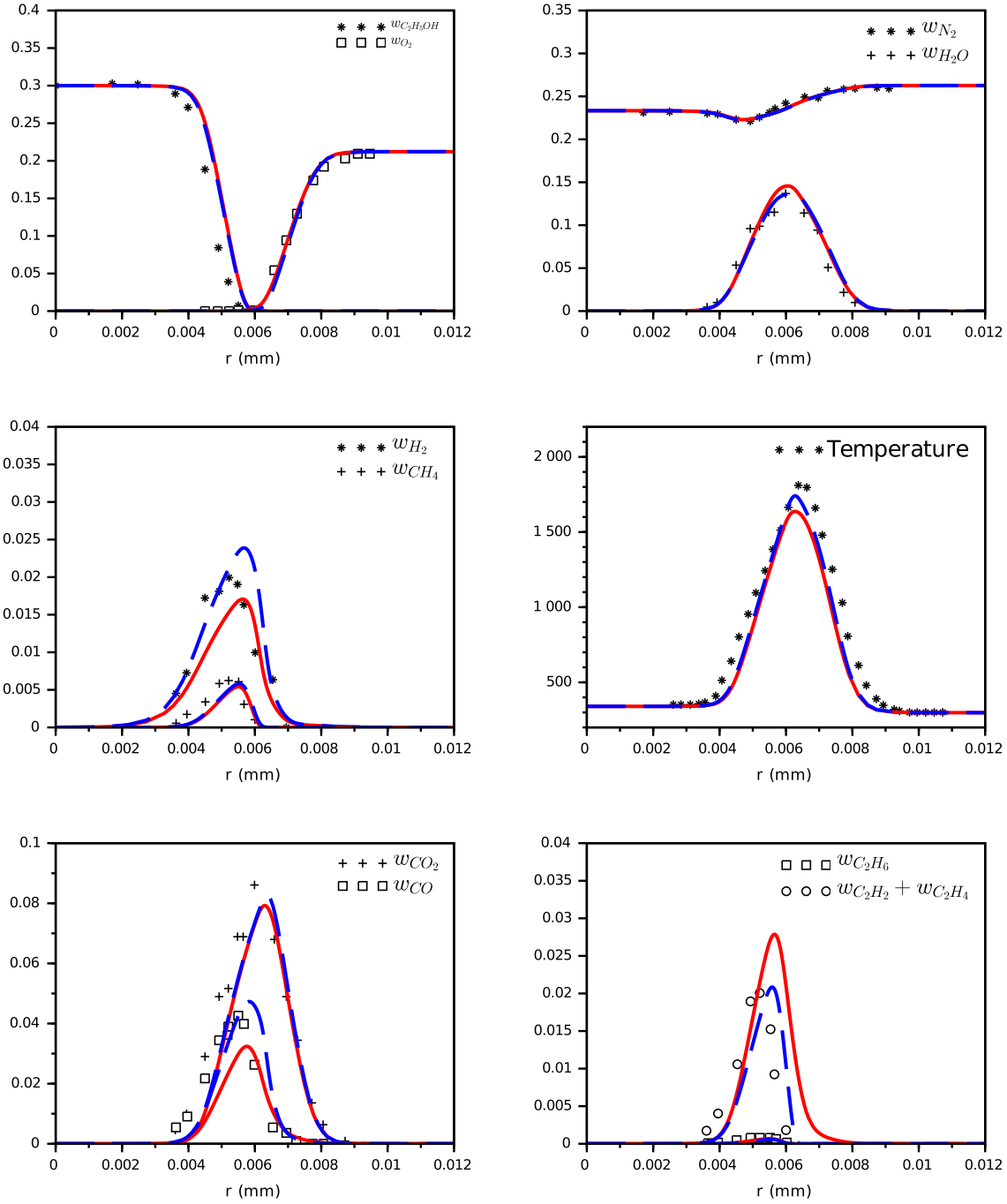

Figure 5.6: Species mass fractions of species and temperature for a non-premixed counterflow flame. Symbols represent experiment [90], blue dashed and red lines are from numerical simulation with detailed and skeletal mechanisms, respectively.

Table 5.2: Conditions used in the simulation of premixed counterflow flames. Species quantities are given in mole fractions.

	Fuel stream	Oxidizer stream
$X_{C_2H_5OH}$	0.1385	0
X_{N_2}	0.6803	0.79
X_{O_2}	0.1812	0.21
Velocity (cm/s)	30.22	30
Temperature (Kelvin)	327	298
Pressure (atm)	1	1

the desired ethanol mole fraction in nitrogen, generates the fuel vapour which flows through a heated line to the lower duct.

Figure 5.6 shows the results of the counterflow non-premixed flame of an ethanol/air mixture. The results of the skeletal mechanism reproduces exactly the detailed for the principal reactants and products. Over-prediction can be seen in the summation of the mass fractions of C_2H_2 and C_2H_4, while under-prediction occurs for CO and H_2. The adiabatic maximum temperature achieved by the skeletal mechanism is $T = 1637K$, while the detailed results in $T = 1740K$ and the experimental value is $T = 1811K$. Despite that, the results of the reduced model shows that it can be used in other simulations, validating that the results will remains in an acceptable error range.

Comparisons are also shown for a premixed counterflow flame in Fig. 5.7, since there is also experimental data available for this configuration. The initial values are displayed in Table 5.2. The same results are observed that from the non-premixed flames, with over-prediction for the summation of C_2H_2 and C_2H_4, and under-prediction for CO and H_2. However, the temperature profile shows exactly the same values for detailed and skeletal mechanism, with a peek in $T = 1990K$ and $T = 1991K$, respectively. The experiment yields $T = 2151K$.

Results for both calculations, premixed and non-premixed, of counterflow flames shows that the skeletal mechanism can reproduce with accuracy the

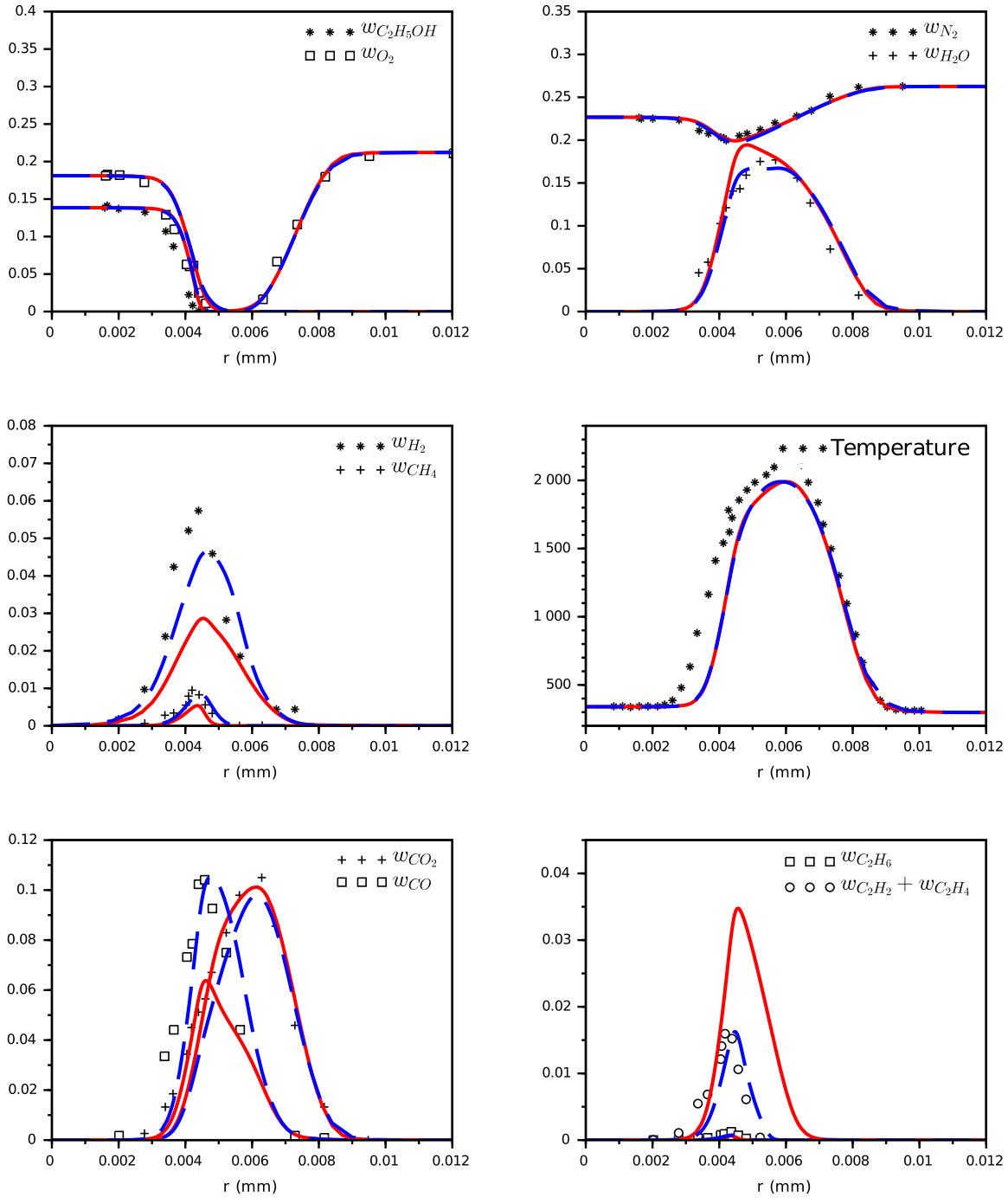

Figure 5.7: Species mass fractions of species and temperature for a premixed counterflow flame. Symbols represent experiment [90], blue dashed and red lines are from numerical simulation with detailed and skeletal mechanisms, respectively.

existing diffusion processes in reactive flow simulations. It is interesting to observe in the previous figures the difference in the results of premixed and non-premixed flames. For instance, the temperature for premixed is approximately 300K higher than that of non-premixed flames, i.e., premixed flames require higher temperatures for reaction to occur.

Another difference that can be seen in the figures is that premixed flames produce higher quantities of CO, while the quantities for CO_2 are practically the same. This can be explained since there is a higher amount of oxygen in the fuel side of the burner, which also makes the production of CO to start sooner in the domain. Presence of oxygen also explains why the fuel is consumed earlier in premixed flames, which influence the mass fraction of H_2, that is almost two times the value for non-premixed.

5.2 REDIM validation

The 2D-REDIM built in section 4.4 is now validated also for a counterflow non-premixed flame. Again, the parameters used are those from Table 4.1, but the simulations were carried out with the code INSFLA, since this code has a subroutine to perform simulations with the reduced model.

Figure 5.8 shows the result of the simulation. The species are given in specific mole fractions, since the parametrization uses this description. It can be seen that the reduced model reproduces exactly the calculation with the detailed mechanism. Also, the results show that the parametrization chosen yields good results, and that a two dimensional slow manifold can reproduce with great capability a one dimensional simulation.

Figure 5.9 shows the comparison between experimental data from [90] and numerical simulation using REDIM. As the REDIM reproduces exactly the

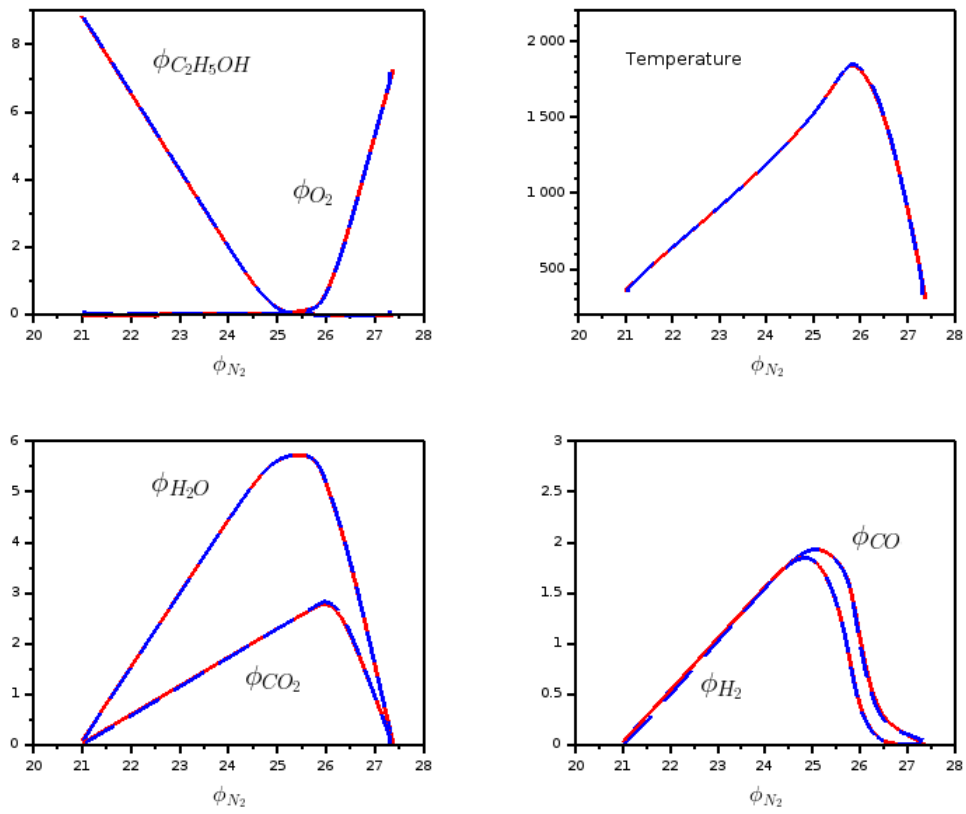

Figure 5.8: Profiles for temperature and specific mole fractions for selected species. The blue dashed lines are the REDIM results and red lines are the simulation with the detailed mechanism.

detailed mechanism (see Fig. 5.8), it's expected that it yields the same behaviour of the full model against the experiment. This happens to all values, but a small difference is observed in the temperature profile. This can be result of numerical instabilities in the different codes that were used for these simulations.

The results for REDIM and the skeletal mechanism presented in the last section can be used to analyze the difference between these two approaches. An advantage of using REDIM is that, for the right set of parametrization, initial and boundaries conditions, it will reproduce the detailed mechanism with almost no difference. This is not seen in the skeletal mechanism since, even though it has an acceptable accuracy, some parameters are either over or under predicted.

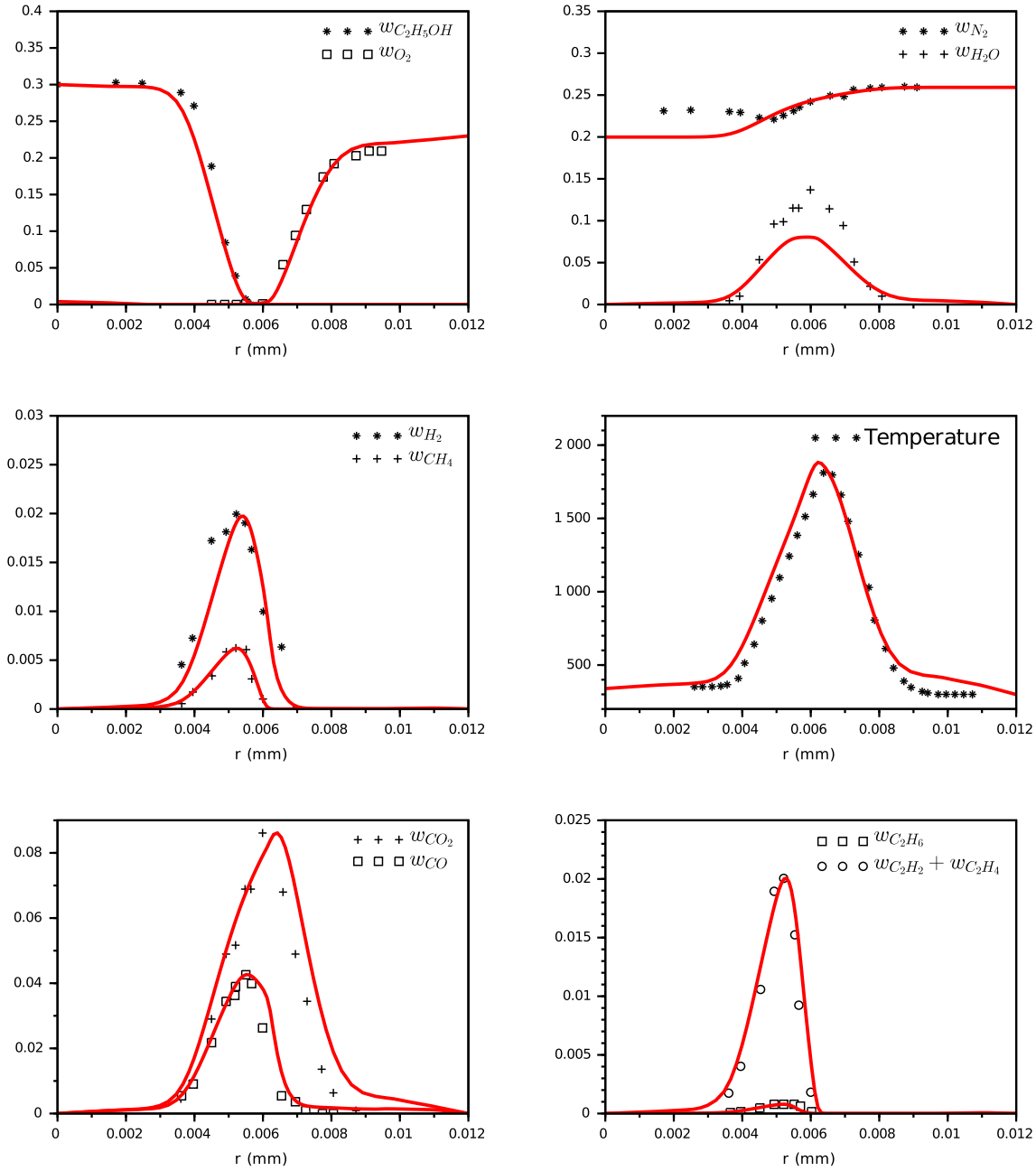

Figure 5.9: Comparison between experiment and simulation using REDIM. Symbols are the experimental data [90] and lines the REDIM.

That difference can be extended between skeletal mechanism generation and model reduction techniques, since the latter will always use the thermodynamic information within the system, while the first needs *a priori* information about the kinetics of the model. The computational cost can also be analyzed and, in this matter, the REDIM resolved faster all simulations that were held in this work.

Nevertheless, it is important to emphasize that, although the time and the results look better for the REDIM, this method is not universal, and different REDIMs may have to be produced for different combustion applications. The more universal character of DRG is an advantage, since even if an application is not used within its implementation, the resulting skeletal mechanism can produce an accurate result for this situation. The studies aiming kinetics information are better appropriate using skeletal mechanisms, while REDIM will be more suitable for heavy computational CFD simulations involving high chain hydrocarbons and alcohols.

5.3 A hybrid DRG-REDIM

Simulations of larger molecules can be computational prohibitive, independent of the technique to be used. For instance, detailed mechanisms of biodiesel fuels can have thousand of reactions and hundreds of species. To reproduce the main features of oxidation, a skeletal mechanism for these fuels will still have a high number of species and reactions. If the REDIM would be applied, the generation of the initial profile and the integration of the REDIM equation until convergence would take a lot of computational time.

Thus, a different approach is presented here. It consists of using both strategies, the DRG and the REDIM. The idea is to develop a skeletal mechanism that accurately reproduces the detailed mechanism and then, uses this mechanism to built the REDIM.

The approach was used for the results obtained in this work. The skeletal mechanism generated was used to built the REDIM with the same configurations that the REDIM built with the detailed mechanism. Figure 5.10 show the simulation of a counterflow non-premixed flame, with the parameters of Table 4.1. The results show the comparison of the skeletal mechanism and the REDIM built with this and, as expected, there is practically no difference.

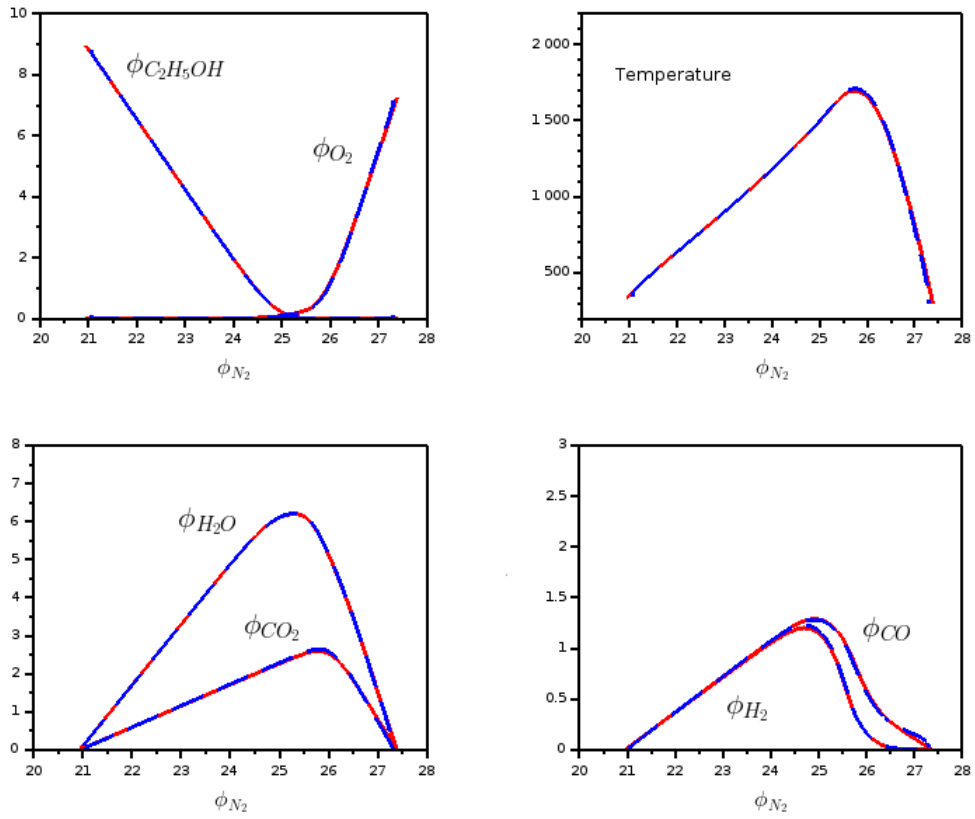

Figure 5.10: Temperature and specific mole fractions of selected species for a counterflow non-premixed flame, using the hybrid DRG-REDIM. Blue dashed lines are the REDIM red lines are the simulation with the detailed mechanism.

The hybrid DRG-REDIM model was also compared with the experimental data, and the results are shown in Fig. 5.11. The model also predicts with good accuracy the experiment, although differences from the REDIM built with the detailed (see Fig. 5.9) are observed. The maximum temperature is achieved ear-

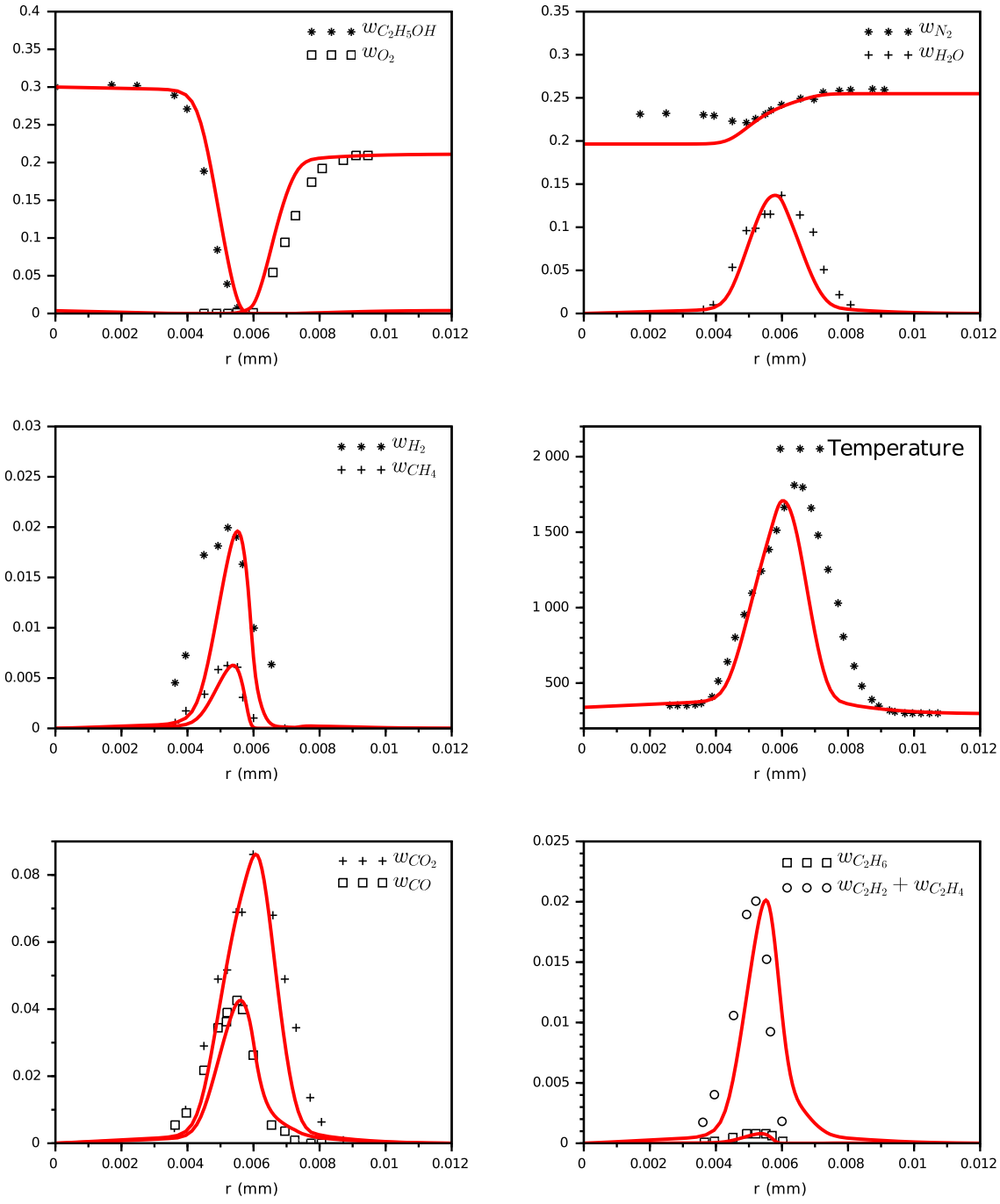

Figure 5.11: Comparison between experiment and simulation using the hybrid DRG-REDIM model. Symbols are the experimental data [90] and lines the REDIM.

lier and has a smaller value compared to the experiment, but within an acceptable range. CO_2 and CO show a very good result, as the standard REDIM had already predicted.

A conclusion that can be done looking to Figs. 5.8 and 5.10 is that the REDIM will predict with accuracy the mechanism that is feed for calculation. This means that, if the skeletal mechanism reproduces with accuracy the full mechanism, the REDIM built for this will also provide good results. This strategy may not show a huge improvement in computational cost for ethanol, but when applied to bigger mechanism, it will provide a very interesting tool. Using the right parameters, a mechanism with thousand of reactions can be reduced to a few hundreds with DRG, and then the REDIM will not be a problem to solve.

6 CONCLUSION

Numerical simulations of reactive flows, such as combustion processes, require high order methods with small time steps for its solution, enhancing the stiffness of the system. The chemical source term, appearing in the species conservation equations, is a difficult task since it is influenced by mixing, molecular transport and chemical kinetics. Thus, modeling is necessary and different strategies for are used to solve this issue.

One type of strategy would be the skeletal mechanism generation, where the kinetic information of the reaction coefficients are often used to describe the relation of species and reactions, and in this way define important, necessary and redundant species, where the latter will be removed, yielding a kinetic mechanism with less reactions. Among the methods, the DRG provides a simple approach to understand the coupling of species and to identify those that are not needed for describing the main features of combustion simulations. It is a simple technique to implement with more general results, depending on the number of application and range of parameters defined.

Time scale analysis is another type of strategy that can be used to reduce chemical kinetics. The idea behind is that in chemical systems, there is a gap in the time scales of species concentration along the oxidation process, and in this way, after some time, the system dynamics will always be described by the slowest time scales. This idea yields the existence of low dimensional manifolds in the state space that attracts all trajectories of species concentration and therefore can be used to calculate all thermodynamical properties of the system. In this sense, the advantage of REDIM among the techniques is that it takes into account both reaction and transport to find the low-dimensional manifold.

The main difference of these type of strategies is that while the skeletal mechanism explicitly generates a new mechanism, with less species and reactions, the manifolds technique is used to reduce the number of equations that will be used to solve the reactive system. The latter states that all thermodynamic variables will be calculated as a function of the variables that parametrizes the manifold.

The purpose of the present work was to analyze the difference between these two techniques (DRG and REDIM) for the oxidation of ethanol, a biofuel that has been an increasing usage in industry. A comprehensive study that compares which type of strategy produces a more reliable result with less computational effort was performed, and numerical simulations of premixed and non-premixed configurations, as well as 0D scenarios, were used to validate the models.

The advantage of using REDIM is that, for the right set of parametrization and initial guess, it will reproduce the detailed mechanism with almost no difference. This is not seen in the skeletal mechanism since, even though it has an acceptable accuracy, some parameters are either over or under predicted. That difference can be extended between skeletal mechanism generation and model reduction techniques, since the latter will always use the thermodynamic information within the system, while the first needs *a priori* information about the kinetics of the model. Nevertheless, REDIM is not universal, and different REDIMs may have to be produced for different combustion applications. The more universal character of DRG is an advantage, since even if an application is not used within its implementation, the resulting skeletal mechanism can produce an accurate result for this situation.

The simulations with both strategies leads to the idea of coupling them, which can be used for high chain hydrocarbons and alcohols. The DRG is first applied to a large mechanism to produce a smaller one, which then is used to built the REDIM. This strategy will decrease the computational cost of generating the initial guess and integration of the REDIM. If the skeletal mechanism reproduces

with accuracy the full mechanism, the REDIM built for this will also provide good results.

Another conclusion that can be made using the hybrid DRG-REDIM is that the REDIM will always reproduce with a very good accuracy the detailed model. Thus, the better the skeletal mechanism, the better will be the results of the REDIM. This is an important feature since, to produce a most accurate model with DRG, a higher set of applications and parameter's range ought to be used, enhancing the size of the skeletal mechanism. The results presented in this work show that a reduction of approximately 50% in the number of reactions to obtain the skeletal mecanism will provide a good result for REDIM. When dealing with mechanisms with thousands of reactions, the hybrid model can produce a large reduction in computational cost.

Therefore, the contributions that were developed in this work are summarized as:

1. a new skeletal mechanism for ethanol consisting of 37 species and 184 reactions that reproduces the detailed mechanism with accuracy and has a comparable size to others found in the literature;
2. a REDIM for ethanol that can be used for CFD simulations;
3. a new methodology consisting of a hybrid DRG-REDIM, that yields accurate results and it is aimed to be applied to very large detailed mechanisms.

BIBLIOGRAFIA

[1] International workshop on measurement and computation of turbulent nonpremixed flames. *[Online]. Available: http://www.sandia.gov/TNF/abstract.html*.

[2] Akih-Kumgeh, B., and Bergthorson, J. M. Skeletal chemical kinetic mechanisms for syngas, methyl butanoate, n-heptane, and n-decane. *Energy & Fuels 27*, 4 (2013), 2316–2326.

[3] An, H., Yang, W., Maghbouli, A., Li, J., and Chua, K. A skeletal mechanism for biodiesel blend surrogates combustion. *Energy Conversion and Management 81* (2014), 51–59.

[4] Barlow, R., and Frank, J. Effects of turbulence on species mass fractions in methane/air jet flames. In *Symposium (International) on Combustion* (1998), vol. 27, Elsevier, pp. 1087–1095.

[5] Benzinger, M.-S., Schiessl, R., and Maas, U. A versatile coupled progress variable/REDIM model for auto-ignition and combustion. *Proceedings of the Combustion Institute 36*, 3 (2017), 3613–3621.

[6] Bilger, R. W. Turbulent mixing and reaction. In *Proceeding of the 11th Australian Fluid Mechanics Conference* (1992), pp. 1–9.

[7] Bodenstein, M. Eine theorie der photochemischen reaktionsgeschwindigkeiten. *Zeitschrift für Physikalische Chemie 85*, 1 (1913), 329–397.

[8] Brakora, J. L., Ra, Y., Reitz, R. D., McFarlane, J., and Daw, C. S. Development and validation of a reduced reaction mechanism for biodiesel-fueled engine simulations. *SAE International Journal of Fuels and Lubricants 1*, 1 (2009), 675–702.

[9] Bykov, V., and Maas, U. The extension of the ILDM concept to reaction–diffusion manifolds. *Combustion Theory and Modelling 11*, 6 (2007), 839–862.

[10] Bykov, V., and Maas, U. Extension of the ILDM method to the domain of slow chemistry. *Proceedings of the Combustion Institute 31*, 1 (2007), 465–472.

[11] Bykov, V., and Maas, U. Problem adapted reduced models based on reaction–diffusion manifolds (REDIMs). *Proceedings of the Combustion Institute 32*, 1 (2009), 561–568.

[12] Bykov, V., Neagos, A., and Maas, U. On transient behavior of non-premixed counter-flow diffusion flames within the REDIM based model reduction concept. *Proceedings of the Combustion Institute 34*, 1 (2013), 197–203.

[13] Chandel, A. K., Junqueira, T. L., Morais, E. R., Gouveia, V. L. R., Cavalett, O., Rivera, E. C., Geraldo, V. C., Bonomi, A., and da Silva, S. S. Techno-economic analysis of second-generation ethanol in Brazil: competitive, complementary aspects with first-generation ethanol. In *Biofuels in Brazil*. Springer, 2014, pp. 1–29.

[14] Chrigui, M., Masri, A., Sadiki, A., and Janicka, J. Large eddy simulation of a polydisperse ethanol spray flame. *Flow, Turbulence and Combustion 90*, 4 (2013), 813–832.

[15] Claramunt, K., Consul, R., Carbonell, D., and Pérez-Segarra, C. Analysis of the laminar flamelet concept for nonpremixed laminar flames. *Combustion and Flame 145*, 4 (2006), 845–862.

[16] Co, P. British Petroleum Company. *BP Statistical Review of World Energy 2017* (2017).

[17] Coelho, P., and Costa, M. *Combustão*, vol. 1. 2007.

[18] Cohen, S. D., Hindmarsh, A. C., Dubois, P. F., et al. CVODE, a stiff/nonstiff ODE solver in C. *Computers in Physics 10*, 2 (1996), 138–143.

[19] Cuenot, B. The flamelet model for non-premixed combustion. In *Turbulent Combustion Modeling*. Springer, 2011, pp. 43–61.

[20] Curran, H. J., Dunphy, M. P., Simmie, J. M., Westbrook, C. K., and Pitz, W. J. Shock tube ignition of ethanol, isobutene and MTBE: experiments and modeling. In *Symposium (International) on Combustion* (1992), vol. 24, Elsevier, pp. 769–776.

[21] De Bortoli, A. L., Andreis, G. S. L., and Pereira, F. N. *Modeling and Simulation of Reactive Flows*. Elsevier Science Publishing Co Inc, 2015.

[22] Dunphy, M. P., Patterson, P. M., and Simmie, J. M. High-temperature oxidation of ethanol. part 2. kinetic modelling. *Journal of the Chemical Society, Faraday Transactions 87*, 16 (1991), 2549–2559.

[23] Dunphy, M. P., and Simmie, J. M. High-temperature oxidation of ethanol. part 1. ignition delays in shock waves. *Journal of the Chemical Society, Faraday Transactions 87*, 11 (1991), 1691–1696.

[24] Egolfopoulos, F., Du, D., and Law, C. A study on ethanol oxidation kinetics in laminar premixed flames, flow reactors, and shock tubes. In *Symposium (international) on Combustion* (1992), vol. 24, Elsevier, pp. 833–841.

[25] Fischer, S., Markus, D., Ghorbani, A., and Maas, U. PDF simulations of the ignition of hydrogen/air, ethylene/air and propane/air mixtures by hot transient jets. *Zeitschrift für Physikalische Chemie 231*, 10 (2017), 1773–1796.

[26] Gao, Y., Shan, R., Lyra, S., Li, C., Wang, H., Chen, J. H., and Lu, T. On lumped-reduced reaction model for combustion of liquid fuels. *Combustion and Flame 163* (2016), 437–446.

[27] Gicquel, O., Darabiha, N., and Thévenin, D. Laminar premixed hydrogen/air counterflow flame simulations using flame prolongation of ILDM with differential diffusion. *Proceedings of the Combustion Institute 28*, 2 (2000), 1901–1908.

[28] Glassman, I., Yetter, R. A., and Glumac, N. G. *Combustion*. Academic press, 2014.

[29] Golub, G. H., and Van Loan, C. F. *Matrix computations*, vol. 3. JHU Press, 2012.

[30] Goodwin, D. G., Moffat, H. K., and Speth, R. L. CANTERA: An object-oriented software toolkit for chemical kinetics, thermodynamics, and transport processes, 2017. Version 2.3.0.

[31] Gorban, A. N., and Karlin, I. V. Method of invariant manifold for chemical kinetics. *Chemical Engineering Science 58*, 21 (2003), 4751–4768.

[32] Goussis, D. A., and Maas, U. Model reduction for combustion chemistry. In *Turbulent Combustion Modeling*. Springer, 2011, pp. 193–220.

[33] Griffiths, J. Reduced kinetic models and their application to practical combustion systems. *Progress in Energy and Combustion Science 21*, 1 (1995), 25–107.

[34] Heye, C., Raman, V., and Masri, A. R. LES/probability density function approach for the simulation of an ethanol spray flame. *Proceedings of the Combustion Institute 34*, 1 (2013), 1633–1641.

[35] Huang, H., Fairweather, M., Griffiths, J., Tomlin, A., and Brad, R. A systematic lumping approach for the reduction of comprehensive kinetic models. *Proceedings of the Combustion Institute 30*, 1 (2005), 1309–1316.

[36] Kee, R. J., Coltrin, M. E., and Glarborg, P. *Chemically reacting flow: theory and practice*. John Wiley & Sons, 2005.

[37] Kee, R. J., Miller, J. A., Evans, G. H., and Dixon-Lewis, G. A computational model of the structure and extinction of strained, opposed flow, premixed methane-air flames. In *Symposium (International) on Combustion* (1989), vol. 22, Elsevier, pp. 1479–1494.

[38] Konzen, P. H. d. A. *Simulaçao Numérica de Chama Laminar Axisimétrica de Metano/Ar usando REDIM*. PhD thesis, Universidade Federal do Rio Grande do Sul, 2010.

[39] Konzen, P. H. d. A., Richter, T., Riedel, U., and Maas, U. Implementation of REDIM reduced chemistry to model an axisymmetric laminar diffusion methane–air flame. *Combustion Theory and Modelling 15*, 3 (2011), 299–323.

[40] Kovács, T., Zsély, I. G., Kramarics, Á., and Turányi, T. Kinetic analysis of mechanisms of complex pyrolytic reactions. *Journal of Analytical and Applied Pyrolysis 79*, 1 (2007), 252–258.

[41] Kuo, K. K. *Principles of Combustion*, 2nd ed. John Wiley & Sons Inc., 2005.

[42] Kuo, K. K.-y., and Acharya, R. *Fundamentals of Turbulent and Multi-Phase Combustion*. John Wiley & Sons, 2012.

[43] Lam, S. Using CSP to understand complex chemical kinetics. *Combustion Science and Technology 89*, 5-6 (1993), 375–404.

[44] Lam, S., and Goussis, D. Understanding complex chemical kinetics with computational singular perturbation. In *Symposium (International) on Combustion* (1989), vol. 22, Elsevier, pp. 931–941.

[45] Lam, S., and Goussis, D. The CSP method for simplifying kinetics. *International Journal of Chemical Kinetics 26*, 4 (1994), 461–486.

[46] Law, C. K. *Combustion Physics*. Cambridge University Press, 2010.

[47] Lebedev, A., Okun, M., Chorkov, V., Tokar, P., and Strelkova, M. Systematic procedure for reduction of kinetic mechanisms of complex chemical processes and its software implementation. *Journal of Mathematical Chemistry 51*, 1 (2013), 73–107.

[48] Leplat, N., Dagaut, P., Togbé, C., and Vandooren, J. Numerical and experimental study of ethanol combustion and oxidation in laminar premixed flames and in jet-stirred reactor. *Combustion and Flame 158*, 4 (2011), 705–725.

[49] Li, J., Kazakov, A., and Dryer, F. L. Experimental and numerical studies of ethanol decomposition reactions. *The Journal of Physical Chemistry A 108*, 38 (2004), 7671–7680.

[50] Li, R., Li, S., Wang, F., and Li, X. Sensitivity analysis based on intersection approach for mechanism reduction of cyclohexane. *Combustion and Flame 166* (2016), 55–65.

[51] Lin, K. C., Tao, H., Kao, F.-H., and Chiu, C.-T. A minimized skeletal mechanism for methyl butanoate oxidation and its application to the prediction of C3-C4 products in non-premixed flames: A base model of biodiesel fuels. *Energy & Fuels* (2016).

[52] Lipp, S., Magagnato, F., and Maas, U. A hybrid transported PDF/CFD model for turbulent flames using REDIM. In *Proc. of the 4th European Combustion Meeting* (2009).

[53] Liu, W., Kelley, A. P., and Law, C. K. Non-premixed ignition, laminar flame propagation, and mechanism reduction of n-butanol, iso-butanol, and methyl butanoate. *Proceedings of the Combustion Institute 33*, 1 (2011), 995–1002.

[54] Løvås, T. *Model reduction techniques for chemical mechanisms*. INTECH Open Access Publisher, 2012.

[55] Løvås, T., Nilsson, D., and Mauss, F. Automatic reduction procedure for chemical mechanisms applied to premixed methane/air flames. *Proceedings of the Combustion Institute 28*, 2 (2000), 1809–1815.

[56] Lu, T., and Law, C. K. A directed relation graph method for mechanism reduction. *Proceedings of the Combustion Institute 30*, 1 (2005), 1333–1341.

[57] Lu, T., and Law, C. K. Linear time reduction of large kinetic mechanisms with directed relation graph: n-heptane and iso-octane. *Combustion and Flame 144*, 1 (2006), 24–36.

[58] Lu, T., and Law, C. K. On the applicability of directed relation graphs to the reduction of reaction mechanisms. *Combustion and Flame 146*, 3 (2006), 472–483.

[59] Lu, T., Plomer, M., Luo, Z., Sarathy, S. M., Pitz, W. J., Som, S., and Longman, D. E. Directed relation graph with expert knowledge for skeletal mechanism reduction. In *US National Combustion Institute Meeting* (2011).

[60] Luo, Z., Lu, T., Maciaszek, M. J., Som, S., and Longman, D. E. A reduced mechanism for high-temperature oxidation of biodiesel surrogates. *Energy & Fuels 24*, 12 (2010), 6283–6293.

[61] Luo, Z., Plomer, M., Lu, T., Som, S., Longman, D. E., Sarathy, S. M., and Pitz, W. J. A reduced mechanism for biodiesel surrogates for compression ignition engine applications. *Fuel 99* (2012), 143–153.

[62] Maas, U. *Automatische reduktion von reaktionsmechanismen zur simulation reaktiver strömungen*. PhD thesis, Institut für Technische Verbrennung, Universität Stuttgart, Germany, 1993.

[63] Maas, U., and Pope, S. Simplifying chemical kinetics: intrinsic low-dimensional manifolds in composition space. *Combustion and Flame 88*, 3 (1992), 239–264.

[64] Marinov, N. M. A detailed chemical kinetic model for high temperature ethanol oxidation. *International Journal of Chemical Kinetics 3*, 2 (1999), 257–263.

[65] Masri, A., and Gounder, J. Turbulent spray flames of acetone and ethanol approaching extinction. *Combustion Science and Technology 182*, 4-6 (2010), 702–715.

[66] Merci, B., Naud, B., Roekaerts, D., and Maas, U. Joint scalar versus joint velocity-scalar PDF simulations of bluff-body stabilized flames with REDIM. *Flow, Turbulence and Combustion 82*, 2 (2009), 185–209.

[67] Nagy, T., and Turányi, T. Reduction of very large reaction mechanisms using methods based on simulation error minimization. *Combustion and Flame 156*, 2 (2009), 417–428.

[68] Ng, H. K., Gan, S., Ng, J.-H., and Pang, K. M. Development and validation of a reduced combined biodiesel–diesel reaction mechanism. *Fuel 104* (2013), 620–634.

[69] Niemeyer, K. E., Sung, C., and Raju, M. P. Skeletal mechanism generation for surrogate fuels using directed relation graph with error propagation and sensitivity analysis. *Combustion and Flame 157*, 1 (2010), 1760–1770.

[70] Niemeyer, K. E., and Sung, C.-J. Reduced chemistry for a gasoline surrogate valid at engine-relevant conditions. *Energy & Fuels 29*, 2 (2015), 1172–1185.

[71] O'Conaire, M., Curran, H. J., Simmie, J. M., Pitz, W. J., and Westbrook, C. K. A comprehensive modeling study of hydrogen oxidation. *International Journal of Chemical Kinetics 36*, 11 (2004), 603–622.

[72] Oijen, J. v., and Goey, L. D. Modelling of premixed laminar flames using flamelet-generated manifolds. *Combustion Science and Technology 161*, 1 (2000), 113–137.

[73] Okuyama, M., Hirano, S., Ogami, Y., Nakamura, H., Ju, Y., and Kobayashi, H. Development of an ethanol reduced kinetic mechanism based on the quasi-steady state assumption and feasibility evaluation for multi-dimensional flame analysis. *Journal of Thermal Science and Technology 5*, 2 (2010), 189–199.

[74] Pepiot, P., and Pitsch, H. Systematic reduction of large chemical mechanisms. In *4th joint meeting of the US Sections of the Combustion Institute, Philadelphia, PA* (2005).

[75] Pepiot-Desjardins, P., and Pitsch, H. An automatic chemical lumping method for the reduction of large chemical kinetic mechanisms. *Combustion Theory and Modelling 12*, 6 (2008), 1089–1108.

[76] Pepiot-Desjardins, P., and Pitsch, H. An efficient error-propagation-based reduction method for large chemical kinetic mechanisms. *Combustion and Flame 154*, 1 (2008), 67–81.

[77] Peters, N. Laminar diffusion flamelet models in non-premixed turbulent combustion. *Progress in energy and combustion science 10*, 3 (1984), 319–339.

[78] Peters, N. Fifteen lectures on laminar and turbulent combustion. *ERCOFTAC Summer School 1428* (1992).

[79] Peters, N. *Turbulent combustion*. Cambridge University Press, 2000.

[80] Peters, N., and Rogg, B. *Reduced Kinetic Mechanisms for Applications in Combustion Systems*, vol. 15. Springer Science & Business Media, 1993.

[81] Pierce, C. D., and Moin, P. Progress-variable approach for large-eddy simulation of non-premixed turbulent combustion. *Journal of Fluid Mechanics 504* (2004), 73–97.

[82] Pitsch, H., and Peters, N. A consistent flamelet formulation for non-premixed combustion considering differential diffusion effects. *Combustion and Flame 114*, 1 (1998), 26–40.

[83] Poinsot, T., and Veynante, D. *Theoretical and Numerical Combustion*, 3rd ed. RT Edwards, Inc., 2011.

[84] Portal Brasil. Etanol atingiu produção recorde de 30 bilhões de litros em 2015, 2016.

[85] Powers, J. M. Intrinsic low-dimensional manifold method for rational simplification of chemical kinetics.

[86] Prasad, V. N., Masri, A. R., Navarro-Martinez, S., and Luo, K. H. Investigation of auto-ignition in turbulent methanol spray flames using large eddy simulation. *Combustion and Flame 160*, 12 (2013), 2941–2954.

[87] Rodriguez, A., Herbinet, O., Battin-Leclerc, F., Frassoldati, A., Faravelli, T., and Ranzi, E. Experimental and modeling investigation of the effect of the unsaturation degree on the gas-phase oxidation of fatty acid methyl esters found in biodiesel fuels. *Combustion and Flame 164* (2016), 346–362.

[88] Röhl, O., and Peters, N. A reduced mechanism for ethanol oxidation. In *4th European Combustion Meeting (ECM 2009), Vienna, Austria, April* (2009), pp. 14–17.

[89] Sacomano Filho, F. L., Fukumasu, N. K., and Krieger, G. C. Numerical simulation of an ethanol turbulent spray flame with RANS and diffusion combustion model. *Journal of the Brazilian Society of Mechanical Sciences and Engineering 35*, 3 (2013), 189–198.

[90] Saxena, P., and Williams, F. A. Numerical and experimental studies of ethanol flames. *Proceedings of the Combustion Institute 31*, 1 (2007), 1149–1156.

[91] Schiessl, R., Bykov, V., Maas, U., Abdelsamie, A., and Thévenin, D. Implementing multi-directional molecular diffusion terms into reaction diffusion manifolds (REDIMs). *Proceedings of the Combustion Institute 36*, 1 (2017), 673–679.

[92] Schlichting, H. *Boundary-layer theory*. McGraw-Hill, 1968.

[93] Seshadri, K., Lu, T., Herbinet, O., Humer, S., Niemann, U., Pitz, W. J., Seiser, R., and Law, C. K. Experimental and kinetic modeling study of extinction and ignition of methyl decanoate in laminar non-premixed flows. *Proceedings of the Combustion Institute 32*, 1 (2009), 1067–1074.

[94] Shi, Y., Ge, H.-W., Brakora, J. L., and Reitz, R. D. Automatic chemistry mechanism reduction of hydrocarbon fuels for HCCI engines based on DRGEP and PCA methods with error control. *Energy & Fuels 24*, 3 (2010), 1646–1654.

[95] Smith, G. P., Golden, D. M., Frenklach, M., Moriarty, N. W., Eiteneer, B., Goldenberg, M., Bowman, C. T., Hanson, R. K., Song, S., Gardiner, W. C., Jr., V. V. L., and Qin, Z. GRI-MECH 3.0. *GRI-Mech Home Page, http://www. me. berkeley. edu/gri_ mech/(accessado 06/01/2017)* (2011).

[96] Stagni, A., Frassoldati, A., Cuoci, A., Faravelli, T., and Ranzi, E. Skeletal mechanism reduction through species-targeted sensitivity analysis. *Combustion and Flame 163* (2016), 382–393.

[97] Stahl, G., and Warnatz, J. Numerical investigation of time-dependent properties and extinction of strained methane and propane-air flamelets. *Combustion and Flame 85*, 3-4 (1991), 285–299.

[98] Steinhilber, G., Bykov, V., and Maas, U. REDIM reduced modeling of flame-wall-interactions: Quenching of a premixed methane/air flame at a cold inert wall. *Proceedings of the Combustion Institute 36*, 1 (2017), 655–661.

[99] Steinhilber, G., and Maas, U. Reaction-diffusion manifolds for unconfined, lean premixed, piloted, turbulent methane/air systems. *Proceedings of the Combustion Institute 34*, 1 (2013), 217–224.

[100] Tomlin, A. S. The role of sensitivity and uncertainty analysis in combustion modelling. *Proceedings of the Combustion Institute 34*, 1 (2013), 159–176.

[101] Tomlin, A. S., Turányi, T., and Pilling, M. J. Mathematical tools for the construction, investigation and reduction of combustion mechanisms. *Comprehensive chemical kinetics 35* (1997), 293–437.

[102] Turányi, T. Reduction of large reaction mechanisms. *New Journal of Chemistry 14* (1990), 795–803.

[103] Turányi, T. Sensitivity analysis of complex kinetic systems. Tools and applications. *Journal of Mathematical Chemistry 5*, 3 (1990), 203–248.

[104] Turányi, T. Applications of sensitivity analysis to combustion chemistry. *Reliability Engineering & System Safety 57*, 1 (1997), 41–48.

[105] Turányi, T., Bérces, T., and Tóth, J. The method of quasi-stationary sensitivity analysis. *Journal of Mathematical Chemistry 2*, 4 (1988), 401–409.

[106] Turanyi, T., Berces, T., and Vajda, S. Reaction rate analysis of complex kinetic systems. *International Journal of Chemical Kinetics 21*, 2 (1989), 83–99.

[107] Turanyi, T., Tomlin, A., and Pilling, M. On the error of the quasi-steady-state approximation. *The Journal of Physical Chemistry 97*, 1 (1993), 163–172.

[108] Turányi, T., and Tomlin, A. S. *Analysis of kinetic reaction mechanisms*. Springer, 2014.

[109] Turns, S. *An Introduction to Combustion: Concepts and Applications*, 2 ed. McGraw-Hill Hight Education, 2000.

[110] Vajda, S., and Turányi, T. Principal component analysis for reducing the Edelson-Field-Noyes model of the Belousov-Zhabotinskii reaction. *The Journal of Physical Chemistry 90*, 8 (1986), 1664–1670.

[111] Vajda, S., Valko, P., and Turányi, T. Principal component analysis of kinetic models. *International Journal of Chemical Kinetics 17*, 1 (1985), 55–81.

[112] Van Oijen, J., and De Goey, L. Modelling of premixed counterflow flames using the flamelet-generated manifold method. *Combustion Theory and Modelling 6*, 3 (2002), 463–478.

[113] Veynante, D., and Poinsot, T. Reynolds averaged and large eddy simulation modeling for turbulent combustion. In *New tools in turbulence modelling*. Springer, 1997, pp. 105–140.

[114] Wang, P., Fröhlich, J., Maas, U., He, Z.-x., and Wang, C.-j. A detailed comparison of two sub-grid scale combustion models via large eddy simulation of the PRECCINSTA gas turbine model combustor. *Combustion and Flame 164* (2016), 329–345.

[115] Wang, P., Platova, N., Fröhlich, J., and Maas, U. Large eddy simulation of the PRECCINSTA burner. *International Journal of Heat and Mass Transfer 70* (2014), 486–495.

[116] Wang, P., Zieker, F., Schiessl, R., Platova, N., Fröhlich, J., and Maas, U. Large eddy simulations and experimental studies of turbulent premixed combustion near extinction. *Proceedings of the Combustion Institute 34*, 1 (2013), 1269–1280.

[117] Wang, Q.-D., Fang, Y.-M., Wang, F., and Li, X.-Y. Systematic analysis and reduction of combustion mechanisms for ignition of multi-component kerosene surrogate. *Proceedings of the Combustion Institute 34*, 1 (2013), 187–195.

[118] Wang, X., Liu, H., Zheng, Z., and Yao, M. Development of a reduced n-butanol/biodiesel mechanism for a dual fuel engine. *Fuel 157* (2015), 87–96.

[119] Wang, X., Liu, H., Zheng, Z., and Yao, M. A skeletal mechanism of a biodiesel surrogate fuel for compression ignition engines. *Energy & Fuels 29*, 2 (2015), 1160–1171.

[120] Warnatz, J., Maas, U., and Dibble, R. *Combustion: Physical and Chemical Fundamentals, Modeling and Simulation, Experiments, Pollutant formation. 2006*, 4th ed. Springer.

[121] Wei, Z., Zhen, H., Leung, C., Cheung, C., and Huang, Z. Heat transfer characteristics and the optimized heating distance of laminar premixed biogas-hydrogen bunsen flame impinging on a flat surface. *international journal of hydrogen energy 40*, 45 (2015), 15723–15731.

[122] Westbrook, C. K., Pitz, W. J., Westmoreland, P. R., Dryer, F. L., Chaos, M., Osswald, P., Kohse-Höinghaus, K., Cool, T. A., Wang, J., Yang, B., et al. A detailed chemical kinetic reaction mechanism for oxidation of four small alkyl esters in laminar premixed flames. *Proceedings of the Combustion Institute 32*, 1 (2009), 221–228.

[123] Whitehouse, L., Tomlin, A., and Pilling, M. Systematic reduction of complex tropospheric chemical mechanisms, Part I: sensitivity and time-scale analyses. *Atmospheric Chemistry and Physics 4*, 7 (2004), 2025–2056.

[124] Williams, F. Recent advances in theoretical descriptions of turbulent diffusion flames. In *Turbulent Mixing in Nonreactive and Reactive Flows*. Springer, 1975, pp. 189–208.

[125] Williams, F. A. *Combustion Theory: the Fundamental Theory of Chemical Reacting Flow Systems*. The Benjamin/Cummings Publishing Company, 1985.

[126] Xia, A., Michelangeli, D., and Makar, P. Mechanism reduction for the formation of secondary organic aerosol for integration into a 3-dimensional regional air quality model: α-pinene oxidation system. *Atmospheric Chemistry and Physics 9*, 13 (2009), 4341–4362.

[127] Yu, C., Minuzzi, F., and Maas, U. Numerical simulation of turbulent flames based on a hybrid RANS/Transported-PDF method and REDIM method. *Eurasian Chemico-Technological Journal 20*, 1 (2018), 23–31.

[128] Zheng, X., Lu, T., and Law, C. Experimental counterflow ignition temperatures and reaction mechanisms of 1, 3-butadiene. *Proceedings of the Combustion Institute 31*, 1 (2007), 367–375.

APÊNDICE A SKELETAL MECHANISM FOR ETHANOL

This appendix provides the skeletal mechanism for ethanol developed in this work, with the corresponding kinetics parameters.

Table A.1: Skeletal mechanism for ethanol developed with DRG; unity are mol, cm^3, s, K and cal/mol.

Reaction	A	b	E_a
H_2+OH=H+H_2O	$2.140E+08$	1.520	3449.00
O+OH=H+O_2	$2.020E+14$	-0.400	0.00
H_2+O=H+OH	$5.060E+04$	2.670	6290.00
H+O_2(+M)=HO_2(+M)	$4.52000E+13$	0.000	0.00
Low pressure limit	$1.05000E+19$	-1.257	0.00
Efficiency of M:			
$CO_2 = 3.8$, CO = 1.9, $H_2 = 0.0$,			
$H_2O = 0.0$, $CH_4 = 10.0$, $N_2 = 0.0$.			
H+O_2(+N2)=HO_2(+N2)	$4.52000E+13$	0.000	0.00
Low pressure limit	$2.03000E+20$	-1.590	0.00
H+O_2(+H_2)=HO_2(+H_2)	$4.52000E+13$	0.000	0.00
Low pressure limit	$1.52000E+19$	-1.133	0.00
H+O_2(+H_2O)=HO_2(+H_2O)	$4.52000E+13$	0.000	0.00
Low pressure limit	$2.10000E+23$	-2.437	0.00
HO_2+OH=H_2O+O_2	$2.130E+28$	-4.827	3500.00
Duplicate			
HO_2+OH=H_2O+O_2	$9.100E+14$	0.000	10964.00
Duplicate			
H+HO_2=2OH	$1.500E+14$	0.000	1000.00
H+HO_2=H_2+O_2	$6.630E+13$	0.000	2126.00
H+HO_2=H_2O+O	$3.010E+13$	0.000	1721.00

Table A.1 continued

Reaction	A	b	E
HO_2+O=O_2+OH	$3.250E+13$	0.000	0.00
2OH=H_2O+O	$3.570E+04$	2.400	−2112.00
2H+M=H_2+M	$1.000E+18$	−1.000	0.00
Efficiency of M:			
$H_2 = 0.0$, $H_2O = 0.0$.			
2H+H_2=2H_2	$9.200E+16$	−0.600	0.00
2H+H_2O=H_2+H_2O	$6.000E+19$	−1.250	0.00
H+OH+M=H_2O+M	$2.210E+22$	−2.000	0.00
Efficiency of M:			
$H_2O = 6.4$.			
H+O+M=OH+M	$4.710E+18$	−1.000	0.00
Efficiency of M:			
$H_2O = 6.4$.			
2O+M=O_2+M	$1.890E+13$	0.000	−1788.00
2HO_2=H_2O_2+O_2	$4.200E+14$	0.000	11982.00
Duplicate			
2HO_2=H_2O_2+O_2	$1.300E+11$	0.000	−1629.00
Duplicate			
2OH(+M)=H_2O_2(+M)	$1.24000E+14$	−0.370	0.00
Low pressure limit	$3.04000E+30$	−4.630	2049.00
Troe parameters:			
$a = 0.47$, $T^{***} = 100.0$, $T^{*} = 2000.0$ $T^{**} = 1e+15$.			
H+H_2O_2=H_2+HO_2	$1.980E+06$	2.000	2435.00
H+H_2O_2=H_2O+OH	$3.070E+13$	0.000	4217.00
H_2O_2+O=HO_2+OH	$9.550E+06$	2.000	3970.00
H_2O_2+OH=H_2O+HO_2	$2.400E+00$	4.042	−2162.00
2CH_3(+M)=C_2H_6(+M)	$9.22000E+16$	−1.174	636.00
Low pressure limit	$1.14000E+36$	−5.246	1705.00

Table A.1 continued

Reaction	A	b	E
Troe parameters:			
$a = 0.405$, $T^{***} = 1120.0$, $T^{*} = 69.6$ $T^{**} = 1e + 15$.			
Efficiency of M:			
$H_2 = 2.0$, $H_2O = 5.0$, $CO_2 = 3.0$, CO = 2.0.			
CH_3+H(+M)=CH_4(+M)	$2.14000E + 15$	-0.400	0.00
Low pressure limit	$3.31000E + 30$	-4.000	2108.00
Troe parameters:			
$a = 0.0$, $T^{***} = 1e - 15$, $T^{*} = 1e - 15$ $T^{**} = 40.0$.			
Efficiency of M:			
$H_2 = 2.0$, $H_2O = 5.0$, $CO_2 = 3.0$, CO = 2.0.			
CH_4+H=CH_3+H_2	$2.200E + 04$	3.000	8750.00
CH_4+OH=CH_3+H_2O	$4.190E + 06$	2.000	2547.00
CH_4+O=CH_3+OH	$6.920E + 08$	1.560	8485.00
CH_4+HO_2=CH_3+H_2O_2	$1.120E + 13$	0.000	24640.00
CH_3+HO_2=CH_3O+OH	$7.000E + 12$	0.000	0.00
CH_3+HO_2=CH_4+O_2	$3.000E + 12$	0.000	0.00
CH_3+O=CH_2O+H	$8.000E + 13$	0.000	0.00
CH_3+O_2=CH_3O+O	$1.450E + 13$	0.000	29209.00
CH_3+O_2=CH_2O+OH	$2.510E + 11$	0.000	14640.00
CH_3O+H=CH_3+OH	$1.000E + 13$	0.000	0.00
CH_2OH+H=CH_3+OH	$1.000E + 13$	0.000	0.00
CH_3+OH=CH_2(s)+H_2O	$2.000E + 13$	0.000	550.00
CH_3+OH=H_2+HCOH	$1.000E + 10$	0.000	-415.00
CH_3+M=CH+H_2+M	$6.900E + 14$	0.000	82469.00
CH_2O+H(+M)=CH_3O(+M)	$5.40000E + 11$	0.454	2600.00
Low pressure limit	$1.50000E + 30$	-4.800	5560.00
Troe parameters:			
$a = 0.758$, $T^{***} = 94.0$, $T^{*} = 1555.0$ $T^{**} = 4200.0$.			

Table A.1 continued

Reaction	A	b	E
Efficiency of M:			
$H_2O = 5.0$.			
CH_2O+H(+M)=CH_2OH(+M)	$5.40000E+11$	0.454	3600.00
Low pressure limit	$9.10000E+31$	−4.820	6530.00
Troe parameters:			
$a = 0.7187$, $T^{***} = 103.0$, $T^{*} = 1291.0$ $T^{**} = 4160.0$.			
Efficiency of M:			
$H_2O = 5.0$.			
CH_3+CH_3O=CH_2O+CH_4	$1.200E+13$	0.000	0.00
CH_3O+H=CH_2O+H_2	$2.000E+13$	0.000	0.00
CH_2OH+H=CH_2O+H_2	$2.000E+13$	0.000	0.00
CH_3O+OH=CH_2O+H_2O	$1.000E+13$	0.000	0.00
CH_2OH+OH=CH_2O+H_2O	$1.000E+13$	0.000	0.00
CH_3O+O=CH_2O+OH	$1.000E+13$	0.000	0.00
CH_2OH+O=CH_2O+OH	$1.000E+13$	0.000	0.00
CH_3O+O_2=CH_2O+HO_2	$6.300E+10$	0.000	2600.00
CH_3O+CO=CH_3+CO_2	$4.680E+02$	3.160	5380.00
CH_2OH+O_2=CH_2O+HO_2	$1.570E+15$	−1.000	0.00
Duplicate			
CH_2OH+O_2=CH_2O+HO_2	$7.230E+13$	0.000	3577.00
Duplicate			
HCOH+OH=H_2O+HCO	$2.000E+13$	0.000	0.00
H+HCOH=CH_2O+H	$2.000E+14$	0.000	0.00
HCOH+O=CO+H+OH	$8.000E+13$	0.000	0.00
HCOH+O_2=CO+2OH	$1.000E+13$	0.000	0.00
HCOH+O_2=CO_2+H_2O	$1.000E+13$	0.000	0.00
HCOH=CH_2O	$2.100E+19$	−3.070	31700.00
CH_2(s)+CH_4=2CH_3	$4.000E+13$	0.000	0.00

Table A.1 continued

Reaction	A	b	E
C_2H_6+CH_2(s)=C_2H_5+CH_3	$1.200E+14$	0.000	0.00
CH_2(s)+O_2=CO+H+OH	$7.000E+13$	0.000	0.00
CH_2(s)+H_2=CH_3+H	$7.000E+13$	0.000	0.00
C_2H_4+CH_2(s)=aC_3H_5+H	$1.300E+14$	0.000	0.00
CH_2(s)+O=CO+2H	$3.000E+13$	0.000	0.00
CH_2(s)+OH=CH_2O+H	$3.000E+13$	0.000	0.00
CH_2(s)+H=CH+H_2	$3.000E+13$	0.000	0.00
CH_2(s)+CO_2=CH_2O+CO	$3.000E+12$	0.000	0.00
CH_2(s)+CH_3=C_2H_4+H	$2.000E+13$	0.000	0.00
CH+O_2=HCO+O	$3.300E+13$	0.000	0.00
CH+O=CO+H	$5.700E+13$	0.000	0.00
CH+OH=H+HCO	$3.000E+13$	0.000	0.00
CH+CO_2=CO+HCO	$3.400E+12$	0.000	690.00
CH+H_2O=CH_2O+H	$1.170E+15$	−0.750	0.00
CH+CH_3=C_2H_3+H	$3.000E+13$	0.000	0.00
CH+CH_4=C_2H_4+H	$6.000E+13$	0.000	0.00
CH_2O+OH=H_2O+HCO	$3.430E+09$	1.180	−447.00
CH_2O+H=H_2+HCO	$2.190E+08$	1.770	3000.00
CH_2O+M=H+HCO+M	$3.310E+16$	0.000	81000.00
CH_2O+O=HCO+OH	$1.800E+13$	0.000	3080.00
HCO+O_2=CO+HO_2	$7.580E+12$	0.000	410.00
HCO+M=CO+H+M	$1.860E+17$	−1.000	17000.00
Efficiency of M:			
$H_2 = 1.87$, $CH_4 = 2.81$, $H_2O = 5.0$,			
$CO_2 = 3.0$, CO = 1.87.			
HCO+OH=CO+H_2O	$1.000E+14$	0.000	0.00
H+HCO=CO+H_2	$1.190E+13$	0.250	0.00
HCO+O=CO+OH	$3.000E+13$	0.000	0.00

Table A.1 continued

Reaction	A	b	E
HCO+O=CO_2+H	$3.000E+13$	0.000	0.00
CO+OH=CO_2+H	$9.420E+03$	2.250	−2351.00
CO+O+M=CO_2+M	$6.170E+14$	0.000	3000.00
CO+O_2=CO_2+O	$2.530E+12$	0.000	47688.00
CO+HO_2=CO_2+OH	$5.800E+13$	0.000	22934.00
C_2H_5OH(+M)=CH_2OH+CH_3(+M)	$5.94000E+23$	−1.680	91163.00
Low pressure limit	$2.88000E+85$	−18.900	109914.00
Troe parameters:			
$a = 0.5$, $T^{***} = 200.0$, $T^{*} = 890.0$ $T^{**} = 4600.0$.			
Efficiency of M:			
$H_2 = 2.0$, $H_2O = 5.0$, $CO_2 = 3.0$, CO = 2.0.			
C_2H_5OH(+M)=C_2H_5+OH(+M)	$1.25000E+23$	−1.540	96005.00
Low pressure limit	$3.25200E+85$	−18.810	114930.00
Troe parameters:			
$a = 0.5$, $T^{***} = 300.0$, $T^{*} = 900.0$ $T^{**} = 5000.0$.			
Efficiency of M:			
$H_2 = 2.0$, $H_2O = 5.0$, $CO_2 = 3.0$, CO = 2.0.			
C_2H_5OH(+M)=C_2H_4+H_2O(+M)	$2.79000E+13$	0.090	66136.00
Low pressure limit	$2.57000E+83$	−18.850	86452.00
Troe parameters:			
$a = 0.7$, $T^{***} = 350.0$, $T^{*} = 800.0$ $T^{**} = 3800.0$.			
Efficiency of M:			
$H_2O = 5.0$			
C_2H_5OH(+M)=CH_3HCO+H_2(+M)	$7.24000E+11$	0.095	91007.00
Low pressure limit	$4.46000E+87$	−19.420	115586.00
Troe parameters:			
$a = 0.9$, $T^{***} = 900.0$, $T^{*} = 1100.0$ $T^{**} = 3500.0$.			
Efficiency of M:			

Table A.1 continued

Reaction	A	b	E
$H_2O = 5.0.$			
$C_2H_5OH+OH=C_2H_4OH+H_2O$	$1.740E+11$	0.270	600.00
$C_2H_5OH+OH=CH_3CHOH+H_2O$	$4.640E+11$	0.150	0.00
$C_2H_5OH+OH=CH_3CH_2O+H_2O$	$7.460E+11$	0.300	1634.00
$C_2H_5OH+H=C_2H_4OH+H_2$	$1.230E+07$	1.800	5098.00
$C_2H_5OH+H=CH_3CHOH+H_2$	$2.580E+07$	1.650	2827.00
$C_2H_5OH+H=CH_3CH_2O+H_2$	$1.500E+07$	1.600	3038.00
$C_2H_5OH+O=C_2H_4OH+OH$	$9.410E+07$	1.700	5459.00
$C_2H_5OH+O=CH_3CHOH+OH$	$1.880E+07$	1.850	1824.00
$C_2H_5OH+O=CH_3CH_2O+OH$	$1.580E+07$	2.000	4448.00
$C_2H_5OH+CH_3=C_2H_4OH+CH_4$	$2.190E+02$	3.180	9622.00
$C_2H_5OH+CH_3=CH_3CHOH+CH_4$	$7.280E+02$	2.990	7948.00
$C_2H_5OH+CH_3=CH_3CH_2O+CH_4$	$1.450E+02$	2.990	7649.00
$C_2H_5OH+HO_2=CH_3CHOH+H_2O_2$	$8.200E+03$	2.550	10750.00
$C_2H_5OH+HO_2=C_2H_4OH+H_2O_2$	$1.230E+04$	2.550	15750.00
$C_2H_5OH+HO_2=CH_3CH_2O+H_2O_2$	$2.500E+12$	0.000	24000.00
$CH_3CH_2O+M=CH_3HCO+H+M$	$1.160E+35$	−5.890	25274.00
$CH_3CH_2O+M=CH_2O+CH_3+M$	$1.350E+38$	−6.960	23800.00
$CH_3CH_2O+O_2=CH_3HCO+HO_2$	$4.000E+10$	0.000	1100.00
$CH_3CH_2O+CO=C_2H_5+CO_2$	$4.680E+02$	3.160	5380.00
$CH_3CH_2O+H=CH_2OH+CH_3$	$3.000E+13$	0.000	0.00
$CH_3CH_2O+H=C_2H_4+H_2O$	$3.000E+13$	0.000	0.00
$CH_3CH_2O+OH=CH_3HCO+H_2O$	$1.000E+13$	0.000	0.00
$CH_3CHOH+O_2=CH_3HCO+HO_2$	$4.820E+14$	0.000	5017.00
Duplicate			
$CH_3CHOH+O_2=CH_3HCO+HO_2$	$8.430E+15$	−1.200	0.00
Duplicate			
$CH_3CHOH+O=CH_3HCO+OH$	$1.000E+14$	0.000	0.00

Table A.1 continued

Reaction	A	b	E
$CH_3CHOH+H=C_2H_4+H_2O$	$3.000E+13$	0.000	0.00
$CH_3CHOH+H=CH_2OH+CH_3$	$3.000E+13$	0.000	0.00
$CH_3CHOH+HO_2=CH_3HCO+2OH$	$4.000E+13$	0.000	0.00
$CH_3CHOH+OH=CH_3HCO+H_2O$	$5.000E+12$	0.000	0.00
$CH_3CHOH+M=CH_3HCO+H+M$	$1.000E+14$	0.000	25000.00
$CH_3HCO+OH=CH_3CO+H_2O$	$9.240E+06$	1.500	−962.00
$CH_3HCO+O=CH_3CO+OH$	$1.770E+18$	−1.900	2975.00
$CH_3HCO+H=CH_3CO+H_2$	$4.660E+13$	−0.350	2988.00
$CH_3+CH_3HCO=CH_3CO+CH_4$	$3.900E-07$	5.800	2200.00
$CH_3HCO+HO_2=CH_3CO+H_2O_2$	$2.400E+19$	−2.200	14030.00
$CH_3HCO+O_2=CH_3CO+HO_2$	$1.000E+14$	0.000	42200.00
$C_2H_6+CH_3=C_2H_5+CH_4$	$5.500E-01$	4.000	8300.00
$C_2H_6+H=C_2H_5+H_2$	$5.400E+02$	3.500	5210.00
$C_2H_6+O=C_2H_5+OH$	$3.000E+07$	2.000	5115.00
$C_2H_6+OH=C_2H_5+H_2O$	$7.230E+06$	2.000	864.00
$C_2H_5+H=C_2H_4+H_2$	$1.250E+14$	0.000	8000.00
$C_2H_5+H=2CH_3$	$3.000E+13$	0.000	0.00
$C_2H_5+H=C_2H_6$	$3.000E+13$	0.000	0.00
$C_2H_5+OH=C_2H_4+H_2O$	$4.000E+13$	0.000	0.00
$C_2H_5+O=CH_2O+CH_3$	$1.000E+14$	0.000	0.00
$C_2H_5+HO_2=C_2H_6+O_2$	$3.000E+12$	0.000	0.00
$C_2H_5+HO_2=CH_3CH_2O+OH$	$3.000E+13$	0.000	0.00
$C_2H_5+O_2=C_2H_4+HO_2$	$2.890E+28$	−5.400	7585.00
$C_2H_5+O_2=CH_3HCO+OH$	$4.900E+11$	−0.480	8357.00
$C_2H_4+OH=C_2H_4OH$	$1.290E+12$	0.000	−817.00
$C_2H_4OH+O_2=HOC_2H_4O_2$	$1.000E+12$	0.000	−1100.00
$HOC_2H_4O_2=2CH_2O+OH$	$6.000E+10$	0.000	24500.00
$C_2H_4+OH=C_2H_3+H_2O$	$2.020E+13$	0.000	5936.00

Table A.1 continued

Reaction	A	b	E
C_2H_4+O=CH_3+HCO	$1.020E+07$	1.880	179.00
C_2H_4+CH_3=C_2H_3+CH_4	$6.620E+00$	3.700	9500.00
C_2H_4+H=C_2H_3+H_2	$3.360E-07$	6.000	1692.00
C_2H_4+H(+M)=C_2H_5(+M)	$1.08000E+12$	0.454	1822.00
Low pressure limit	$1.11200E+34$	−5.000	4448.00
Troe parameters:			
$a = 1.0$, $T^{***} = 1e-15$, $T^{*} = 95.0$ $T^{**} = 200.0$.			
Efficiency of M:			
$H_2 = 2.0$, $H_2O = 5.0$, $CO_2 = 3.0$, CO = 2.0.			
C_2H_4(+M)=C_2H_2+H_2(+M)	$1.80000E+14$	0.000	87000.00
Low pressure limit	$1.50000E+15$	0.000	55443.00
C_2H_3+H(+M)=C_2H_4(+M)	$6.10000E+12$	0.270	280.00
Low pressure limit	$9.80000E+29$	−3.860	3320.00
Troe parameters:			
$a = 0.782$, $T^{***} = 208.0$, $T^{*} = 2663.0$ $T^{**} = 6095.0$.			
Efficiency of M:			
$H_2O = 5.0$.			
C_2H_3+H=C_2H_2+H_2	$9.000E+13$	0.000	0.00
C_2H_3+O_2=CH_2O+HCO	$1.700E+29$	−5.312	6500.00
C_2H_3+O_2=C_2H_2+HO_2	$2.120E-06$	6.000	9484.00
C_2H_3+OH=C_2H_2+H_2O	$2.000E+13$	0.000	0.00
C_2H+C_2H_3=2C_2H_2	$3.000E+13$	0.000	0.00
C_2H_3+CH_3=aC_3H_5+H	$4.730E+02$	3.700	5677.00
C_2H_3+CH_3=C_2H_2+CH_4	$2.000E+13$	0.000	0.00
C_2H_2+OH=C_2H+H_2O	$3.370E+07$	2.000	14000.00
C_2H_2+OH=CH_3+CO	$4.830E-04$	4.000	−2000.00
C_2H_2+O=C_2H+OH	$3.160E+15$	−0.600	15000.00
C_2H_2+CH_3=C_2H+CH_4	$1.810E+11$	0.000	17289.00

Table A.1 continued

Reaction	A	b	E
C_2H_2+M=C_2H+H+M	$4.200E+16$	0.000	107000.00
C_2H_2+H(+M)=C_2H_3(+M)	$3.11000E+11$	0.580	2589.00
Low pressure limit	$2.25000E+40$	-7.269	6577.00
Troe parameters:			
$a = 1.0$, $T^{***} = 1e-15$, $T^{*} = 675.0$ $T^{**} = 1e+15$.			
Efficiency of M:			
$H_2 = 2.0$, $H_2O = 5.0$, $CO_2 = 3.0$, CO = 2.0.			
CH_3CO(+M)=CH_3+CO(+M)	$3.00000E+12$	0.000	16722.00
Low pressure limit	$1.20000E+15$	0.000	12518.00
C_2H+H_2=C_2H_2+H	$4.090E+05$	2.390	864.30
C_2H+O=CH+CO	$5.000E+13$	0.000	0.00
C_2H+O_2=2CO+H	$9.040E+12$	0.000	-457.00
C_2O+H=CH+CO	$1.000E+13$	0.000	0.00
C_2O+O=2CO	$5.000E+13$	0.000	0.00
C_2O+OH=2CO+H	$2.000E+13$	0.000	0.00
C_2O+O_2=2CO+O	$2.000E+13$	0.000	0.00
CH_3CHCO+H=C_2H_5+CO	$2.000E+13$	0.000	2000.00
CH_3CHCO+O=CH_3+CO+HCO	$3.000E+07$	2.000	0.00
aC_3H_5+O_2=C_2H_2+CH_2O+OH	$2.780E+25$	-4.800	15468.00
O_2+pC_3H_5=CH_3HCO+HCO	$1.090E+23$	-3.290	3892.00
O_2+pC_3H_5=CH_3CHCO+H+O	$1.600E+15$	-0.780	3135.00
O+pC_3H_5=CH_3CHCO+H	$1.000E+14$	0.000	0.00
H+pC_3H_5=aC_3H_5+H	$1.000E+14$	0.000	0.00